ANALYSIS OF OLFACTORY EVOKED POTENTIALS

A Thesis Submitted to
the Graduate School of Engineering and Sciences of
İzmir Institute of Technology
in Partial Fulfilment of the Requirements for the Degree of

MASTER OF SCIENCE

in Electronics and Communication Engineering

by
Bilal Orkan OLCAY

July 2014
İZMİR

We approve the thesis of **Bilal Orkan OLCAY**

Examining Committee Members:

_____
Prof. Dr. Ferit Acar SAVACI
Department of Electrical and Electronics Engineering, Izmir Institute of Technology

_____
Prof. Dr. Murat ÖZGÖREN
Department of Biophysics, Dokuz Eylul University

_____
Assist. Prof. Dr. Mustafa Aziz ALTINKAYA
Department of Electrical and Electronics Engineering, Izmir Institute of Technology

11 July 2014

_____
Prof. Dr. Ferit Acar SAVACI
Supervisor
Department of Electrical and Electronics Engineering, Izmir Institute of Technology

_____   _____
Prof. Dr. Mehmet Salih DİNLEYİCİ   **Prof. Dr. R. Tuğrul SENGER**
Head of the Department of   Dean of the Graduate School of
Electrical and Electronics Engineering   Engineering and Sciences

ACKNOWLEDGEMENTS

ABSTRACT

ANALYSIS OF OLFACTORY EVOKED POTENTIALS

With the growing opportunities of laboratories and measurement techniques, cognitive science attracts many researchers interest from other branches of science. In the literature, lack of studies related to the brain's responsiveness against the olfactory stimuli has been the main source of motivation for our work on this issue.

In this thesis, it is examined by means of time-dependent wavelet entropy of Electroencephalographic (EEG) signals which is collected from individuals that how olfactory and trigeminal effective odor stimuli affects responsiveness of the brain. Significance and meaningfulness of the results are shown with statistical tests of average entropy in the discrete time windows.

Due to its nature of small amplitude in comparison with ongoing EEG activity, it's hard to observe the components of olfactory evoked potentials and trigeminal evoked potentials. In order to separate these components from ongoing EEG, different signal processing techniques have been employed in this thesis. And, findings from these techniques have been conveyed to statistical tests to determine the most suitable technique for that purpose.

Additionally, a novel smell performance identification metric have been offered for clinical studies that is not affected by basal activity of brain and subjective review, for objective assessment of smell performance. Statistical test result have shown that, results of this technique which is performed on 19 participants, and their TDI scores obtained from Sniffin' Stick test battery, are in a strong correlation.

ÖZET

OLFAKTÖR UYARILMIŞ POTANSİYELLERİN ANALİZİ

Günümüz teknolojisi ile birlikte gelişim gösteren laboratuvar ve ölçümleme olanakları, beyin araştırmalarını çeşitli bilim dallarının ilgi odağı haline getirmiştir. Literatürde, beynin koku uyaranına karşı göstermiş olduğu yanıtlılığının incelenmesi ile ilgili yapılan çalışmaların azlığı, bu konu üzerinde çalışmamız için ana motivasyon kaynağı olmuştur. Yapılan bu tezde, olfaktör ve trigeminal etkili koku uyaranların, beyin yanıtlılığını nasıl etkilediği, kişilerden toplanan Elektroensefalogram (EEG) işaretlerinin zamana bağlı dalgacık entropisi ile incelenmiş ve ayrık zaman pencereleri ile ortalama entropinin anlamlılık derecesi istatistiksel testler ile gösterilmiştir.

Koku performansının klinik olarak değerlendirilmesi esnasında önemli öznitelikler olan olfaktör uyarılmış potansiyeller ve trigeminal uyarılmış potensiyellerin bileşenleri, EEG işaretine kıyasla düşük genliklidir. Bu potansiyellerin EEG işaretlerinden ayrıştırılması için farklı sinyal işleme teknikleri denenmiş ve en uygun teknik çeşitli istatistiksel kıyaslamalar ile belirlenmiştir. Bütün bunların yanı sıra, klinik çalışmalara katkı sağlayacak, kişinin bazal aktivitesinden etkilenmeyen ve sübjektif yorumlara kapalı bir koku performans metriği önerilmiştir. 19 hasta üzerinde uygulanan bu metriğin sübjektif koku performans testleri ile ilintili olduğu istatistiksel testler ile gösterilmiştir.

TABLE OF CONTENTS

LIST OF FIGURES

LIST OF TABLES

LIST OF ABBREVIATIONS

AA	Acquired Anosmia
AD	Alzheimer Disease
ADC	Analog Digital Converter
AL	Antennal Lobe
ANN	Artificial Neural Network
ATP	Adenosine Triphosphate
CDA	Canonical Discriminant Analysis
cAMP	Cyclic Adenosine Monophosphate
CN-1	Cranial Nerve-1
CN-5	Cranial Nerve-5
CNN	Cellular Neural Network
CNS	Central Nervous System
CO_2	Carbon dioxide
CSEP	Chemosensory Evoked Potentials
CSERP	Chemosensory Event-Related Potentials
CWT	Continuous Wavelet Transform
DFT	Discrete Fourier Transform
DWT	Discrete Wavelet Transform
ECG	Electrocardiogram
EEG	Electroencephalogram
EF	Enhancement Factor
EMD	Empirical Mode Decomposition
EP	Evoked Potentials
ERD	Event-Related Desynchronisation
ERP	Event-Related Potentials
ERS	Event-Related Synchronization
FIR	Finite Impulse Response
FSE	Fourier Spectral Entropy
iICA	Iterative Independent Component Analysis
IDT	Inter Digital Transducer
IMF	Intrinsic Mode Function

ISI	Interstimulus Interval
LN	Local Neurons
LVQ	Learning Vector Quantization
MMSE	Minimum Mean Square Error
MOS	Metal Oxide Semiconductor
NMP	Negative Mucosal Potential
OB	Olfactory Bulb
OERP	Olfactory Event-Related Potentials
OEP	Olfactory Evoked Potentials
OR	Olfactory Receptor
ORN	Olfactory Receptor Neuron
PCA	Principal Component Analysis
PEA	Phenyl Ethyl Alcohol
PN	Projection Neurons
QCM	Quartz Crystal Microbalance
REM	Rapid Eye Movement
RMS	Root Mean Square
RMS	Rostral Migratory Corridor
SAW	Surface Acoustic Wave
SNR	Signal-to-Noise Ratio
STFT	Short-Time Fourier Transform
SVM	Support Vector Machine
SVZ	Supra Ventricular Zone
TDI	Threshold-Discrimination-Identification
TERP	Trigeminal Event-Related Potentials
TEP	Trigeminal Evoked Potentials
TRI	Trigeminal
TW	Time Window
UPSIT	University of Pennsylvania Smell Identification Test
URTI	Upper Respiratory Tract Infection
WSS	Wide Sense Stationary

CHAPTER 1

INTRODUCTION

Did you ever measure a smell?
Can you tell me one smell is just twice strong as another?
It's very obvious that we have very many different kinds of smell, all the way from odor of violets
and roses to asafetida.
But until you measure the likeness and differences, you can have no science of odor.
If you are ambitious to find a new science, measure the smell.
Alexander Graham Bell, 1914

In comparison with the other senses such as somatosensory (i.e. tactile sensation), visual or auditory, olfaction or namely sense of smell is the most disregarded perception. This is because, olfaction is the least required sense in human's daily life and it is hard to evaluate the performance of olfaction in clinical conditions due to its subjectivity. It is noticed that, unlike in other sensory modalities, there is an unclear relation between stimulus and perception. This implies that there is an unclear sensory information processing in olfactory system. The subjective parameters of affecting the performance of sense of smell are hormonal cycle, subject's vigilance, sensitivity to odors, gender, substance usage, eating disruption, congenital or acquired disease, pregnancy, mood…etc. The external factors are relative humidity of ambient, molecular shape of odorant molecules, temperature and concentration of odors…etc. However, recently, it is recognized that olfaction is the one of the vital sensations in humans and animals [1].

Especially in animals, sense of smell gives a lot of information about their surroundings and also shapes the behavioral patterns such as identification of foods, territorial defense, awareness of dangers, kinship recognition and sexual attitude [2]. Also in humans, role of olfaction starts in neonatal life and takes an active role in throughout the life. Mate selection, emotional responses, social options are in strong correlation with sense of smell.

It is reported that olfaction is the oldest sensory modality in phylogenetic history in mammals and also, the similarity of parts of olfaction system between wide apart species such as rodents, insects and fruit fly points out the common evolutionary ancestry [3].

Nobody knew that EEG is the fundamental tool that demonstrates the memory building and integrative brain function until the slogan 'The EEG is quasi-deterministic response or represents chaotic behavior of brain, shouldn't be considered as background noise' came up. That was the renaissance of brain electrophysiology. A theory which follows Newton's, Einstein's and Galilee's pathway, states that brain waves are the language of brain and oscillations in different frequency tones creates the words and super-synergy between neuronal structures are the sentences of this language [4].

Pioneer of study of neuroscience is Hans Berger who had discovered the EEG in humans [5]. In his first study, he worked with string galvanometer. After that, he started to use Siemens double coil galvanometer which is a more powerful tool for analyzing brain rhythms. He published his first paper in 1929 that involves three minutes EEG recording on photographic paper. In that study, he claimed that alpha activity of brain rhythms is the major component of EEG.

There were no study found to examine the effect of olfactory stimulation on livings central nervous system. A study was done by Fleischl von Marxow in 1883 showing that he was the first discoverer of the relation between odor and brain oscillations in livings. He realized the fact that ammonia produced electrical fluctuations in rabbit's brain.

In humans, this relation was first described by Moncrieff in 1962. In his experiment, he recorded subjects' brain electrical activity while presenting different odors such as floral perfumes, oils, butanol and fresh chives. He realized that several odors can reduce the alpha activity.

First quantitative EEG changes upon odor stimulation for adults was published by Van Toller [6].

Discovery of olfactory evoked potentials (and olfactory event-related potentials) has attracted deserved interest of scientific or clinical community. Briefly, ERP and EP are EEG derived polyphasic deflections due to electromagnetic field of activated cortical neurons.

In 1966, Finkenzeller was the first discoverer of olfactory evoked potentials (OEP) by using blast olfactometer [7]. After that, in 1967 Allison and Geoff did the same experiment with constant flow olfactometer which is an improved version of blast olfactometer. These studies are milestones in this research area [8].

In early years, blast olfactometers were the most popular devices. As a short description, olfactometer is an instrument that can create and deliver rectangular shaped

odorant pulses to subject's nose in a controlled fashion for advanced clinical researches. Blast olfactometer creates a pressurized odorized air puffs and sends it through the subject's nostrils. However, the main drawback of using such an olfactometer is, it creates tactile stimuli by activating mechano-receptors due to air puffs in subject's nostril and evokes trigeminal afferents which lies in nasal cavity for transmission of tactile stimulation to second somatosensory cortex. This causes several problems that odorant which have no trigeminal effect, can generate trigeminal evoked potentials (TEP) in human brain. Using such a device causes some recordable evoked potential on the scalp on people who don't have ability to detect odorized air. To overcome this problem, an olfactometer, capable of creating odorized air stimulation under constant air flow by switching vacuum line, developed by Kobal and Plattig [9], has allowed researchers to interest in various problems in how brain processes olfactory information [8].

Before the chemosensory event related potentials and evoked potentials became popular in clinical manner, there wasn't any international standardized olfactory performance test. Even though these smell tests are easy to implement and validated by some clinics, there are many drawbacks. Outcomes of such tests are easily affected by subject's response bias [10]. This means that, it is hard to identify malingering and impaired subjects [11].

Sniffin' Stick test is a performance evaluation tool that measures subject's olfaction ability under definite procedures [12]. In the first stage of this test, olfactory threshold (T) value is determined by presentation of n-butanol by stepwise increasing dilution with sixteen felt-tip pens. The lowest concentration that subject can detect, is the threshold score of the subject. As a second step, the subject need to perform a triple forced-choice task by using sixteen triplet of odorant. Target pen contains different type of odorant than other remaining two pens. Discrimination score (D) of subject is assessed in this step and finally identification (I) performance is tested by selection of sixteen odorant names from a forced-choice list. All the results are summed to obtain subject's TDI score. For TDI score with smaller than 16.5, patient is functionally anosmic. For TDI score greater than 30.5, patient is called normosmic and otherwise patient is said to be hyposmic or anosmic. Anosmia is defined as the inability to perceive the odors or it can be said that lack of olfactory functioning. Hyposmia is known as degradation of smell performance due to various reasons. Normosmic people show normal smell performance [13].

Another commonly used technique is the UPSIT (University of Pennsylvania Smell Identification Test) [14]. UPSIT was developed by Doty and colleagues in USA in 1984. In this test, odorants are presented via pen-like sticks to the participants. About 40 different odors are used and subjects are requested to choose one of the four odorant name from forced-choice list. Numbers of correctly identified odors are the score of the subject's performance.

SOIT (Scandinavian Odor Identification Test) was developed by Nordin in 1998 with the basis of north Europe cultural pedestals. In this test, liquid odors are injected to stype in order for saturation. About 16 different type of odors (anasone, vanilla, apple, clove, almond…etc.) are able to activate and test trigeminal and olfactory afferents separately. Same as UPSIT, participants are requested to choose one of the best-matched odor name from a forced choice list [15].

Olfactory event-related potentials (OERP) and olfactory evoked potentials (OEP) have proven to be a good tool for assessment of olfaction performance and diagnosis of some neurodegenerative diseases due to its direct correlation with neuronal activation. However, there are some disadvantages such as;

- It can be affected by motor and movement artifacts.
- Vigilance decreases and olfactory fatigue can be seen with repeated stimuli.
- It is hard to observe pure OERP due to background EEG activity.

These drawbacks bring the main question about the probability of recording an OERP. In study [16], functional relation between TDI score and probability of observing the OERP is given as,

$$p = \frac{1}{1 + \left(\frac{TDI}{\alpha}\right)^{-\beta}}$$
(1.1)

where p is the probability of observing OERP when psychophysical score is TDI. Parameters α and β are turning point of probability function and steepness of function respectively. With the help of logistic regression, the turning point of TDI is found about 22.6 for men that observation of OERP is more than chance. This score is almost 0.8 times lower for women participants. It is pointed out in this study that occurrence of OERP is a fingerprint of olfactory ability but vice versa is not correct.

Congenital anosmia, (i.e. Kalmann Syndrome), known to be the absence of olfactory function due to several congenital or subsequent reasons such as dysgenesis/agenesis of receptor cells and/or olfactory bulb. In study [17], olfactory event-related potentials were recorded for 9 anosmic and age matched 9 control subjects. Assessment of olfactory performance was evaluated by using P1, N1, P2, N2 potentials. Isoamyl acetate was used as olfactory and chloracetyl phenone as trigeminal stimulant. For congenital anosmic subject, no reproducible components were recorded in isoamyl acetate stimulation and there were no significant differences found anosmic and control group for chloracetyl phenone stimulation.

Post-infectious olfactory loss is defined as an unannounced impairment of olfactory functioning due to upper respiratory tract infection (URTI) mainly due to toxic attack or virus spread of olfactory pathways. As a brief information, such a dysfunction can be seen in %11 of whole population [18]. By utilizing the power of OERP, recovery from this deficit can be estimated. In [18], 27 patients suffering from URTI were included. All psychophysical and electrophysiological tests evaluated twice at distinct times. Subjects who elicit recordable OERP in the first meeting, show improved (i.e. recovered) olfactory functioning. Vital finding from this study is that, a participant who elicits OERP when suffering from an olfactory dysfunction, has more chance to recover from such a disease.

Studies about interaction between trigeminal and olfactory systems mainly utilize the subjects with olfactory dysfunction such as acquired anosmia (AA) who displays larger peripheral responses and smaller cerebral response amplitudes. In [19], a total number of 123 subjects that 73 of them suffers from AA, attended in this study. Negative mucosal potential (NMP) results of acquired anosmic patients demonstrate higher NMP activity than healthy group. However, examining the TERP results, AA subjects elicit smaller P2 and N1/P2 amplitudes. It was inferred by the authors that, olfactory system is in a close interaction with trigeminal system and changes in central nervous system (CNS) due to olfactory loss results in attenuated trigeminal responsiveness. In this line of sight, it is hypothesized from this study; such a result is greatly due to impairment of excitatory cells in olfactory bulb.

Alzheimer, the most encountered form of dementia [20], is a kind of neurodegenerative disease that shows itself by decrease in cognitive functions and also, some neuropsychiatric changes can be seen in time courses. One of the early symptoms of Alzheimer disease is reduction in the sense of smell. This is because, regions are

involved in olfaction, also demonstrates some deterioration in Alzheimer disease [21]. Additionally, according to Braak and his colleague, the initial suffered limbic structure is transentorhinal cortex, which is associated with memory, emotion and olfaction. As an important outcome referred in [22] that volume of olfactory bulb decreases dramatically in Alzheimer Disease (AD) patients in comparison with age-matched controls. This study shows the ability of olfactory event-related potentials that helps diagnosis of Alzheimer disease in clinical context. 12 AD and 12 age-matched controls were attended in that study. Two type of stimulus modality were handled. In olfactory stimulations, AD patients elicit significantly prolonged P3 latency. AD patients also show longer latencies of N1, P2 and N2 than control subjects. As a consequence, dementia status is highly correlated with OERP latencies.

Loss of olfactory performance in Parkinsonism has been well documented by several authors. It is stated that about %95 of Parkinson patient suffers from olfactory loss [23]. Prior to motor symptoms, Parkinson demonstrates itself with degradation of sense of smell with 4-6 months earlier than clinical motor impairments [24]. A general characteristic of people who suffer from idiopathic Parkinson disease is delayed or absent OERP. Apart from psychophysical tests, OERP can be utilized to investigate smell performance [25]. But functional neuro-imaging studies reveal that both ERP detected (ERP+) and non-detected (ERP-) participants elicit central activation during odorant stimuli. In [26], both electrophysiological and FMRI responses were discussed for 24 subjects. ERP+ participant showed higher TDI scores than ERP-. Both groups elicit in left and right superior temporal gyrus but additionally, ERP+ group display activation in orbitofrontal region and inferior frontal gyrus. And also, ERP+ participants demonstrate higher activation in left and right inferior temporal gyrus for both sided stimulations. Such a discrepancy might be due to neuro-degeneration of olfactory related areas occurring dramatically in ERP- group. As a consequence presence of OERP is prognostic sign for activation of several brain areas and it may be a fingerprint of recovery of the olfactory function [18, 26].

Aging is an important factor that causes degradation in smell performance. Entorhinal cortex, hippocampus, amygdala and temporal lobe are the most affected olfactory regions from aging progress. In 1983, Murphy pointed out that older subject demonstrates higher threshold values than younger subjects [27]. In [28], totally 16 participant divided into three groups by considering their age. Youngest group comprises 15-34 year-old subjects, middle aged group involve 35-54 and final group consist of 55-

74 year-old people. N1/P2, N1, P2 amplitudes and latencies were handled in order for assessment of the effect of aging. For elderly people, N1/P2 interpeak amplitude significantly smaller in comparison with other two groups for olfactory stimulation with H_2S. P2 amplitude demonstrates a dramatical decrease for both olfactory and trigeminal stimulations with aging. Besides them, prolongation of N1 peak increases for both trigeminal and olfactory test with increasing age. Along with this study, study done by Charlie D. Morgan et.al. participated 8 male and 8 female [29]. Being consistent with other age-related studies, younger participants elicit larger amplitude and shorter latency for all different electrode site and different ISI conditions. Furthermore, most interesting finding is that, the older males elicit more attenuated OERP amplitude in comparison with older females. This can be due to greater brain atrophy occurs in elderly men than age-matched females.

Besides aging, gender effect [30] is another important factor that affects the olfactory performance. In [31], in addition to gender and aging, effect of side of stimulation and concentration of odor is also discussed. For both women and men, aging causes linear decrease of olfactory ability and propensity for olfactory adaptation. Psychophysical test result shows the factor 'gender' is significant in lateralization task that women demonstrates higher scores for trigeminal stimulation than men. For olfactory function, aging shows itself by elevation of olfactory threshold that young and middle aged participants outperform the psychophysical discrimination task in Sniffin' Stick test battery. Electrophysiological results point the degradation in P2 amplitudes and increment of N1 latency with advancing age for olfactory stimulation. Besides, gender related differences show that women elicit larger P2 and shorter N1 latency than men. Electrophysiological outcomes are in strong correlation with psychophysical findings that odor threshold and odor discrimination scores are in strong correlation with P2 amplitude while odor identification has a strong correlation with latency of P2. For trigeminal function, higher lateralization task scores are also associated with shorter peak amplitude and shorter latencies. Stimulation through right or left nostril doesn't give any novel result except that women give larger P2 amplitude to right-sided olfactory stimulation. It is underlined in this study is that such a result might be raised from hemispheric olfactory information processing differences between men and women.

Study [32] examines the effect of gender by utilizing chemosensory perception scores and evaluation of chemosensory event-related potentials (CSERP). Pyridine, known to be dual olfactory/trigeminal stimulant is used for both psychophysical and

electrophysiological sessions. Psychophysical tests consist of nasal intensity, pleasantness and sensory irritation tests. Electrophysiological test consist of measurement of CSERP's. Results demonstrate for both psychophysical and electrophysiological outcomes, women scores higher than men. Identifiability of P1, N1 and P2/P3 complex is greater in women. It can be inferred that women display higher signal-to-noise (SNR) ratio than men. Study [33] examines the intranasal trigeminal sensitivity and potentials hemispheric in the sense of gender difference. Significant differences found in latencies that women elicit shorter in left-hemispheric recordings and mean amplitude, especially in cognitive P3 component, in greater in women for both hemi-sphere recordings.

It is well-known that, late latency (P3) component has strong correlation with cognitive functions and dominates the delta band response [34]. It arises when stimulus has a novelty or contains a cognitive task. A study done by Morgan & Murphy [35], demonstrates the OERP P3 changes for young, middle and older age groups in active/passive task conditions. As a comparison, they utilized a visual stimulus with both active and passive conditions. Results display that older participants elicits longer latency values than younger participants in both olfactory and visual stimuli and for both task conditions. While in active visual stimuli shows shorter P3 latency than passive task, olfactory P3 doesn't display any significant change. As a significant finding, older participants show the longest latency in passive task for olfactory modality. As a consequence, younger participants' shows reduced P3 latency for both stimulus modalities. According to Karayanidis and coworkers, these prolonged latencies and attenuated amplitudes with aging, are due to reduced information filtering for older subjects that neural system has to process irrelevant information besides important ones.

Many studies demonstrate the hypersensitivity in women during pregnancy. In pregnancy, there exists a hedonic shift of odors from pleasant to unpleasant. Olofsson et.al. utilized CSERPs in response to olfactory and trigeminal stimuli to represent the hypersensitivity while in pregnancy [36]. In comparison with non-pregnant women, pregnant women elicit larger amplitude and shorter latency for P3 component rather than early sensory components such as N1, P1. It is outlined that, this hypersensitivity comes from neural basis of cognitive processing of odorant information that serves a protection mother and embryo from certain foods such as coffee, alcohol, protein-rich foods which they originates toxic effect.

There are many factors affecting signal-to-noise ratio of CSEP/CSERP such as, subject's vigilance, basal activity, adaptation/habituation, hormonal cycle, gender,

smoking and psychological state. Classical way to enhance the signal-to-noise ratio (SNR) of CSEP/CSERP is conventional time domain averaging. In general, event-related-potentials (ERP) and evoked potentials (EP) are assumed to be the time-locked brain's stationary response under same stimuli conditions. Besides, ongoing EEG oscillations, whose amplitude is bigger than ERP/EP, can obscure them. By utilizing the EEG's non-stationary property, averaging across many trials can attenuate the ongoing EEG oscillations and enhance the SNR of event-related potentials. In [37], the question how many single trials are needed to obtain the optimal event-related response is discussed. It is found that, for trigeminal ERP, there is no further improvement beyond averaging 60 single trials and for olfactory ERP, obtaining optimal SNR ratio requires averaging about 80 single trials. Further averaging for both responses of subsystems, attenuation of N1P2 inter-peak can be seen due to temporal jitter. Temporal jitter can be considered as brain's variable reaction time to stimuli. It causes deterioration of the ERP so that it becomes unpredictable. Intracellular transduction, trial by trial variation, changing cortical dynamics, fatigue and loss of vigilance are the well-known jitter sources.

It has been demonstrated that, there is an interrelation between effect of aging and stimulus intensity. Intensity of odor affects the generation time (latency) and amplitude of OERP components. Increasing concentration demonstrates increase in amplitude and decrease in latency. The study [38] was carried out with 14 young and 14 normal older adults. Results are consistent with previous studies that younger participants demonstrate shorter latency and larger amplitude in comparison with older participants. Decrease in concentration shows itself by prolongation of latency variables. These findings are consistent across all age groups.

In 1978, Cain demonstrated that there is a functional relationship between odorant concentration and perceived magnitude [39]. He manifested this relation by the formula,

$$\psi = k\varphi^{\beta} \qquad\qquad (1.2)$$

where ψ is the perceived magnitude, φ represents the concentration and β is the steepness of the function. When examining the equation (1.2) it can be easily seen that, increase in concentration results in an enhancement the perceived magnitude in olfactory system. A study [40] deals with the correlation between physiological and psychological outcomes in variation of intensity of odor. Isoamyl acetate known to be pure olfactory stimulant is represented to subjects via Lorig design continuous flow olfactometer [41]. Psychological

responses obtained from the subjects that they were requested to press a button to each perceived stimuli. Electrophysiological responses are the recorded OERP amplitudes. Results show that decrease in interstimulus interval (ISI) elicits smaller OERP amplitudes due to adaptation/habituation. Besides, increase in stimulus intensity lead to an increment in OERP amplitude. As a psychological result, subjects become unable to detect the odors with shorter ISI's. As a consequence for this study, with higher intensities, both physiological and psychological results demonstrates significant correlation with lower stimulus frequency that does not cause adaptation/habituation in olfactory pathway and/or higher order brain centers.

Interstimulus interval (ISI) is an important factor for evaluation of OERP and TERP in clinical context. Short ISI can causes adaptation in olfactory receptor cells and also habituation in neuronal structures. Wetter et.al. proposed a paradigm for measuring OERP efficiently by 10 minute-ISI and fewer trial [11]. OERP amplitudes and latencies were recorded three times for each 10 participant with 10 min ISI paradigm. Results show that none of OERP amplitude and latency demonstrates dramatic increase or drop in three sessions. To conclude, by utilizing 10-min ISI, stable OERP recordings can be obtained without any habituation and/or adaptation. On the contrary, utilization of longer ISI might cause boost in alpha activity which is associated with variability of ERPs and such activity enhancement can interfere with stimulus evoked potentials. Mental task load is known to be a attenuator of alpha rhythms in indirect way [42]. Nordin et.al. employed visuomotor tracking task to analyze the effects of mental task versus eyes open/close conditions on olfactory induced potentials in young and older subjects. However there weren't any significant difference in sense of amplitude but in P2 latency. In consistent with other studies related with aging, young subjects produce larger amplitude in entire conditions than older ones. Latencies of N1 and P2 are smaller in younger participants. The only task related differences was seen in P2 latency that tracking task produces shorter latencies than others. All these differences are known to relate with aging, it can be stated that, type of the task does not influence the OERP components significantly.

Usage of different stimulant can also affect latency and amplitude of OEP. Study [43] uses skatole which is a flowery smell and amyl-acetate as olfactory stimulant. New stimulation technique is employed which combines led light pulse and odorant stimuli. According to findings, usage of different odors changes the latency values.

OERP gives us a chance to assess the neuronal resource allocation for information processing in the brain. It is hypothesized in [44] that amplitude of CSERP shows amount

of neuronal resources. In attended (active) condition subjects required some additional effort such as estimation of stimulus strength, button pressing, counting the less frequent stimuli. Ignore (passive) condition does not load any extra task to participant. In [45], totally 26 participant were included to study. Participants, who passed the series of psychophysiological tests, were conveyed to electrophysiological session. Amyl acetate and ammonia were presented for excitation of olfactory and trigeminal afferent respectively. It is found in attended condition that, latencies of exogenous (N1) component and endogenous (P3) component were shorter than ignored stimuli condition for both olfactory and trigeminal stimuli. Amplitudes, A-N1/P2 and A-P3 were higher in attended condition. All these finding suggest that extra workload like in attended condition, demands more neuronal resources than ignored condition.

Like in wakefulness, chemosensory stimuli activate neuronal resources during different sleep stages. Study [46] analyzed the alteration of chemosensory ERP potentials in different sleep stages such as light sleep, slow wave sleep and REM sleep with 15 female participants for both olfactory and trigeminal stimuli. Averaged P1N1 and N1P2 amplitudes and latency of N1 and P2 components were observed. Number of subjects that demonstrated recordable olfactory and trigeminal event-related potentials as in Table 1,

Table 1. Number of subjects demonstrates recordable ERP

	Light Sleep	Slow Wave Sleep (SWS)	REM-sleep
Olfactory (H_2S)	6	8	1
Trigeminal (CO_2)	2	3	4

In olfactory stimulation, N1 component elicited longest latency during light sleep and latency of P2 component were reach its largest value during slow wave sleep. By comparing with other sleep stages, N1/P2 amplitude reaches its maximum value during slow wave sleep. In trigeminal stimuli, the longest latencies were seen in light sleep cycle. Amplitudes were smaller in slow wave sleep and REM-sleep compared to the baseline values. During the sleep, in despite of more neuronal resources are available to process the information, it remains unclear that, the reason why such longer latencies and smaller amplitudes have been observed. As a consequence, brain continues the exogenous information processing during sleep.

All these aforementioned studies requires time domain averaging of olfactory responses over many trials due to the signal-to-noise ratio of single trials. However, this conventional method incorporate many drawbacks. First of all, averaging enhances event-related potentials (ERP), but it attenuates event-related synchronization (ERS) and event-related desynchronisation (ERD). Second, requirement of many trials require longer experiment time. Exposure of odorant so long causes olfactory fatigue, decrease of vigilance, adaptation and habituation. In this respect, working with single trial responses becomes important owing to the aforementioned shortcomings.

Due to nonstationary property of EEG signals, wavelet transform has attracted deserved interest in neuroscience and biomedical engineering [47]. In [48], C. Huart et.al. utilized continuous wavelet transform in their study and compare the performance with classical time domain averaging. Time domain features were amplitude and latency values of N1 and P2 were for both olfactory and trigeminal responses. Time-frequency representations of both olfactory and trigeminal responses were handled in order for selection of reliable distinct features. A comparison was done in the sense of sensitivity and selectivity of the features. For trigeminal response, selected all of three time-frequency domain features were able to classify the presence or absence of olfactory function in participants. Somehow, only one time-frequency feature of olfactory response were reached significant sensitivity and selectivity level. In both case no reliable time domain feature was found except for trigeminal P2 (TRI-P2). As a consequence, time-frequency domain features are good indicator tools for olfactory functioning and also time-frequency representation enables the determination of phase locked and non-phase locked responses and also it enhances the signal-to-noise ratio of elicited response. It is proven that CWT is suitable tool for clinical OERP researches [2].

Extraction of P300 response from ongoing EEG is mostly done by task based selection method. However, Demiralp et.al. proposed a new method utilizing wavelet decomposition with B-Spline wavelet functions to extract more suitable features in order for extraction of P300 wave [34]. P300 wave is mostly correlated with fourth delta band coefficient after the stimulus onset. By using this method authors found enhanced and clearer averaged response of P300 obtained in comparison with task based selection method.

Owing to the fact that ERPs are small amplitude signals in comparison with ongoing EEG, extraction of such signal requires advanced signal processing techniques. Wavelet denoising which is utilized in a part of our study is a successful method that

provides an estimation of amplitudes and latencies of ERPs. R. Quian Quiroga et.al. employed Wiener filter and wavelet denoising in [49] to extract simulated ERP with different signal-to-noise ratio. After that, both algorithms were applied to visual and auditory event-related potentials. Results show that, for all 3 dataset, wavelet denoising gives good estimation of ERP than Wiener filter.

Manual selection of ERP/EP related wavelet coefficients can be time consuming and requires huge number of analysis due to subject-to-subject variability. An automatic denoising algorithm which is improved version of the algorithm [50] was demonstrated in [51] gives better performance in the sense of resulting ERP.

An alternative approach for estimation of single-trial responses was given in [52]. In addition to wavelet denoising, Woody filter was employed for latency correction [53]. In this study, algorithm was applied to synthetic data with contaminated white and iso-spectral noise. Findings from this study shows that, time adaptive denoising algorithm gives satisfactory result than other filtering techniques.

Independent component analysis is a kind of blind source separation technique that is developed for seeking statistically independent sources from their observations. In [54], a comparison was done between wavelet denoising proposed by Donoho and an iterative algorithm iterative ICA (iICA). Outcomes of two methods show that, iICA method extracts individual components clearly, but wavelet denoising elicits smoother approximation of single trial response.

Empirical mode decomposition (EMD), proposed by Huang et.al. is a data-driven nonlinear time series analysis tool that decomposes signal into intrinsic mode functions (IMF's) [55]. Study [56] utilized the power of EMD to observe the inter-trial variations of OERP. Subject-specific frequency band and spatial template was determined to obtain stimulus related IMF's. Candidate IMF's are classified by using K-means clustering and reconstructed by summating all the related IMFs. Such an algorithm is useful for rejection of stimulus unrelated brain oscillations and analysis of inter-trial variability between single-trials.

Entropy has proven to be a useful analysis technique for demonstration of degree of disorder. The conventional approach to determine the degree of disorder of EEG was Fourier spectral entropy (FSE). However, the main drawback is that, Fourier spectral entropy requires stationary data. To overcome this, orthogonal discrete wavelet transform is proposed by Daubechies [57]. In [58, 59], wavelet Shannon entropy was employed for analysis of auditory event-related potentials. Results show that major entropy decrease

occurs at short after the stimulus onset and it indicates that stimulus forces the brain to enter more ordered microstates. In [60], again discrete wavelet transform and Shannon entropy is employed for detection of changes in brain dynamics in pre-ictal, ictal and post-ictal stages. In the ictal stage, structures create rhythmic oscillations in order to synchronous neuronal discharge. Wavelet entropy analysis demonstrates that the lowest entropy values can be seen in ictal seizures because of synchronization in specified frequencies. As a consequence wavelet entropy elicits reliable quantities about system's complexity.

Both continuous and discrete time wavelet entropy was employed in [61] for analysis of auditory evoked potentials for both target and non-target stimulations. As entropy measures, Shannon [62] and Tsallis [63] entropies are employed to demonstrate degree of disorder with time evolution. While continuous time wavelet entropy can elicit more detailed entropy changes with time, discrete time wavelet entropy represents the bulk evolution. Findings are consistent with previous studies that major entropy decrease occurs in post-stimulus time period.

Like audition, visual stimulation also evokes some oscillation in human brain. As so in aforementioned studies, [64] utilizes the wavelet entropy as time-varying measurement tools of order of brain oscillations. According to the resonance hypothesis that was put forward by Erol Basar, which is referred in [65], that ERP is emerged from EEG due to coherent oscillations of neuronal pattern generators upon any endogenous or exogenous stimulation. In this study, visual evoked potentials were quantified by wavelet Shannon entropy as in previously mentioned studies. Time evolution of wavelet Shannon entropy clearly specified the entropy decrease due to visual stimulation.

Remainder of this thesis is organized as follows. In chapter 2, initially, definition of odor is given. Human and insects olfactory system is reviewed and brief information and literature survey about electronic nose which is a device that mimicks insects olfactory system is given. Also, brief information about brain rhythms, evoked/event-related potentials is given. At the end of chapter 2, the procedure of obtaining CSEP have been described. Chapter 3 provides some information about time-frequency analysis methods and denoising scheme by using time-frequency components is described. Chapter 4 gives some basic information about Wiener filters and usage of Wiener filters for obtaining CSEP. Chapter 5 describes Empirical Mode Decomposition and how to utilize the EMD method for single trial EP extraction is detailed. In chapter 6, we have proposed a metric, which is called "Enhancement Factor" for obtaining subjects' smell

performance. Chapter 7 provides a conclusion for studied techniques and also, some future works for this study is given.

CHAPTER 2

BACKGROUND

2.1. Definition of Odor

Odor is the emotion that can be solved and diluted in ambient air and generates a perception in sensation part of olfaction system. Detection of odors depend not only the concentration in ambient air but also depends on the molecular shape of the odor.

Assessment of the odors can be done in many quantitative ways such as,

- Concentration measurement
- Intensity
- Hedonic tone assessment
- Character
- Dispersion modeling

Among these measurements, intensity and hedonic tone assessment are the best known and most used quantities. Intensity can be defined as the strength of odor. In most clinical study, subjects are asked to quantify odor intensity by verbal description. A numerical value can be assigned to odor by the subject. The most common used intensity scale in many rhinology clinic is;

0- No odor
1- Very weak
2- Weak
3- Distinct
4- Strong
5- Very Strong
6- Intolerable

Hedonic tone assessment is the scoring of odors from unpleasant to pleasant scale. Main drawback of this procedure is odor perception can change between subjects and perception of one odor can change from pleasant to unpleasant with increasing concentration.

Researchers still tries to find a way to describe the relation between physico-chemical features of the molecules and perception of odors. The complexity of physico-chemical space is well documented in many studies, however, several studies proposed some metric features to describe the perceptual differences that points the variations in neuro-physiological data in humans. In addition to molecular complexity of odors, Kermen et.al. concluded that besides other derived features, molecular length and weight also contribute confusion to pleasantness and perceptive differences [66].

2.2. Olfaction in Insects

Olfaction in insects and vertebrates starts in olfactory receptor neurons (ORN). ORN's are located in dendrites of olfactory receptor cells inside sensilla that they are in charge for odorant detection from the environment. It is reported that, in insects, they have approximately 50,000-300,000 ORNs to capture different kinds of odorants molecules. It is important to note that identification and quantification of an odor in a short time is the fascinating features of insect's olfaction system [67].

Drosophila's olfaction system has been a basis for study of olfaction and also it has attracted much interest from scientists. By looking closer at the insect's olfactory system it consist of three main part,

- Antenna
- Antennal Lobe
- Mushroom Body
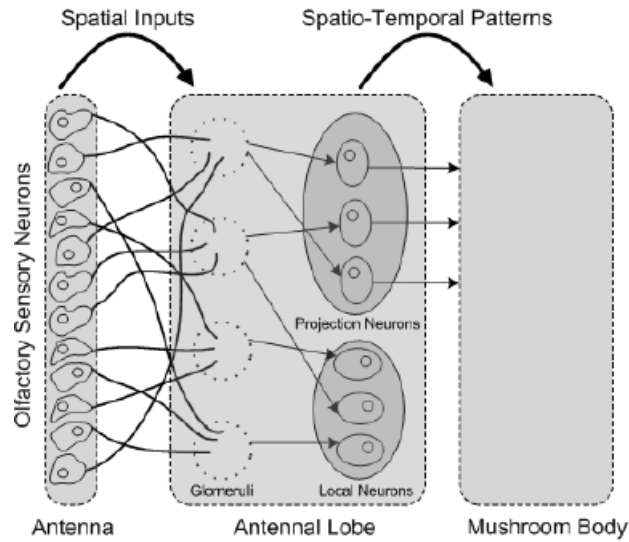
Figure 1. Block diagram of insect's olfactory system [67]

Antenna comprises immense number of olfactory receptors which appear in chemosensory sensilla. They are responsible for binding the odorant molecules. Short after the onset of binding process, olfactory receptors create electrical impulses to activate the higher order structures.

Antennal lobe (AL) is said to be the biggest neuropil of the insects' higher order nervous system (see Figure 2) [67]. Main purpose of this structure is to converts the olfactory code which is generated by olfactory receptor neurons to spatio-temporal code. Consistent with this finding, it is pointed out in [68] that, there is a nonlinear signal transformation in AL.

AL is structured by local neurons (LN), projection neurons (PN) and glomeruli [69]. Projection neurons and local neurons elicit strong interaction in AL. Projection neuron responses are the input of the local neurons. After the reciprocal information processing, processed information conveyed to mushroom body via projection neurons. In this structure glomeruli acts as an interface between antenna and projection/local neurons. In the above block diagram, it can be seen that, every projection neuron is in collaboration with a glomeruli. Odorant information which is received from antenna is converted to spatio-temporal code by excitatory and inhibitory processes in antennal lobe. Analysis of AL demonstrates that odorant information is projected to lower dimensional feature space with lower variability between same types of odors. As a consequence antennal lobe reduces within class scatter and increases the inter-class scatter working as a non-linear filter.
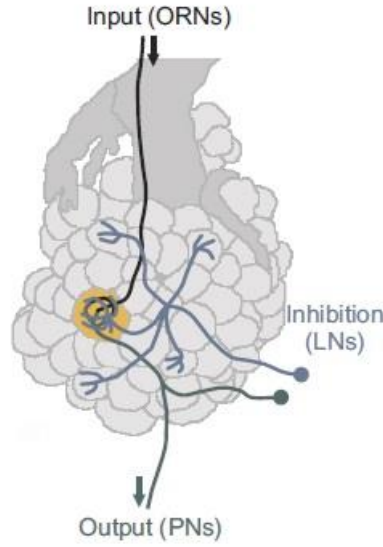
Figure 2. Schematic view of Antennal Lobe with its glomerular structure [70]

Settling time of ORN lasts hundreds of milliseconds but pattern recognition process is completed in 30-40 milliseconds. This fact displays that pattern recognition uses transient response of ORNs.

In [71], It is stated that antennal lobe is the analogous of the vertebrates olfactory bulb. Muezzinoglu & Vergara et.al. modelled the insects' antennal lobe by means of projection and local neurons.

$$\beta_i^E \frac{dx_i(t)}{dt} = K_i^E . \Theta \left(-\sum_{j=1}^{N_I} w_{ij}^{EI} \ y_j(t) + g_{INP}^E \ S_i^E(t) \right) - x_i(t) + \mu_i^E(t) \tag{2.1}$$

$$\beta_i^I \frac{dy_i(t)}{dt} = K_i^I . \Theta \left(\sum_{j=1}^{N_E} w_{ij}^{IE} \ x_j(t) + g_{INP}^I \ S_i^I(t) \right) - y_i(t) + \mu_i^I(t) \tag{2.2}$$

In equations (2.1) and (2.2), E and I stands for excitatory (projection) and inhibitory (local) neurons respectively. Synaptic connection weight w^{EI} represents the connection from a projection neuron to local neuron and w^{IE} represents the connection from local neuron to projection neuron and μ is the noise that is infected from ambient air and other factors. S_a^B represents the input from a^{th} glomeruli and $\theta(.)$ is the Heaviside function.

The network topology is formed by using Bernoulli process such as

$$w_{a,b}^{AB} = \begin{cases} 1, & with\ p^{AB} \\ 0, & with\ 1 - p^{AB} \end{cases}$$

(2.3)

Mushroom body is responsible for learning and memory processes. It is analogous to mammalian cerebral cortex. In some other kind of insects, mushroom body governs the associative memory and motor control.

2.3. Human Olfaction

The vital requirement for sensing the odorant is the arrival of the odorized air to the olfactory epithelium (regio olfactoria) which is located at the roof of the nasal cavity. Olfactory epithelium consists of 4 different cell types. These are;

- Support cells
- Microvillus cells
- Stem cells
- Olfactory receptor cells

Among these, there are also four types of olfactory receptor subgroups that can be found in distinct locations within olfactory neuroepithelium in humans. In these subgroups, approximately 900 billion of receptor variations are assumed to be found. In mammals, sub genome of olfactory receptors are occupied the one percentile of gene families and number of functional OR types varies from 600 to 1400 in vertebrates [3].

These OR cells are located in different sides of the olfactory mucosa. In this region, odorants are encoded with activation of different kinds of olfactory receptors. Response of the olfactory receptors to any odorant stimulus is known to be encoded by combinational way. It can be also stated that activation of specific receptors are the vital part of the odorant encoding as demonstrated in Figure 3.
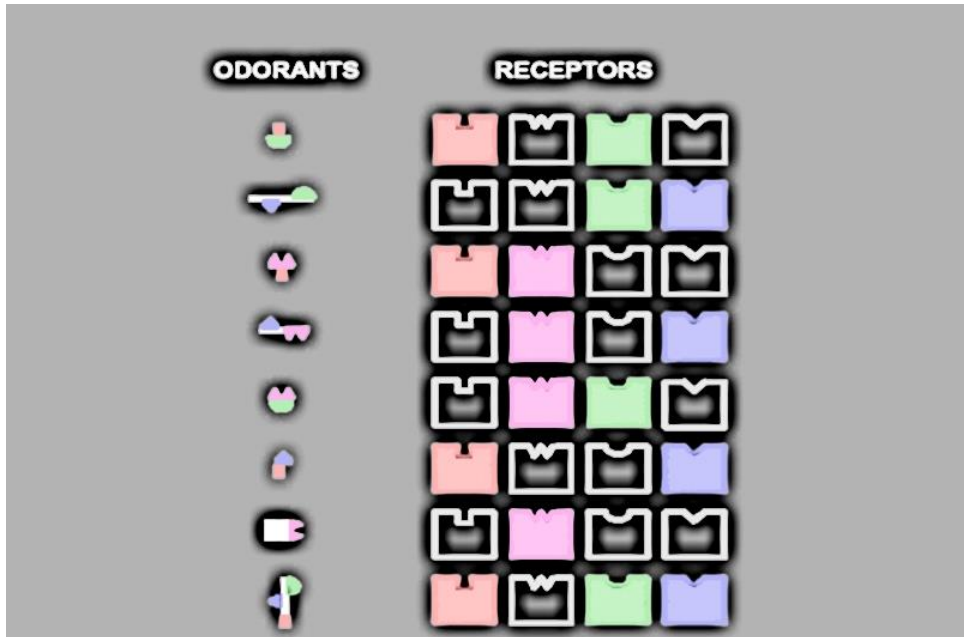
Figure 3. Illustration of process of encoding for any odorant molecule

Olfactory cell is a kind of a nerve cell that can be found about a number of 50 million in humans. An olfactory receptor consists of cilia carrying dendrites and axons that connect directly to CN-1 olfactory nerve. Many of these olfactory receptors constitute the nerve bundles and passes through the cribriform plate and directed to the olfactory bulbs (bulbus olfactoria).

Olfactory receptor cells are known to be a candidate of large subfamily G-Protein [72]. In olfactory mucosa, odorant molecules are captured by means of binding process and transmitted to olfactory receptor, causes fracture of a sub-unit α (see Figure 4). This sub-unit activates the adenylate cyclase and activation of this matter causes convertion of ATP (adenosine triphosphate) to cAMP (cyclic adenosine monophosphate). As a final step, cAMP opens the cyclic nucleotide bodied sodium-potassium channel of the olfactory receptor. Activated olfactory receptor causes a signal running to olfactory bulb in the brain [73]. Thus, transported information by an odor molecule is transferred to neural domain.
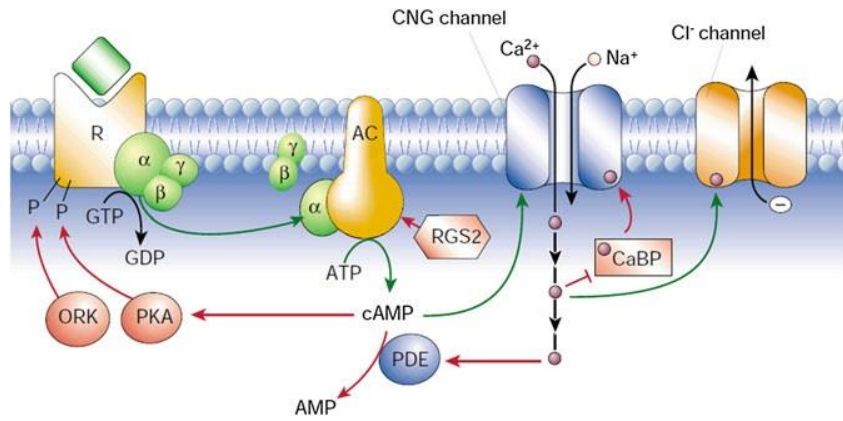
Figure 4. Sensory transduction [74]

2.3.1. Olfactory Pathway

Olfactory receptor neurons are the first neuron of the olfactory pathway that locates within olfactory neuroepithelium (regio olfactoria). These neurons are bipolar type nerve cells. Only one dendrite stem from its apical pole, and then it constitutes an extension region. From that point, 5-20 cilias directed to olfactory mucosa in order for swaying unrestrainedly. Basal pole of the olfactory receptor neuron is directed to the olfactory bulb to transmit the odorant information to higher order brain centers. Axons of these neurons projects synapse with specialized cells of olfactory bulb (OB) by passing through the cribriform plate. Any fracture in cribriform plate due to head trauma causes damage of these nerves which results with complete or partial acquired anosmia.

In the central domain, OB is of great importance in processing of information that comes from periphery. It can be seen in Figure 5 that OB is located in the anterior cranial fossa, above the cribriform plate and under the frontal lobe [75]. Odorant information is encoded in OB. Within the OB, glomerulus has great importance in olfaction. Axons of ORNs are made synapse with glomeruli and also with periglomerular sub-neurons which surround the glomerular layer.

Clustering of many glomeruli produces glomerular sheets. Glomerular sheet is found for 2-dimensional representation of multidimensional odor space [69]. First study was done by Adrian in 1953 that he discovered the spatial representation of odors in the related structures. Also it is believed that first neural processing of odors is handled by glomerular layer. Anatomical and physiological evidences and energy demand of these

activated interconnections shows that glomerulus has a great importance in chemosensory signal processing.

Axons of mitral and tufted cells which are the outputs of olfactory bulbs are coalesced and directed to olfactory cortex by forming the olfactory tract (tractus olfactus) [75].
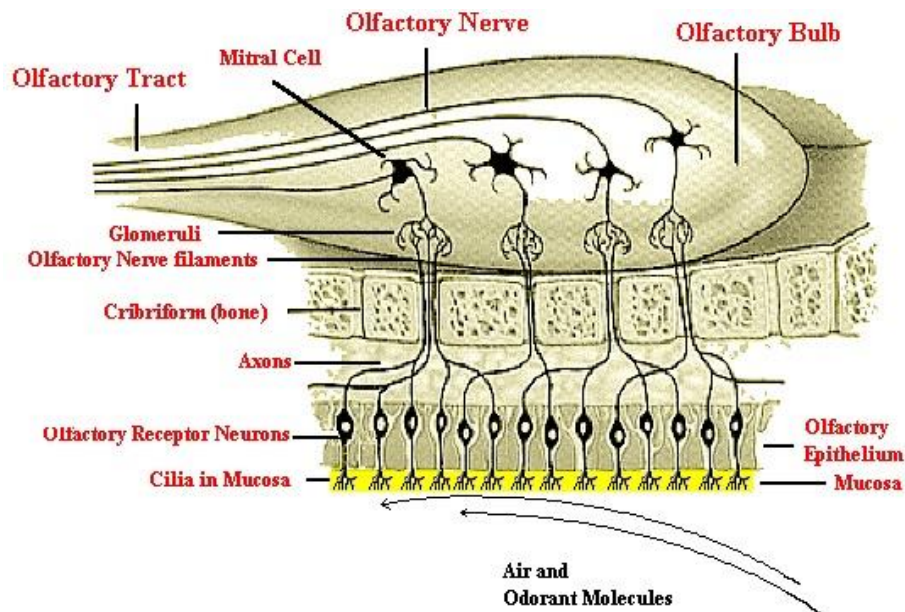
Figure 5. Schematic view of the olfactory regions [76]

From the olfactory cortex, olfactory information is sent by means of mediodorsal nucleus of the thalamus to the insular and orbitofrontal cortex (see Figure 6). Not only olfactory information but also gustatory signals are received to that area. It is a common belief that insular cortex is a special region in brain that meets olfactory and gustatory information together and integration of these signals produces the term 'flavor'.

Medial olfactory region ends in anterior and superior regions of the hypothalamus. This region consists of septum pellicidum, gyrus suballocus, olfactory trigon, medial lobe of anterior perforated substance, lateral lobe of anterior perforated substance, uncus and amygdaloidal nucleus [77].

Fibers which are the outputs of medial and lateral side of olfactory region are directed to the region of hippocampus, hypothalamus and brain stem.

Amygdala is known to be a large nuclear structure which is responsible for,

- Control of emotion
- Control of sexual behavior
- Control of water and food intake

For this sense, amygdala has an important role on olfactory information processing. Pleasantness and unpleasantness of odors are decided in this region [78].
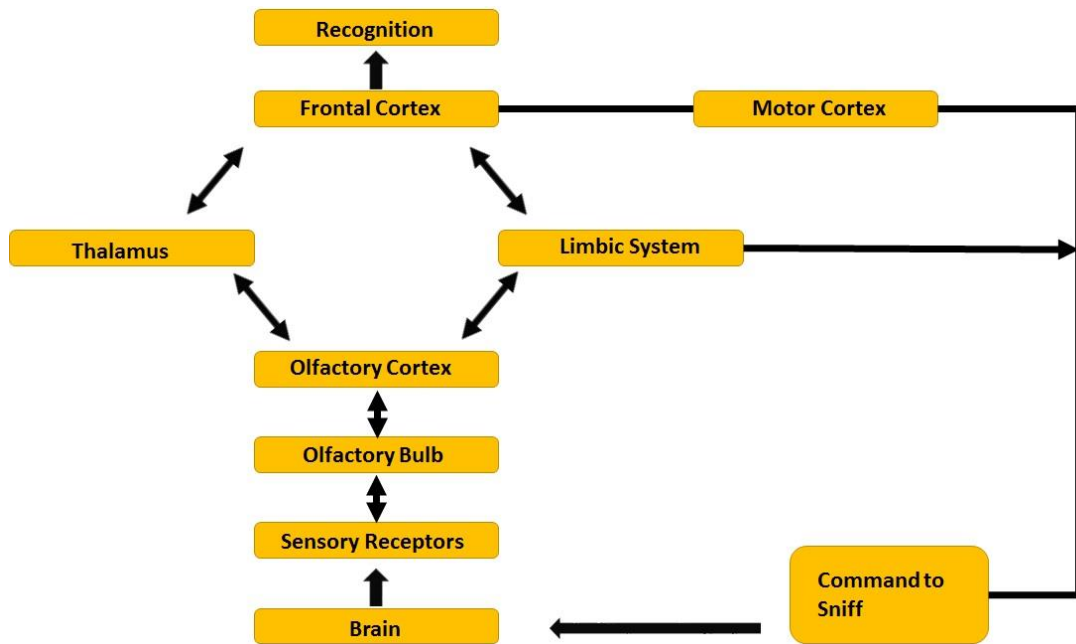
Figure 6. Olfactory Pathway [79]

Plasticity of human olfactory system is still under discussion. Many studies were done with in vivo and in vitro animals that highlight the two main neurogenesis processes. The first type of neurogenesis that occurs in olfactory neuroepithelium that contains proliferating cells. Such cells are capable of reproducing olfactory receptor neurons throughout the life. Second observation of neurogenesis is seen in supraventricular zone (SVZ) of lateral ventricle. Within this area, stem cells causes generation of neuroblasts. These neuroblasts form a chain-like structure and tend to pass away to olfactory bulbs by using migration corridor (RMS). In OB, these neurons are believed to involve in sophisticated functions such as olfactory memory, social interactions [80].

Another rough idea for neurogenesis process is self-plasticity of OB that carries its own progenitor cells. Many MRI studies states the plasticity of OB that volume of OB varies as a function of gender, age and disorders. In [81], authors observed the decline in

24

bulb volume and number of mitral cells with advancing age. More interestingly, some researchers claim that there is a linear relationship between bulbar volume and TDI score of Sniffin' Stick test [75].

2.3.2. Trigeminal Pathway

The term common chemical sense stands for trigeminal sensing system that is specialized for chemical irritant recognition.

The name 'Trigeminal' is the type of nerve that contains three major nerve branches. Ophthalmic nerve (V_1), Maxillary nerve (V_2), Mandibular nerve (V_3).

Trigeminal afferents innervates the nasal cavity with ophthalmic and maxillary branches. There are two major fiber types. The first one is the C-fibers that are stand for sense of burning and the second one is A_{delta}-fibers which are specialized for stinging sensation. It's important to note that, C-fibers and A_{delta}-fibers responses are different for repeated stimuli. For C-fibers, summation of the response could be observed for repeated stimuli whereas no summation occurs for A_{delta}-fibers [73].

Trigeminal information is relayed from caudal solitary tract by lateral parabranchial complex and transmitted to amygdala which is locate within temporal lobe of medial nuclei of hypothalamus.

It is noteworthy that, electrophysiological techniques indicate the anterior third septum is the area that shows an elevated activation during trigeminal chemosensory activation in both nostrils. Projections of the ventral posterior medial nucleus terminated in primary somatosensory cortex which is known to involved pain perception [73].

Repeated stimuli with odors show a reduction in stimulus intensity rating in case of a longer interstimulus interval.

In trigeminal stimulations, shorter ISI causes enhancement of rating of stimulus intensity. This phenomenon is called sensitization. Researches with capsaicin [82] highlights that, ISI with shorter than one minute causes enhanced burning sensation in nostrils.

On the other hand, ISI with larger value causes degradation of intensity of stimulus rating called desensitization. [83] underlines the effect of larger ISI that repeated stimuli with about 3-4 minutes causes desensitization.

2.4. Electronic Nose

An electronic nose is a device that is developed for mimicking the sense of smell of humans. These devices have ability to detect and distinguish odors in a complex environment precisely [84]. As in Figure 7, such systems contain three main part,

- Data acquisition and Signal Conditioning (Sensing Layer)
- Signal Processing and feature extraction (Pattern Recognition)
- Odor Prediction (Decision)
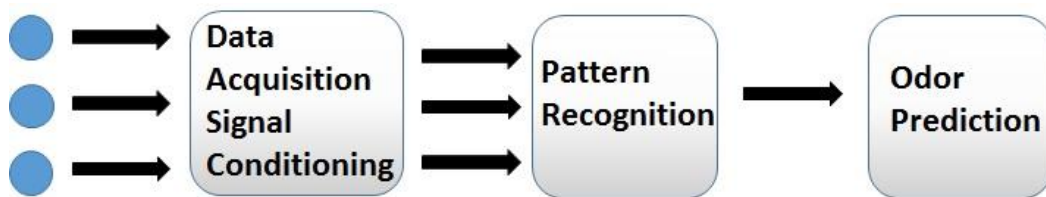
Figure 7. Simple block diagram of E-nose

Electronic noses have wide usage areas.

- Military industry
- Food quality control
- Environmental check
- Chemical analysis
- Medical industry

Inspection of these devices, in the sensing layer, odor information is gathered and sampled via gas sensors and conveyed to signal processing and feature extraction stage. In this stage, dimensionality is reduced and useful information from the signal, which comes from sensing layer, is extracted. Independent component analysis (ICA), Principal component analysis (PCA), Canonical discriminant analysis (CDA) are the most preferred dimensionality reduction techniques in an e-nose structure. In the final stage, a classifier like K-Means Clustering, Support Vector Machine (SVM) and Artificial Neural Network (ANN) is employed for making decision.

Heart of such an electronic nose system is the gas sensor arrays. Sensor array are used to collect the information from environment and convert it to spatial pattern such as conductance, frequency change, voltage, current, resistance, etc… [67]. A typical gas

sensor array contains 6-30 gas sensors. In this structure every gas sensor is covered with different active film layer. There are five types of sensors that are frequently used in e-nose,

- MOS (metal oxide semiconductor) gas sensors
- QCM (Quartz crystal microbalance) gas sensors
- SAW (Surface acoustic wave) gas sensor
- IDT (Inter digital transducer) gas sensors
- Optical Sensors

Among these, MOS and QCM are the famous and mostly used gas sensor types. Metal Oxide gas sensors are made up of tin oxide and or zinc oxide. One of the models that describe the gas reaction mechanism with MOS sensor is Ionosorption model. In this model gas reacts with ionosorbed oxygen. The conductivity of sensitive layer changes when concentration of absorbed oxygen changes. As a result, due to this concentration change, resistance of MOS sensor changes (see Figure 8 and Figure 9) [85].
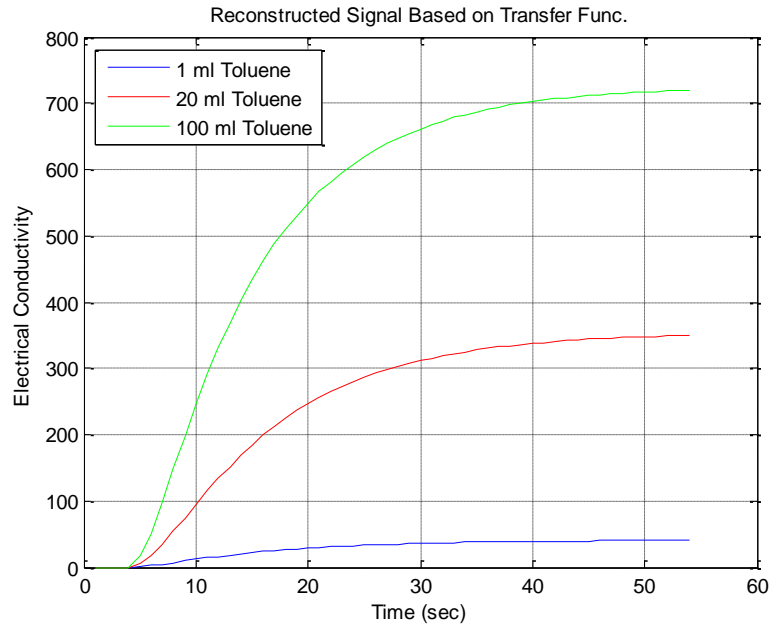
Figure 8. Electrical conductivity of an MOS sensor
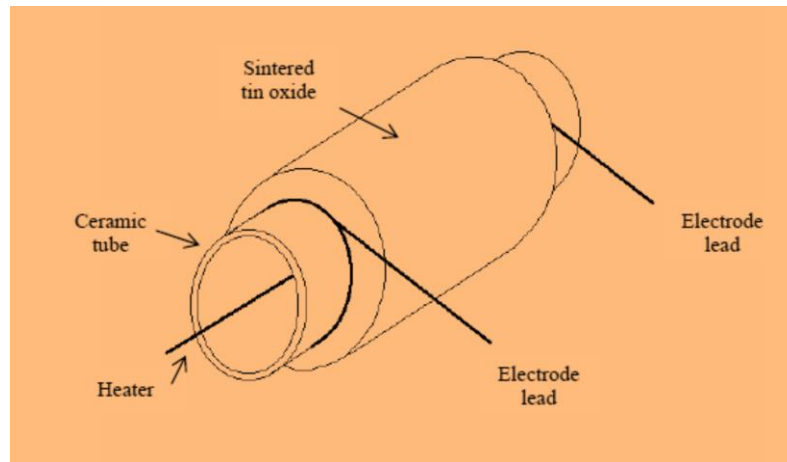
Figure 9. Basic configuration of tin dioxide gas sensor [86]

The working principle of QCM gas sensors are based on change on oscillating frequency with exposure of active layer to odorant molecules like in Figure 10,

$$\Delta f = \frac{C_f \, f_0^2}{A} \Delta m \qquad (2.4)$$

where C_f is the mass sensitivity constant, f_0 is the fundamental oscillation frequency, A is the area of active layer and Δm is the mass change on active layer.
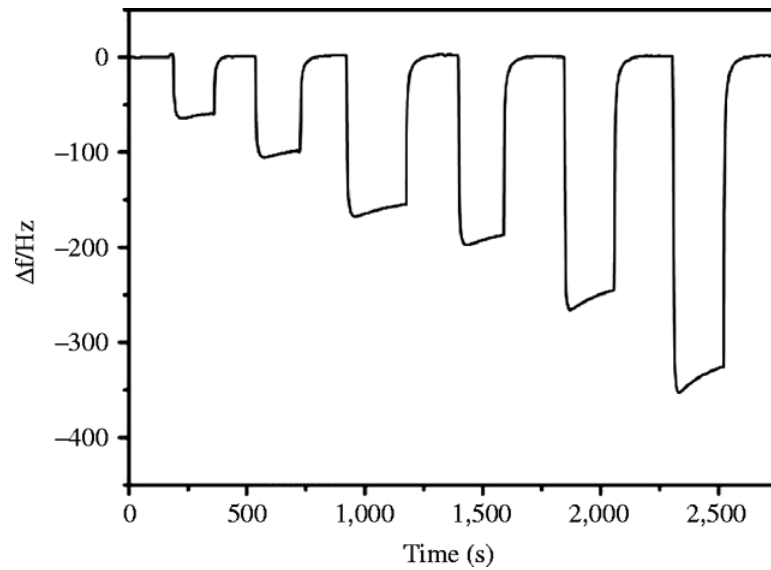
Figure 10. Frequency change with time due to gas exposure [87]

There are some challenges for sensor arrays. First one is about measurements speed of the sensors, which lasts about 80-100 seconds to reach steady-state. Second problem is about robustness of the sensors. In an e-nose system, sensors should be robust to the noise, humidity and temperature change. Life time, recovery time, sensor poisoning, drifting are more or less important drawbacks that might be confront of researchers.

2.4.1. E-Nose in Literature

Since 1982 Persaud and Dodd came with an idea that odor sensing technology with a pattern recognition algorithm and e-nose prototype in Warwick University Olfaction Research Group in 1987 had been pioneering, there are various studies can be found. In [88], instead of time domain representation, a new representation space was demonstrated called *Similarity Space.* In that space, odor samples were represented by a similarity measure between them.

Nimsuk & Nakamoto employed short-time Fourier transform and stepwise discriminant analysis for feature extraction [89]. As a classifier, Learning Vector Quantization (LVQ) was used in this study. Robustness of this algorithm was in satisfying level though the odorant concentration was changing with time.

In [90], classifier which is called *Inhibitory Support Vector Machine* that is inspired from animal's neural system was utilized to overcome varying temperature wind

speed, concentration and measurement distance. Odor classification results showed that temperature and measurement distance were the major factors that affect the classification performance.

As mentioned above, humidity is a significant external factor that causes performance degradation for odor sensation for e-noses. Study [91] comprises a compensation technique by using artificial neural network without any humidity monitoring system or any compensation module. As feature dimension reduction, Principal Component Analysis and as a classifier Feed-Forward neural network was used. By using ANN, classification error due to humidity is reduced to levels of %1.15.

Noise is always known to be a performance degrader factor in a system. But in non-linear systems, noise can enhance information transmission, detection performance or system response. In [92], the phenomenon Stochastic Resonance was utilized to recognize bacteria types which causes infectious disease. Single threshold device was inserted to obtain a cross correlation between bacteria classes.

Study [93] utilized orthogonal discrete wavelet transform and Support Vector Regression to predict odor mixture responses. Odor recorder is a device that blends two or more fragrance at a desired level. Performance of the system was measured by closeness of estimated and real sensory responses.

In [94], it is demonstrated that outliers are the kind of source that causes classification error such as drift effect of sensors. Ekachai Phaisangittisagul proposed an algorithm that rejects the outliers by discarding the responses that lies outside of the maximum and minimum threshold value. After the exclusion, classification performance of system increased significantly.

One of the most industries that employ e-nose is the food industry. In recent years, observation of quality of foods, drinks, beverages is done by e-nose. In the recent past, quality of wines has been scored by experts. Acevedo et.al. studied on classification of wines in the sense of their qualities [95]. As a classifier, Probabilistic Support Vector Machine (PSVM) was used.

Classification speed of an e-nose system is another challenging problem. Exponential moving average, which is borrowed from economics discipline, helps to extract transient features from sensor response to reduce classification time. Extraction of different features by changing the parameter α displays that, transient features carries more useful information than steady-state features [96].

In [97], an electronic nose is mounted on a mobile robot. Aim of this study is to identify odors in a turbulent condition from their transient sensory responses. Attenuation of noise effect is achieved by three type of manipulation. These are differential, relative and fractional manipulations. Features are obtained by using DFT, DWT and curve fitting approximation. After the normalization of features, Relevance Vector Machine (RVM) is employed as a decision part. In comparison with SVM, RVM gives slightly lower classification scores.

In order to reduce the required time for classification, Phaisangittisagul applied DWT to obtain transient features. As feature extractor, Haar, Daubechies, Biorthogonal wavelets were employed. Extracted features were conveyed to the K-means Clustering, Radial Basis Function Network and Back Propagation Neural Network. 5th order Daubechies wavelet gives the best classification result for all classifiers [98].

In [99], feature extraction with short-time Fourier transform is adopted. STFT is applied to all sensor signals to obtain Fourier spectra with high temporal and spatial resolution. Energy, up to 2 Hz is summed and is divided all other sensor energies. These extracted features are conveyed both SVM and Maximum Likelihood Estimation.

2.4.2. CNN based E-nose

The paradigm Cellular Neural Network (CNN) was firstly introduced by Chua and Yang in 1988 [100]. CNN realizes a network that accommodate locally interconnected analog processors, which can be realized with linear and nonlinear circuit elements such as capacitors, resistors, linear and nonlinear controlled sources and independent sources, to perform parallel processing and given computational tasks in real time. Any cell in CNN can be considered as multi-input single output nonlinear subsystem and also it fair to say that each cell communicate each other directly or indirectly. An illustration of a two dimensional cellular neural network is given in Figure 11.

In an MxN CNN structure, any cell denoted by $C_{i,j}$ where $i \in \{1,2,...,M\}$ and $j \in \{1,2,...,N\}$ is a part of the structure and it is locally interconnected to neighbor cells which lies within sphere of influence which is denoted by $S_i(r)$ of radius r [101].

$$S_{i,j}(r) = \{C_{i,j} : \max(|k - i|, |l - j|) \leq r \quad 1 \leq k \leq M; 1 \leq l \leq N \ k \neq i, l \neq j\} \tag{2.5}$$
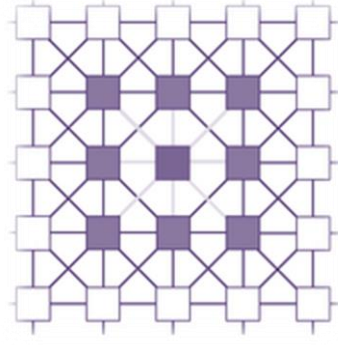
Figure 11. A demonstration of 2-D CNN

where r is a positive integer. In Figure 12, demonstration of a single cell (neuron) with circuit elements is given. Applying Kirchhoff's voltage and current laws, we will obtain the following dynamic representation of the cell. State of a single processor $C_{i,j}$ can be obtained as,

$$
\begin{aligned}
C \frac{dv_{Xi,j}(t)}{dt} = &-\frac{1}{R_x} v_{Xi,j}(t) + \sum_{C(k,l) \in S_{i,j}(r)} A(i,j;k,l)\, v_{Yk,l}(t) \\
&+ \sum_{C(k,l) \in S_{i,j}(r)} B(i,j;k,l)\, v_{Uk,l}(t) + I
\end{aligned}
\tag{2.6}
$$

where $v_{Xi,j}$ demonstrates the state of the corresponding cell $C_{i,j}$, I is the independent current source connected to that cell. In that circuit, input of the cell $v_{Ui,j}$ is modeled as independent voltage source $E_{i,j}$ and output $v_{Yi,j}(t)$ is equal to a output of piece-wise linear function of state of the cell,

$$
v_{Yi,j}(t) = \frac{1}{2} \left(|v_{Xi,j}(t) + 1| - |v_{Xi,j}(t) - 1| \right)
\tag{2.7}
$$

It can be easily seen in given equations, the network dynamics holds both output feedback and input control mechanism.
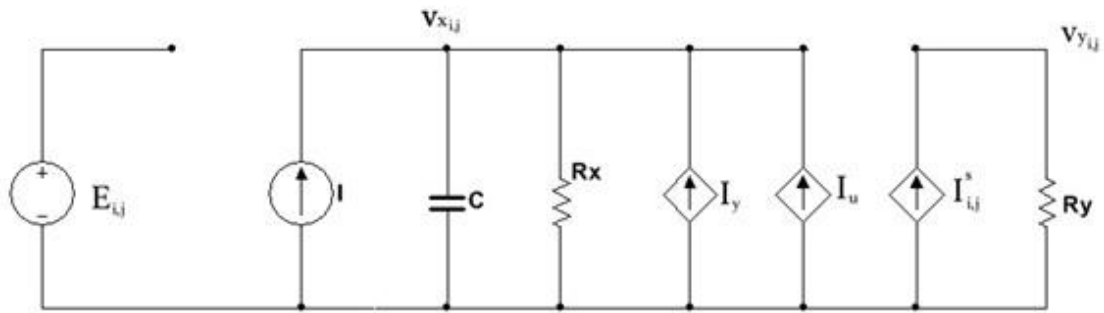
Figure 12. Circuit implementation of one single cell in CNN

Cellular Neural Network (CNN) based artificial olfactory system studies aims to mimic the olfaction system of Drosophila's and vertebrates. However, unlike the regularity of CNN biological information processing structure antennal lobe in insects and olfactory bulb in mammals contains some random connections between their neurons. This reality can be observed in many other biological systems. This phenomenon is called 'Small World'.

The term 'Small-world' was came up in 1960's. But there were no idea about whether it could be applicable to networks. Wattz and Strogatz were the first people that they adapted the Small-world phenomenon to wide variety networks [67].

Briefly, in networks, small world phenomenon ruins the regularity of connection template in network by inserting random connection between cells which are not in their neighborhood.

Like other electronic nose models found in literature, e-nose systems with CNN also consists of three major parts such as,

1. Sensing layer
2. Feature extraction
3. Decision and classification

In studies [67, 102], Cellular Neural Network, which was inspired from the structure of human retina, was employed to extract the relevant features to reach satisfactory classification rates which was used in [71]. Anticipated advantage of using CNN is to speed up the classification progress with utilizing transient features of sensor array responses.

By looking under the hood, inspired from studies on Drosophila's antennal lobe, CNN behaves as an artificial antennal lobe in those studies.

There are 2 kinds of neuronal population is found in CNN based antennal lobe model. The first one is called excitatory cell population and second one is called inhibitory cell population. These excitatory and inhibitory cell populations are inspired from Wilson-Cowan population model. Mathematical description of both one layer and two layer structure can display the dynamics of CNN structure.

One-dimensional neural population model is given for excitatory population as,

$$\beta \frac{dx_{i,j}(t)}{dt} = K\Theta\left(-\sum_{l=-r}^{r}\sum_{k=-r}^{r} A_{k,l}\, C_{i+k,j+l}(t) + g_{i,j}S_{i,j}\right) - x_{i,j}(t) + \mu_{i,j} \qquad (2.8)$$

In above equation $x_{i,j}$ stands for an excitatory processor in one layer network located in i^{th} row, j^{th} column. A is the matrix that demonstrates the connection template with radius r. Template A with r=1 can be demonstrated as follows,

$$A = \begin{bmatrix} A_{-1,-1} & A_{-1,0} & A_{-1,1} \\ A_{0,-1} & A_{0,0} & A_{0,1} \\ A_{1,-1} & A_{1,0} & A_{1,1} \end{bmatrix} \qquad (2.9)$$

and for the inhibitory population is given as,

$$\beta \frac{dy_{i,j}(t)}{dt} = K\Theta\left(-\sum_{l=-r}^{r}\sum_{k=-r}^{r} A_{k,l}\, C_{i+k,j+l}(t) + g_{i,j}S_{i,j}\right) - y_{i,j}(t) + \mu_{i,j}(t) \qquad (2.10)$$

In equations (2.8) and (2.10), $C_{i+k,j+l}$ represents the inhibitory cells and excitatory cells respectively. If neighboring cells are same with considered cell, there is no connections available, which means that $A_{k,l} = 0$. Connection weights between cell and sensor were demonstrated with $g_{i,j}$ and $S_{i,j}$ represented the sensory inputs to considered cell and $\mu_{i,j}$ is the additive zero mean white noise with variance 0.5, Θ is defined as unit ramp function. For the two layer network, population models are given in eq. (2.11) for excitatory and, for inhibitory in eq. (2.12).

$$\beta_{i,j}^{E} \frac{dx_{i,j}(t)}{dt} = K_{i,j}\Theta\left(-\sum_{k=-r}^{r}\sum_{l=-r}^{r} \hat{A}_{k,l}\, y_{i+k,j+l}(t) + g_{inp}S_{i,j}\right) \qquad (2.11)$$
$$- x_{i,j}(t) + \mu_{i,j}(t)$$

$$\beta_{i,j}^{I} \frac{dy_{i,j}(t)}{dt} = K_{i,j}\Theta\left(\sum_{k=-r}^{r}\sum_{l=-r}^{r} \hat{A}_{k,l}\, x_{i+k,j+l}(t) + g_{inp}S_{i,j}\right) - y_{i,j}(t) \qquad (2.12)$$
$$+ \mu_{i,j}(t)$$

where $x_{i,j}(t)$ and $y_{i,j}(t)$ stands for state of a neuron at time t located at ith row and jth column of excitatory and inhibitory neural populations, β and K are the denoted as time constant and gain respectively. Again, $\hat{A}_{k,l}$ is the connection template. As in one layer structure, connection of two neurons in the same population was not allowed.

In that thesis, they aimed to achieve better classification performance with transient response of sensor array by utilizing CNN based model than other proposed e-nose models in literature.

For sensing array, sixteen metal oxide gas sensors was used and, for decision part, public available LibSVM (A library for Support Vector Machines) and PCA (Principal Component Analysis) was employed.

Test of proposed models comprises two sections. The first part involves three kinds of gaseous such as pure toluene, pure acetaldehyde and mixture of them with different concentrations. Performance of one-layer and two-layer CNN models are tested. As a classifier PCA [103] and SVM [104] was adopted. Feature vectors are created in a way that all the neurons which belongs to excitatory population are saving in a vector for every time instant (i.e. $t = 1,2,3, ...$). Then all the feature vectors are conveyed to PCA. For the PCA analysis, results shows that classes become separable nearly at $t = 25$. In Figure 13, results of the both one layer and two layer CNN model can be seen at $t = 100$. It can be inferred that, two layer CNN is more successful at discrimination of the classes than one layered structure.
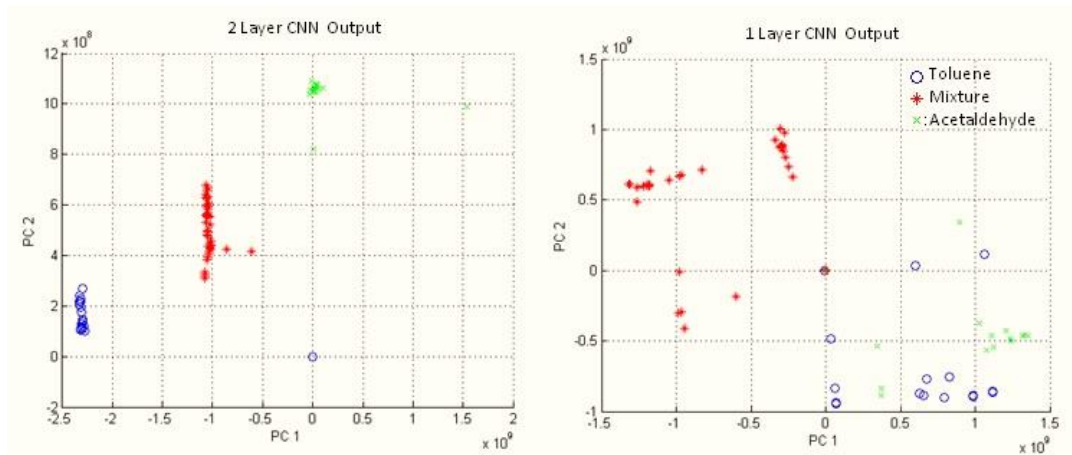
Figure 13. Results with 1-Layer and 2-Layer CNN [67]

As a second part of first session, SVM is employed for classification of the output of the excitatory processors for each feature vector that was obtained from time instants of the excitatory cells again. Totally 80 feature vectors are labeled were used for every odorant classes. For the training of the SVM, linear kernel and LOOCV (leave one out cross validation) technique was preferred. For each classes, one individual sample is used for testing and remaining 79 samples are used in training in memoryless case (see Figure 14).
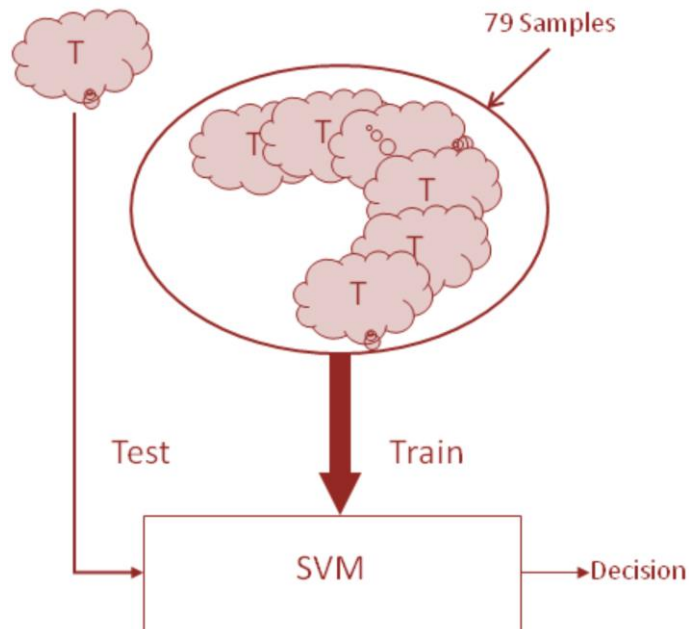
Figure 14. Schematic demonstration of SVM with individual samples [67]

Performance calculation of the classification is formulated as follows,

$$\%Perf = 100 \ x \ \frac{\# \ success}{20} \% \qquad\qquad (2.13)$$

and in case of system with memory, whole time vectors (snapshots) were taken into consideration. Captured time vectors from $t = 0$ to $t = T - 1$ were conveyed to training and, vector captured at $t = T$ was used for classification test.
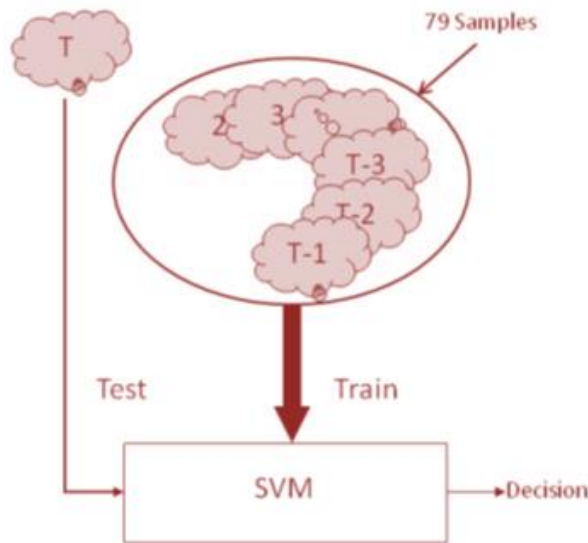
Figure 15. Schematic view of SVM in case of with memory [67]

Results shows that, classification performance of system with memory which is demonstrated in Figure 15, reaches higher classification rates than memoryless case. And it's notably that, in early responses of the sensor array, as in memoryless case, two layer CNN model gives higher classification rates that is nearly %80.

Small-world CNN model was tested in second session. They aimed to observe the effects of random connections on the performance of classification. For that purpose, 4x4 two layer SWCNN model with r=1 was built. In this part, dataset was comprised of 5 different gaseous namely acetone, butane, ethylene, ethane and acetaldehyde. For each scent, fifteen successful measurements were recorded.
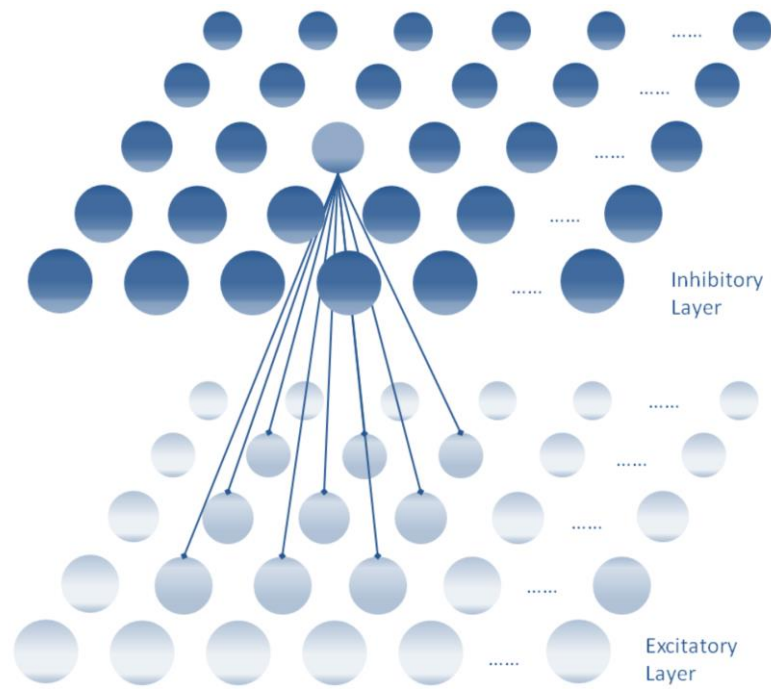
Figure 16. 2-Layer CNN with both inhibitory and excitatory layer [102]

In this session, only SVM was used to see success rate of classification of the SWCNN model. Random connections were created randomly between cells that they are not within their neighborhood r. A number p is defined as number of neurons that makes random connection among whole neural population in both excitatory and inhibitory layer. Starting from $p = 0$, analysis was done with increasing the number p by one in every step to see the effect of number of random connections on classification performance. By looking at Figure 16, CNN was built with pure regular connections ($p = 0$), performance rate increases up to %80 (see Figure 17).
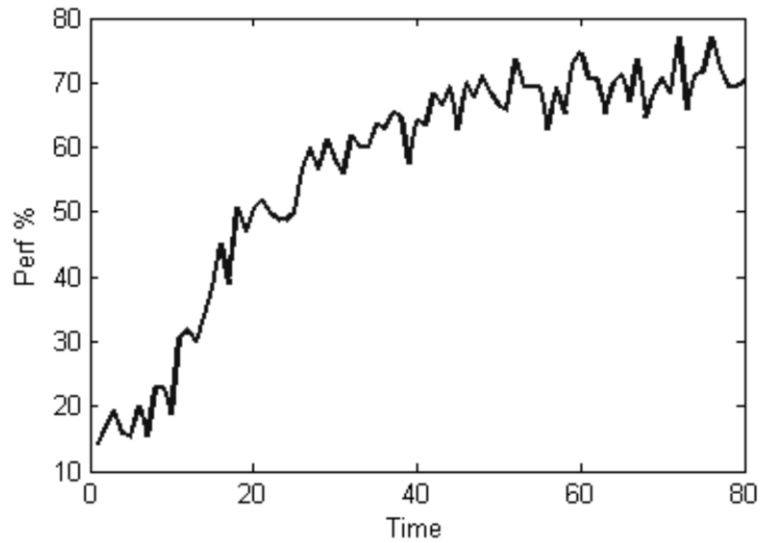
Figure 17. Performance of 2-Layer CNN with regular connections [102]

In Figure 18, it can be seen that, increasing the number of irregular (random) connections (p=1, 2, 3 …) gives at a rate of %85-90 classification performance which is slightly higher than regular connected CNN model.
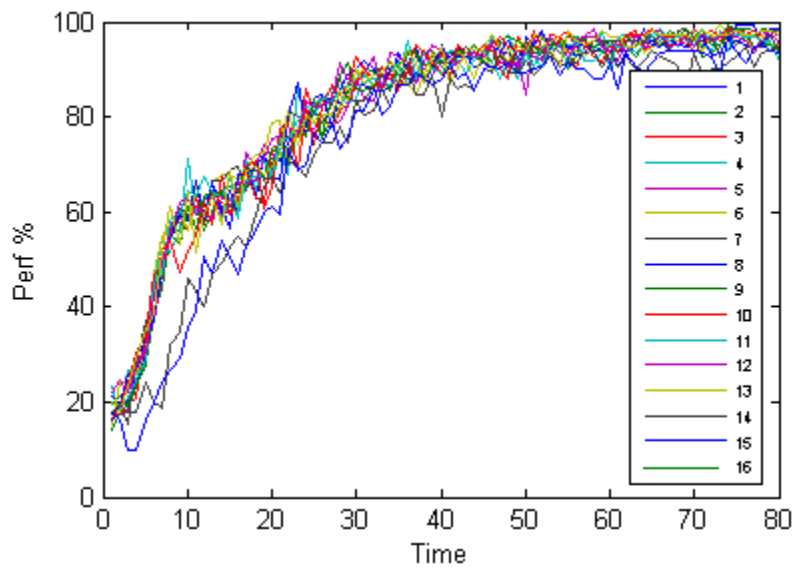
Figure 18. Performance of 2-Layer SWCNN with random connections as increasing number p [67]

It was briefly discussed by the authors, usage of two layer SWCNN increases the classification performance but this elevation does not reach the significant level in

comparison with regular model. However, fault tolerance of SWCNN is much better than regular two layer CNN.

2.5. EEG and Brain Rhythms

EEG is said to be the measurement of voltage fluctuations of neuronal ensembles. This voltage fluctuation is mainly caused by synchronized firing of large number of neurons and also, due to synaptic current passes through in different pyramidal neurons locates in cerebral cortex. This oscillatory activity is the indicator of the functional and physiological changes in the brain with high temporal resolution. It is stated that the first EEG measurement was done by simple galvanometer by Richard Caton in 1875. Discovery of human EEG was achieved by Hans Berger in 1929. Toennies (1902-1970) was the inventor of the first biological amplifier in 1932. After that, the first differential amplifier was developed by the help of Rockefeller foundation.

EEG signals contain many different frequency tones up to 300 hertz and order of microvolt but informative oscillations are restricted up to 100 hertz. But many recent study have found many high frequency informative oscillations between neuronal structures [105].

In computerized measurement system, received oscillations are passed to analog-digital converter (ADC). In such a system, EEG signals are digitalized with a sampling frequency up to 10000 samples/second. However, in most clinics 1000 sample/sec is preferred. After the digitalizing process, signal is conveyed to a bandpass filter with low cut-off frequency 0.5 Hz and 50-70 Hz high cut-off frequency to reject artifacts like motor artifacts, eye movements, electrocardiographic oscillations (ECG), chest movement due to breathing cycle, sweating. Additionally, a 50/60 Hz Notch filter is employed to discard the bus-bar (power-line) effect.

In general, EEG measurement is done by multiple electrodes by placing each of them on the different sides of scalp called multichannel EEG recording. The aim of the multichannel measurement is to detect the correlation (cross-frequency phase synchronization and cross-frequency amplitude envelope correlation) between distal cortical regions during different conditions such as ERP/EP.

With the development of multichannel EEG hardware recording systems many topographic and tomographic signal source localization methods have been raised. The

most used electrode positioning system is International 10-20 positioning system shown in Figure 20 [106].

Measurement of EEG is achieved by two types of recording namely differential and referential. In differential mode, two inputs are selected and conveyed directly to differential amplifier. However in referential mode, at least one reference electrode is selected. In 10-20 positioning system, most used reference electrodes are vertex Cz, link earls, link mastoids, ipsilateral ear and C7.

The 10-10 international positioning system with 64 electrodes is shown in Figure 19. It was first proposed by Chandrian in 1985, is an extended version of international 10-20 with more electrode density.

Figure 19 . International 10-10 positioning system
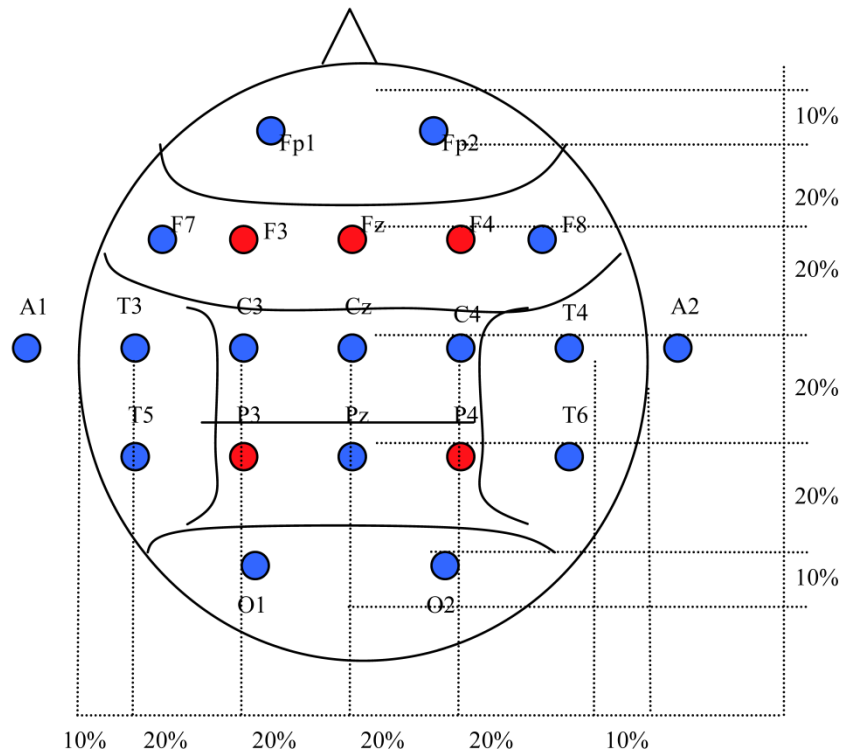
Figure 20. 10-20 positioning system with 21 electrode [107]

As described in many studies, EEG consists of five major oscillatory frequencies as given in Table 2. These are;

- Delta (0.5-4 Hz)
- Theta (4-8 Hz)
- Alpha (8-13 Hz)
- Beta (13-32 Hz)
- Gamma (32-100 Hz)

Delta (δ) oscillations can be seen while deep sleep and state of anesthesia. They are the slowest oscillations but their amplitude is the highest when compared with other frequency bands. In comparison with males, females demonstrate higher amplitude delta waves. According to [4], delta waves are enhanced while in oddball paradigm.

A range of 4-8 Hertz signals belongs to theta (Ɵ) band. It is stated in [108] that theta waves are bearded vital roles in childhood and infancy. Larger amplitudes of theta waves are the indication of abnormalities.

We can observe the alpha (α) oscillations in the posterior half of head and occipital region of the brain. Researches demonstrate that alpha oscillations are in strong correlation with memory and long-term memory engrams. Sinusoidal shape signals in

visual cortex neurons demonstrate a strong correlation with alpha band oscillatory activities. Results of observation in [4] demonstrates that alpha wave oscillations provides functional and communicative interaction between distant structures. Alpha oscillations show a reduction while eyes are open, sleepiness and deep sleep.

Frequency between 13-32 Hertz oscillations are related as beta (β) wave oscillations. Beta waves are known to be the waking oscillations such as thinking attention and focus.

Gamma waves can be found in a range of 32-100 Hertz. Gamma wave sources are localized in fronto-central region of brain. According to Erol Basar [109], gamma responses are vital for building blocks of electrical activity of brain which is related to multiple functions. Gamma waves create interaction between distant structures and shows phase-locking, time-locking or weak time locking. In accordance with [4], gamma oscillations show a universal communication code in central nervous system.

Table 2. The Brain Rhythms and their Specifications

Wave Name	Frequency Range	Source Location
Delta (δ)	Up to 4 Hz.	Frontally in adults posterior in children
Theta (Θ)	4-8 Hz.	Founds in location not related to task at hand
Alpha (α)	8-13 Hz.	Posterior region of head, central sides (C3,C4) at rest
Beta (β)	13-32 Hz.	Both side, symmetrical distribution
Gamma (γ)	32-100 Hz.	Somatosensory cortex

2.5.1. Evoked Potentials and Event-Related Potentials

Evoked potentials are electrical response of central nervous system to external stimuli. This stimulus can be in modality of somatosensory, auditory, gustatory, visual or olfactory. They are defined as EEG-derived polyphasic signals that can be used in diagnosis of wide variety of neurological diseases. They provide stable monitorization of sensory system, peripheral and central nervous system functioning in clinical context. It can also help to define anatomic distribution of disease and deficiency status over time [110].

Event-related potentials are said to be the electrophysiological response of brain to time- locked to sensory, motor or cognitive events. This electrical activity occurs within a large number of pyramidal cortical neurons that they are oriented similarly. Also, nearly all endogenous or exogenous stimulations creates such an activity in brain, few of them can be detected through the skull. ERP are needed to satisfy some criterions to be detectable [111],

- Stimulation must fire enough number of cortical neurons and these cortical neurons have to elicit relatively strong electrical field.
- Activated neurons must oscillate in coherent way. If not, the response will be diluted over time and potential becomes undetectable.
- Arrangement of activated neuronal assemblies must be an open-filed structure. Unless, the net field at the outside of the structure will be zero.
- Because of the fact that skull interface acts as low-pass filter, ERP must consist of low frequency components.

Common approach for demonstration of ERP and EP components is the usage of polarity and latency value such as P300, N200. In this demonstration type 'P', or 'N' displays the polarity is positive of negative. Numbers 200, 300 appearance time in milliseconds after the stimulus onset. Another demonstration type is uses first argument like P or N but it uses the sequence number like N1, P1 and P2. For chemosensory evoked potentials, the occurrence time and order of the peaks is given as follows,

- The first positive peak P1 which is generally not seen, occurs at 200-310ms.
- N1 peak is the first negative peak, occurs at 320-450ms.
- Second positive peak P2 is seen at time interval of 530-800ms.

Occurrence of these peaks is inferred as the results of chemosensory information processing in the pyramidal cortical neurons. The main reason of such a lagging in comparison with other modalities is described as the sensory transduction (i.e. utilization time of receptors) and also might be a reason of complex olfactory information processing in brain. In Figure 21, illustration of evoked potentials is given.
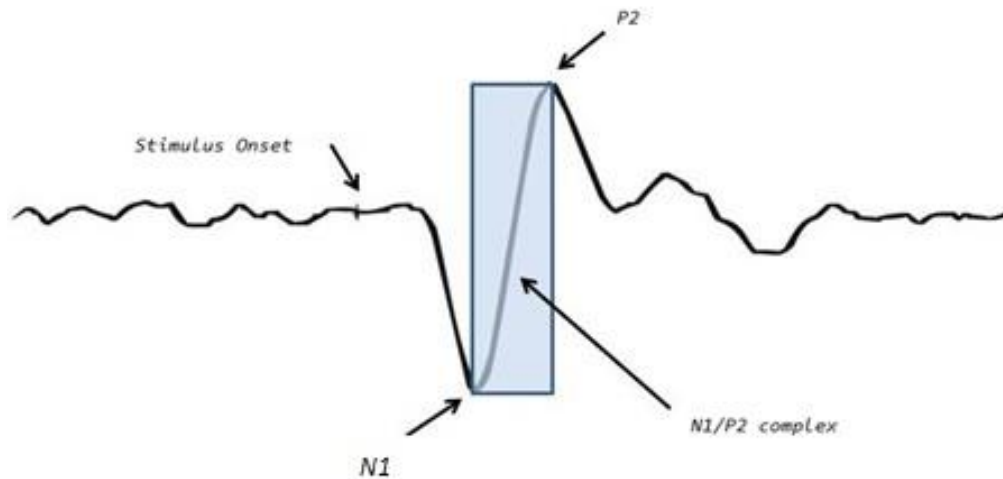
Figure 21. Demonstration of evoked potentials

Chemosensory evoked and event-related potentials are also the brain responses to odorant stimulation giving them into the subject's nostrils. In many clinical studies, H_2S (hydrogen sulfide), PEA (phenyl ethyl alcohol) are the most preferred odorants for excitation of olfactory receptor cells and CO_2, which is known to be a pure trigeminal activator stimulant.

CSEP/CSERP shows itself on all over the scalp. However, they demonstrate itself clearly at the Cz channel which is located on the vertex with the highest amplitudes and minimum latencies [112].

Characteristics of OERP can be affected by many factors. The main external factors are [112],

- Stimulus Intensity [113]
- Stimulus duration [110]
- Airflow
- Quality of odor [78]
- Inter-stimulus interval [37].

The internal factors can be sorted as,

- Subjects' age [29]

- Gender [32]

- Vigilance [45]

- Hormonal cycle

- Pregnancy [36]

- Etc.

2.5.2. Obtaining CSEP in Clinical Context

The data which we have used in this thesis, were acquired from Dokuz Eylul University Brain Biophysics Lab. Om2b (Burghart, Germany) was used as olfactometer. In Figure 22, picture of Om2b olfactometer has been given. This olfactometer has two outputs. One output carries the humidified air with odorant molecules and the other output just carries humidified clean air. This olfactometer has ability to switch from non-odorous air to odorant air in just 20ms. In this system, it is possible to obtain stimuli with different odorant concentrations. Humidity and temperature of the air which is sent to the subject's nostrils are maintained at constant rates so that humidity is about %80 and temperature stabilized to 36ºC to avoid nasal pungency. Airflow is adjusted to 8 liter/min as in [112]. Odors are applied to subject's nostril by means of a Teflon tube with a vacuum line. Vacuum line is preferred to prevent the formation of mechanical vibration on trigeminal nerves.

Figure 22. Om2b-computer controlled olfactometer

In this study, 2 different types of odorants were used. For olfactory stimulations phenyl ethyl alcohol (PEA) is known to be a pure olfactory stimulator and CO_2 is used for trigeminal stimulations. Interstimulus interval has been selected randomly between 15-17 seconds.

Figure 23. Dokuz Eylul University Brain Biophysics lab.

EEG signals are collected by using 10-10 International positioning system with 64 electrodes. But, for the further analysis, CZ channel has been utilized. In order to mask the switching clicks of olfactometer from non-odorous step to odorant step, or vice versa, 60 dB white noise is binaurally given to headphones to subject's ears.

EEG measurements are digitalized at 1 kHz sampling frequency and filtered with a bandpass filter with low cutoff frequency 0.5 Hz and high cutoff frequency 48 Hz. Additionally, 50 Hz Notch filter has been applied to attenuate the power line effects in recordings. EEG epochs are started from -1000ms before stimulus and lasts until 2000ms after stimulus.

Electro ocular activity was recorded by placing electrodes at outer canthus of left and right eye. Trials, in which ocular activity which exceeds 50μV, were discarded.

CHAPTER 3

TIME-FREQUENCY ANALYSIS

3.1. Fourier Transform

There are many different ways to analyze certain characteristics of the signals. Frequency analysis is the most powerful technique that can represent or characterize the signal by its frequency content.

Fourier transform is a popular technique for analysis of frequency content of given signal $x(t)$ by utilizing correlation with sine and cosine function together with specified oscillating frequencies. It was first described by Jean Baptiste Fourier (1768-1830);

$$X(\omega) = \int_{-\infty}^{\infty} x(t) e^{-j\omega t} \, dt \tag{3.1}$$

$$x(t) = \frac{1}{2\pi} \int_{-\infty}^{\infty} X(\omega) e^{j\omega t} \, d\omega \tag{3.2}$$

Equation (3.1) is the analysis and equation (3.2) is the synthesis equations. In above equation, the term 'ω' denotes the angular frequency.

Discretized version of the Fourier transform for an N-sample discrete signal $x[n] = (x_0, x_1, \dots, x_{N-1})$ is given as,

$$X[k] = \sum_{n=0}^{N-1} x[n] \, e^{-j2\pi kn/N} \tag{3.3}$$

where k=0, 1… N-1 and the inverse discrete Fourier transform is defined as,

$$x[n] = \frac{1}{N} \sum_{k=0}^{N-1} X[k] \, e^{j2\pi kn/N} \tag{3.4}$$

And also, discrete frequencies can be obtained as,

$$f_k = \frac{k}{N\,\Delta}$$

(3.5)

where N is the total number of samples and Δ is the sampling period. It is important to highlight that, maximum detectable frequency f_N is called Nyquist frequency which is the half of the sampling frequency f_s and the relationship is given as follows,

$$f_s \geq 2f_N$$

(3.6)

3.2. Short-Time Fourier Transform

Short-time Fourier Transform is a method to observe the time evolution of frequency content. It was introduced by Gabor in 1946. His aim was to divide the signal into pieces with means of a sliding window and taking the Fourier transform of each signal which falls within that window. Representation of short time Fourier Transform of function $f(t)$ is defined as follows,

$$S_f(u,\xi) = \langle f, g_{u,\xi} \rangle = \int_{-\infty}^{\infty} f(t)\,\overline{g(t-u)\,e^{j\xi t}}\,dt$$

(3.7)

Where the window $g \in \mathcal{L}^2(\mathbb{R})$ is real and symmetric and $\|g\| = 1$ also $\|g_{u,\xi}\| = 1$. $\overline{s}$ denotes the complex conjugate of the s. Different types of window can be used in this transform. The most popular windows are given in Table 3.

Table 3. Different types of window functions [114, 115]

Name	g(t)	Δω
Hamming	0.54+0.46cos(2πt)	1.36
Hanning	$cos^2(\pi t)$	1.44
Blackman	0.42+0.5cos(2πt) + 0.08cos(4πt)	1.68
Rectangle	1	0.89

where $\Delta\omega$ is the frequency radius of the corresponding function (see eq. (3.13)).

Gabor transform is a special case for Short-time Fourier transform that window function g_α is selected as Gaussian [116],

$$g_\alpha(t) = \frac{1}{2\sqrt{\pi\alpha}} \, e^{\frac{-t^2}{4\alpha}}$$
(3.8)

And also, Spectrogram is defined as the squared magnitude of the windowed Fourier transform of signal $x(t)$,

$$|S_x(u,\xi)|^2 = \left| \int_{-\infty}^{\infty} x(t) \, g(t-u) \, e^{-j\xi t} \, dt \right|^2$$
(3.9)

Its graphical interpretation in time-frequency plane demonstrates the evolution of energy localization.

The window localized at the time instant u_γ ,

$$u_\gamma = \int_{-\infty}^{\infty} t \left| g_{u,\xi}(t) \right|^2 \, dt$$
(3.10)

Spread around time instant u_γ is,

$$\Delta t = {\sigma_t}^2 = \int_{-\infty}^{\infty} \left(t - u_\xi \right)^2 \left| g_{u,\xi}(t) \right|^2 \, dt$$
(3.11)

Window localized at the frequency ξ_γ is given as,

$$\xi_\gamma = \frac{1}{2\pi} \int_{-\infty}^{\infty} \omega \left| \hat{g}_{u,\xi}(\omega) \right|^2 \, d\omega$$
(3.12)

Spread around frequency is given as σ_ω^2 in equation (3.13),

$$\Delta\omega = \sigma_\omega^2 = \frac{1}{2\pi}\int_{-\infty}^{\infty} (\omega - \xi_\gamma)^2 \left|\hat{g}_{u,\xi}(\omega)\right|^2 d\omega \qquad (3.13)$$

Where $\hat{g}_{u,\xi}(w) = \hat{g}(\omega - \xi)\, e^{(-ju(\omega-\xi))}$. With the help of the parameters Δt and $\Delta\omega$, the area of the window can be found easily,

$$area = 2\Delta t\; 2\Delta\omega = 4\Delta t\Delta\omega \qquad (3.14)$$

According to the Heisenberg uncertainty principle the area of the time-frequency window must be greater than 0.5 in which the relation is given in equation (3.15) as,

$$\Delta t\Delta\omega \geq \frac{1}{2} \qquad (3.15)$$

For the Gabor transform, this time-frequency window area is,

$$\Delta t\Delta\omega = \frac{1}{2} \qquad (3.16)$$

For the short-time Fourier transform, it is discussed in [115] the area of the time-frequency windows unchanged as in Figure 24.
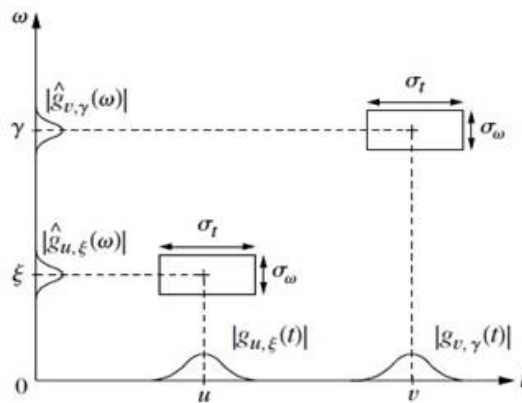
Figure 24. Heisenberg box of two time-frequency atoms [115]

3.3. Wavelet Transform

With the help of Fourier transform, frequency content of signal $f(t)$ can be obtained. However it does not give any time evolution of these elicited components. In short-time Fourier transform this drawback has been partially overcame. But due to the fixed time-frequency windows (tiles), time and frequency resolution is still a problem.

Wavelets and wavelet transform is appropriate tool to overcome this limitations. Wavelets are small wave-shaped and localized functions $\psi \in \mathcal{L}^2(\mathbb{R})$ with zero mean [115] and graphical demonstration of a wavelet is given in Figure 25,

$$\int_{-\infty}^{\infty} \psi(t)dt = 0 \tag{3.17}$$

They are also normalized and centered at t=0. A function can be called a mother wavelet if it can satisfy some mathematical criteria [117],

1. Admissibility constant of selected wavelet must be smaller than infinity.

$$C_\psi = \int_0^{\infty} \frac{|\hat{\psi}(\omega)|^2}{\omega} \, d\omega < \infty \tag{3.18}$$

2. Transported energy in wavelet function must be finite.

$$E = \int_{-\infty}^{\infty} |\psi(t)|^2 \, dt < \infty \tag{3.19}$$

3. Fourier transform of the candidate wavelet function must be real and zero for negative frequency components.

3.3.1. Continuous Wavelet Transform

The continuous wavelet transform of signal $f(t)$ is defined as [57],

$$W_f(u, s) = \int_{-\infty}^{\infty} f(t)\, \psi_{u,s}^*(t)\, dt \tag{3.20}$$

where the parameters u and s denotes the translation and dilation respectively and $*$ denotes the complex conjugate. In the above equation,

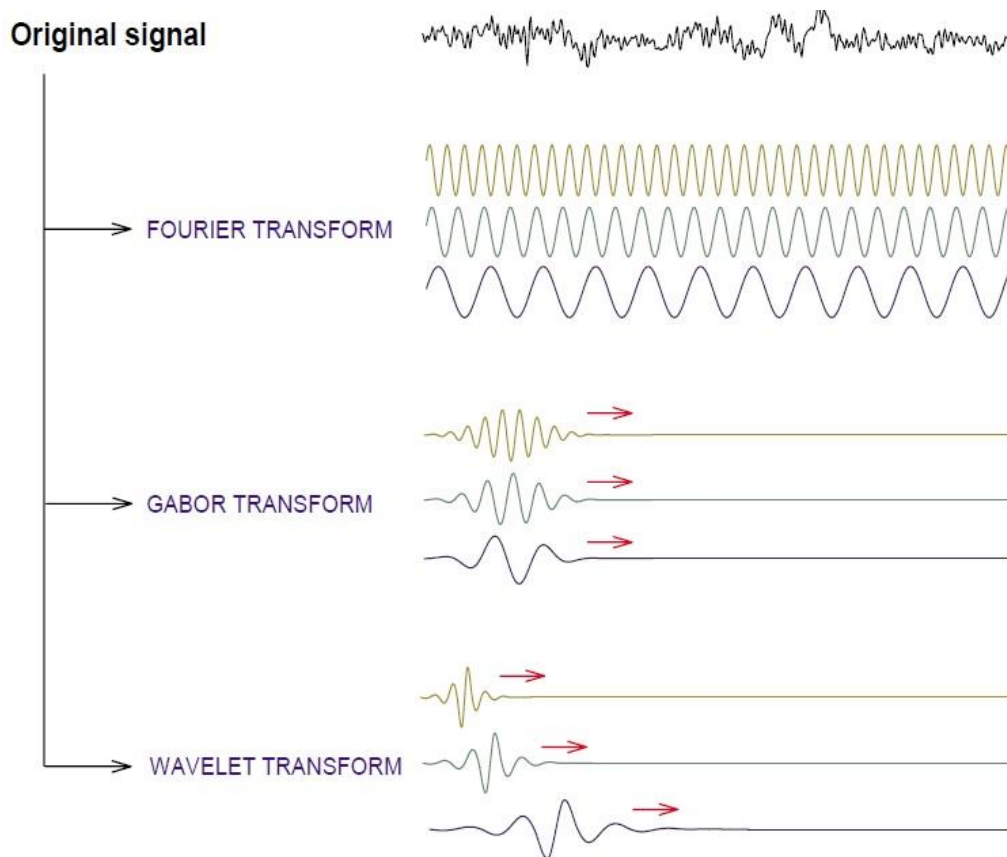$$\psi_{u,s}(t) = \frac{1}{\sqrt{s}}\, \psi\left(\frac{t-u}{s}\right) \tag{3.21}$$

Figure 25. Evolution of the three frequency based methods with time [116]

Recovery of a signal from its wavelet transform can be achieved by integrating over all scales and locations u and s,

$$f(t) = \frac{1}{C_\psi} \int_0^\infty \int_{-\infty}^\infty W_f(u,s) \, \psi_{u,s}(t) \, du \, \frac{ds}{s^2}$$

(3.22)

By confining the integration scale in a finite range, filtering of the original signal is achieved.

The wavelet transform demonstrates the localized energy of the signal $f(t)$ in the time-frequency window called Scalogram [115],

$$P_f W(u,s) \triangleq |W_f(u,s)|^2$$

(3.23)

The total energy of signal $f(t)$ in time domain is equal to total energy of the signal contain in wavelet domain. Such an conservation of the energy is described by the Plancharel's formula [118] is given as,

$$E \triangleq \int_{-\infty}^\infty |f(t)|^2 \, dt = \frac{1}{C_\psi} \int_{-\infty}^\infty \int_0^\infty |W_f(u,s)|^2 \, \frac{ds}{s} \, du$$

(3.24)

3.3.2. Discrete Wavelet Transform

Discrete wavelet transform (DWT) performs multiresolution analysis by using different types of wavelet filters.

Wavelet filters are employed to separate the original signal into several different frequency bands. A high pass filter and a low pass filter separates the frequency content of the signal into equal width but the output of the filter is in same size with original signal. Down sampling by a factor two is essential to prevent the doubling the amount of data (see Figure 26).

Synthesis filters are used to reconstruct the original signal from sub-band coefficients. Up sampling by a factor two is required to obtain original size of the signal.

Analysis Filter Bank   Synthesis Filter Bank
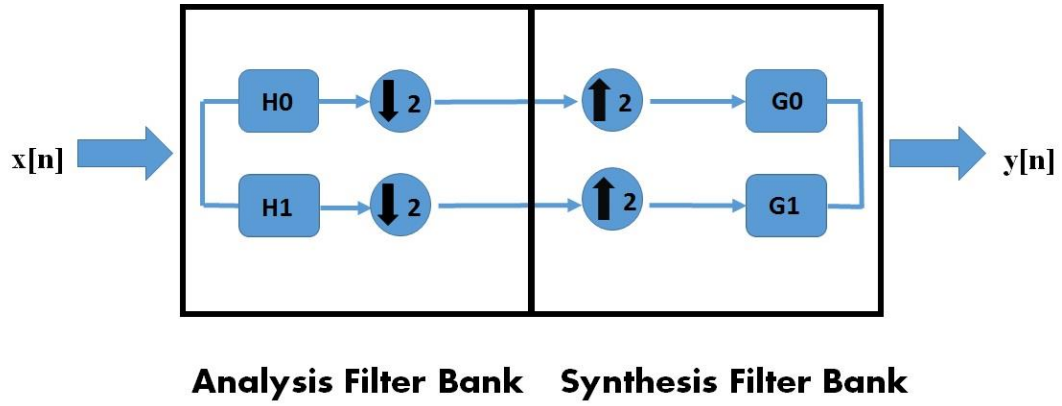
Figure 26. Two channel filter bank

For a perfect reconstruction, selected filter bank should be Biorthogonal and some design criteria should be met,

$$G_0(z) = H_1(-z)$$
$$G_1(z) = -H_0(-z)$$

(3.25)

where H_0 and G_0 are the low pass filters, H_1 and G_1 are the high pass filters of synthesis and analysis section respectively.

Any square integrable function $f(x) \in \mathcal{L}^2(\mathbb{R})$ can be represented by scaling function $\varphi(x)$ and wavelet function $\psi(x)$. Scaled and dilated version of the scaling function and wavelet function can be represented as,

$$\varphi_{j,k} = 2^{j/2} \varphi(2^j x - k)$$

(3.26)

$$\psi_{j,k} = 2^{j/2} \psi(2^j x - k)$$

(3.27)

$$f[n] = \frac{1}{\sqrt{M}} \sum_k W_\varphi(j_0, k) \, \varphi_{j_0,k}[n] + \frac{1}{\sqrt{M}} \sum_{j=j_0}^{\infty} \sum_k W_\psi(j, k) \, \psi_{j,k}[n]$$

(3.28)

where $f[n]$ is the discretized version of square integrable function $f(x)$. Equation (3.28) denotes the inverse discrete wavelet transform of function $f[n]$. Terms W_φ and W_ψ represents the scaling and wavelet coefficients respectively.

56

$$W_\varphi(j_0, k) = \frac{1}{\sqrt{M}} \sum_n f[n]\, \varphi_{j_0, k}[n] \tag{3.29}$$

$$W_\psi(j, k) = \frac{1}{\sqrt{M}} \sum_n f[n]\, \psi_{j, k}[n] \tag{3.30}$$

By putting equation (3.27) into equation (3.30), it yields

$$W_\psi(j, k) = \frac{1}{\sqrt{M}} \sum_n s[n]\, 2^{j/2}\, \psi(2^j n - k) \tag{3.31}$$

where $\psi(n)$ can be demonstrated as scaling function $\varphi(n)$,

$$\psi(n) = \sum_p h_\psi(p)\sqrt{2}\; \varphi(2n - p) \tag{3.32}$$

Scaled and dilated version of equation (3.32) can be written as,

$$\psi(2^j n - k) = \sum_p h_\psi(p)\sqrt{2}\; \varphi(2(2^j n - k) - p) \tag{3.33}$$

By using the equality $p = m - 2k$,

$$\psi(2^j n - k) = \sum_m h_\psi(m - 2k)\sqrt{2}\; \varphi(2^{j+1} n - m) \tag{3.34}$$

Putting the equation (3.34) into (3.30) we could obtain,

$$W_\psi(j, k) = \frac{1}{\sqrt{M}} \sum_n s[n]\, 2^{j/2} \left[\sum_m h_\psi(m - 2k)\sqrt{2}\; \varphi(2^{j+1} n - m) \right] \tag{3.35}$$

Interchanging the order of summation in eq. (3.35) yields

$$W_\psi(j, k) = \sum_m h_\psi(m - 2k) \left[\frac{1}{\sqrt{M}} \sum_n s[n]\, 2^{(j+1)/2}\, \varphi(2^{j+1} n - m) \right] \tag{3.36}$$

As a result, equation (3.36) gives a convolution operation as described below eq. (3.37),

$$W_\psi(j,k) = \sum_m h_\psi(m - 2k) \, W_\varphi(j+1,k)$$

(3.37)

Same as equation (3.37), equation (3.38) displays the scaling coefficients

$$W_\varphi(j,k) = \sum_m h_\varphi(m - 2k) \, W_\varphi(j+1,k)$$

(3.38)

Graphical demonstration of the discrete wavelet transform is given in Figure 27, 28 as,
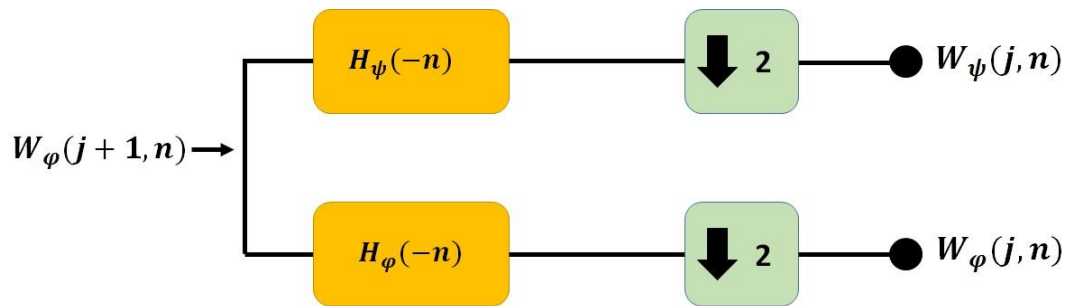

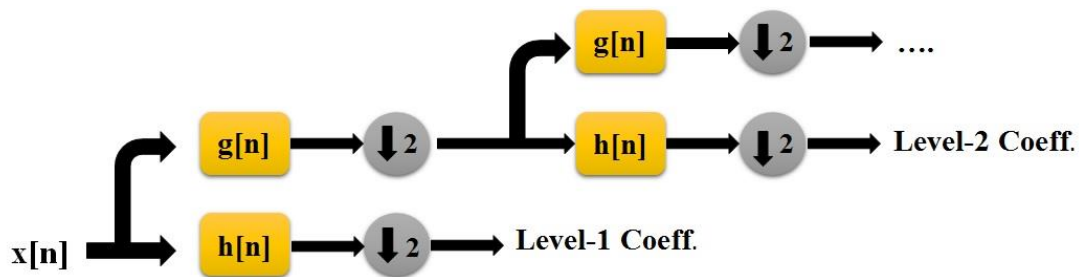Figure 27. Discrete wavelet analysis filter bank

Figure 28. Block diagram of discrete wavelet transform with low pass and high-pass wavelet filters

In p-level decomposition, the highest frequency seen in pth approximation coefficient is,

$$f_{ap-p} = \frac{f_s}{2^{p+1}}$$

(3.39)

3.4. Relative Wavelet Energy and Wavelet Entropy

The relative energy can be obtained as sum of all Scalogram [115] in wavelet domain in specific frequency band of a signal x(t) is given as,

$$E_{[f_j \, f_{j+1}]} = \sum_{m=0}^{(f_{j+1}-f_j)/\Delta f} \sum_{n=0}^{N-1} \left| W_x(t_n, f_j + m\,\Delta f) \right|^2 \tag{3.40}$$

where Δf is the step size of the frequency. Total wavelet energy can be determined by the sum of all relative wavelet energies over all frequency bands [47, 61]. Total wavelet energy at time t_n is defined as,

$$E_{total}(t_n) = \sum_{j} \sum_{m=0}^{(f_{j+1}-f_j)/\Delta f} \sum_{k=0}^{w/T_s} \left| W_x(t_n - \frac{w}{2} + kT_s, f_j + m\,\Delta f) \right|^2 \tag{3.41}$$

In the above equation, w denotes the window size, Δf is the step size of frequency. The probability of signal's having a component at a specific frequency band at time instant t_n is defined as,

$$p_j(t_n) = \frac{E_j(t_n)}{E_{total}(t_n)} \tag{3.42}$$

In information theory, entropy is a measure of degree of disorder of the signal. Shannon entropy [62] and Tsallis entropy [63] have been proven to be a good tool of demonstration of the complexity of signal. Shannon entropy is defined as,

$$WE_{Shannon} = -\sum_{j} p_j \, \ln p_j \tag{3.43}$$

And Tsallis entropy is defined as,

$$WE^q_{Tsallis} = \frac{1}{q-1} \sum_{j} \left(p_j - p_j^q \right) \tag{3.44}$$

where q is called as 'entropic index'.

3.5. Wavelet Denoising

Averaging of many trials to extract the ERP or EP from ongoing EEG many not be a proper solution. Temporal jitter is a major source of low signal-to-noise ratio. In addition to time domain averaging, wavelet denoising is utilized in this thesis [49]. Due to their spatial adaptivity wavelet denoising (shrinkage) is mostly preferred function estimator [119]. Standard wavelet based tools consider the wavelet coefficients individually with soft or hard thresholding function. Besides them, Donoho and Johnstone proposed a universal threshold value $\tau = \sigma\sqrt{2\,\log n}$. However individual consideration of each wavelet coefficient gave not satisfactory results in many applications. To overcome this drawback, Neighcoeff and Neighblock approaches have been demonstrated in [119]. Algorithm step of Neighblock method is given as,

- Transformation of data into wavelet domain via Orthogonal Discrete Wavelet transform

$$\widetilde{\Theta} = W.Y \tag{3.45}$$

- In each scale j wavelet coefficients should be grouped b_i^j with non-overlapping window with length $L_0 = \log n / 2$.
- Extension of each separated blocks with a length of $L_1 = \max(1, [L_0/2])$ in both direction to form overlapping blocks B_i^j with length $L = L_0 + 2L_1$
- Estimation of the thresholding level can be estimated by shrinkage rule

$$\hat{\theta}_{j,k} = \beta_i^j \tilde{\theta}_{j,k} \tag{3.46}$$

where β_i^j is called shrinkage factor and is defined as,

$$\beta_i^j = (1 - \lambda_* L\sigma^2 / \sum_{i,j\,\epsilon B_i^j} \tilde{\theta}_{j,k}^2) \tag{3.47}$$

In this thesis, we have utilized Neighcoeff method which has same procedure as Neighblock method except for $L_0 = L_1 = 1$ and $\lambda = \frac{2}{3}\log n$. The sum of all squared wavelet coefficients in the sliding window must be equal or greater than squared universal threshold value is given as,

$$\tau^2 = 2\sigma^2 \log n \tag{3.48}$$

The algorithm steps which we adopted to use is as follows,

I. Decompose the grand/subject average OEP into wavelet domain by utilizing Discrete Wavelet Transform.

II. Calculate the standard deviation for each scale before the stimulus onset time instants as,

$$\sigma_j = Median\left(\left|w_{j,1} - \overline{w_J}\right|, \left|w_{j,2} - \overline{w_J}\right|, \ldots, \left|w_{j,m} - \overline{w_J}\right|\right)/0.6745 \tag{3.45}$$

Where $w_{a,b}$ denotes the wavelet coefficient of ath scale and b^{th} time instant and also $\overline{w_x}$ represents the mean of the coefficients at x^{th} scale before the stimulus onset.

III. For each frequency band (scale) there must be a specific threshold value T_j. Threshold value for each frequency level j can be calculated as ,

$$T_j = \sigma_j\sqrt{2 \ln K} \tag{3.46}$$

Where parameter K represents the total number of wavelet coefficients in each scale and ln is the natural logarithm.

IV. Instead of using Donoho's individual denoising scheme, we took into consideration of immediate neighbor coefficients [119] due to the fact that the energy cannot be carried by immediate coefficients. The thresholding criterion is as given [51],

$$w_{den}(j,k) = \begin{cases} w(j,k), & w_{j,k-1}^2 + w_{j,k}^2 + w_{j,k+1}^2 > T_j^2 \\ 0, & otherwise \end{cases} \tag{3.47}$$

V. After all procedure completed, zero-tree denoising was applied onto remaining coefficients. In that process, main intention is to discard the insignificant coefficients. Coefficients which are locate at higher decomposition level are called 'parent' coefficients and coefficient that stay in lower levels called children coefficients. Zero-tree denoising sets all children coefficient zero if the parent coefficient is discarded in step IV.

3.6. Results

In this section, wavelet entropy and wavelet denoising results will be demonstrated for average and single trial responses.

3.6.1. Continuous Time Wavelet Entropy for Olfactory Evoked Potentials

We have utilized continuous time wavelet entropy to observe more detailed entropy results in this study. However, many studies [59, 120] utilized discrete time wavelet entropy to observe how brain processes sensory information. In this study, we have analyzed totally 23 response of 20 subjects in this section. Among them, 4 of them are single trial responses of both CO_2 and PEA stimulations of two subjects. As single subject responses, 10 averaged response were collected for CO_2 response analysis and 9 for PEA response analysis. As mother wavelet, we have selected Complex Morlet Wavelet as aforesaid in [2]. However, we have considered different types of wavelets such as Shannon, Frequency B-Spline and Gaussian wavelets with different center frequencies and bandwidths. In Table 4, correlation coefficients between grand average and different wavelets with different center frequency and bandwidth values have been given.

Table 4. Correlation coefficients of different types of wavelets and grand average

Wavelet	1-0.5	1-1	1.5-1.5	N=4	N=5	N=8
CMOR	0.8363	0.8062	0.6355	-	-	-
F.B.Spline	0.7807	0.7833	0.6461	-	-	-
Shannon	0.7836	0.8308	0.7483	-	-	-
Gaussian	-	-	-	0.6268	0.6874	0.7615

We have applied all wavelet types given in table 4. Although it has lesser correlation value, the most successful results have been obtained with complex Morlet wavelet with 1.5 Hz center frequency and 1.5 Hz bandwidth. For the relative energy and wavelet entropy calculations, we used 32 ms rectangular overlapping time window. Since the magnitude of wavelet energy is quite low for gamma band, it was not demonstrated in relative energy figures.

For clearance, we calculate the mean entropy value for numerical demonstration of three distinct time intervals. Time window-1 (TW-1) involves the time instants between -1000ms to -600ms before stimulus. Time window-2 (TW-2) comprises time instants 500-900ms after stimulus that is the time interval which mostly contains chemosensory evoked potential responses. The final time (TW-3) window starts from 1400ms to 1800ms. In TW-3, there are no evoked potentials can be seen. Our main purpose is to demonstrate how brain goes from disordered (i.e. more chaotic state) to more ordered state with respect to given olfactory and trigeminal stimuli in graphical and in numerical results. Table-5 demonstrates the mean Shannon entropy values for aforementioned time windows. After finding the mean entropy values for all time windows, we have applied statistical test to demonstrate relationship between them.

3.6.1.1. Single Trial Entropy Results

In this section, we demonstrate two subjects' wavelet entropy results for olfactory (PEA) and trigeminal (CO_2) stimuli. In Figure 29, Figure 30 and Figure 31, recorded single trial, relative energy and wavelet entropy results of subject-1 to PEA stimuli are given respectively.

Figure 29. Single trial PEA response of Subject-AP1 and computed Scalogram

Figure 30. Time evolution of relative energies for Subject-AP1

Figure 31. Time evolution of normalized wavelet entropy of Subject-AP1 for PEA stimuli

Figure 32. Single trial CO_2 response of Subject-AC1 and computed Scalogram

Figure 33. Time evolution of relative energies of Subject-AC1

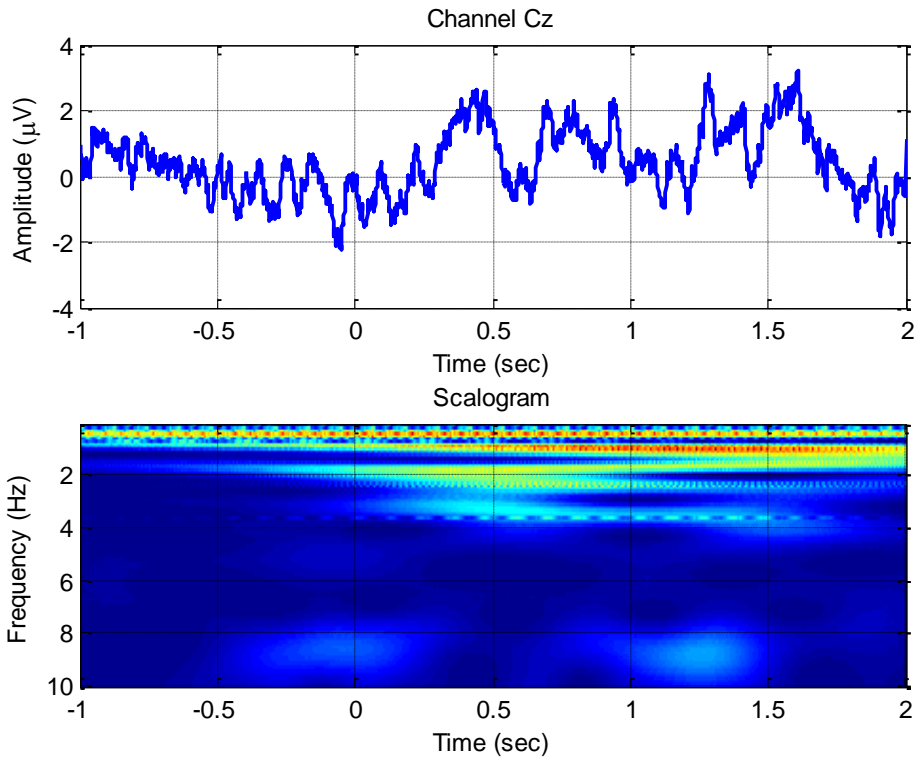Figure 34. Time evolution of normalized wavelet entropies for Subject-AC1

Figure 35. Single trial CO_2 response of Subject-AC2 and computed Scalogram

Figure 36. Time evolution of relative energies of Subject-AC2

Figure 37. Time evolution of normalized wavelet entropies for Subject-AC2

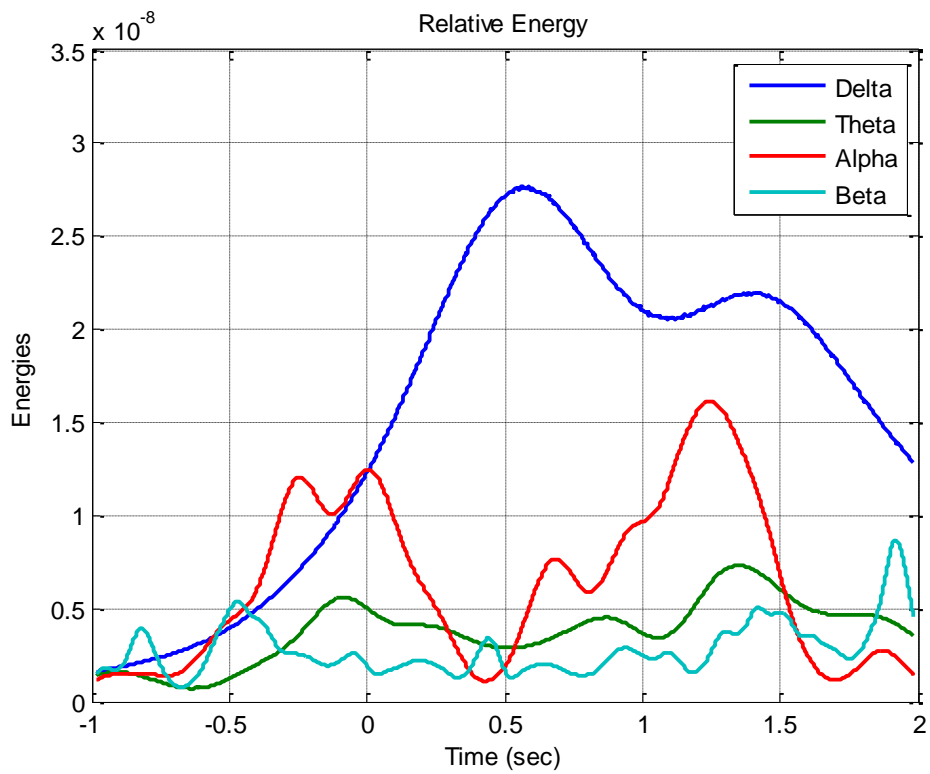Figure 38. Single trial PEA response of Subject-AP2 and computed Scalogram

Figure 39. Time evolution of relative energies of Subject-AP2

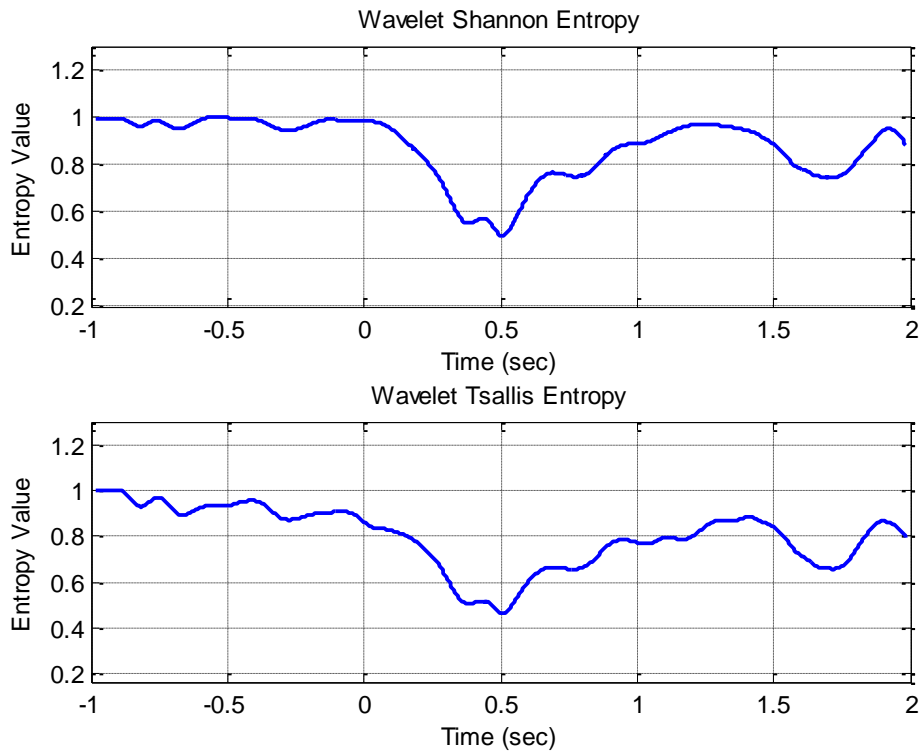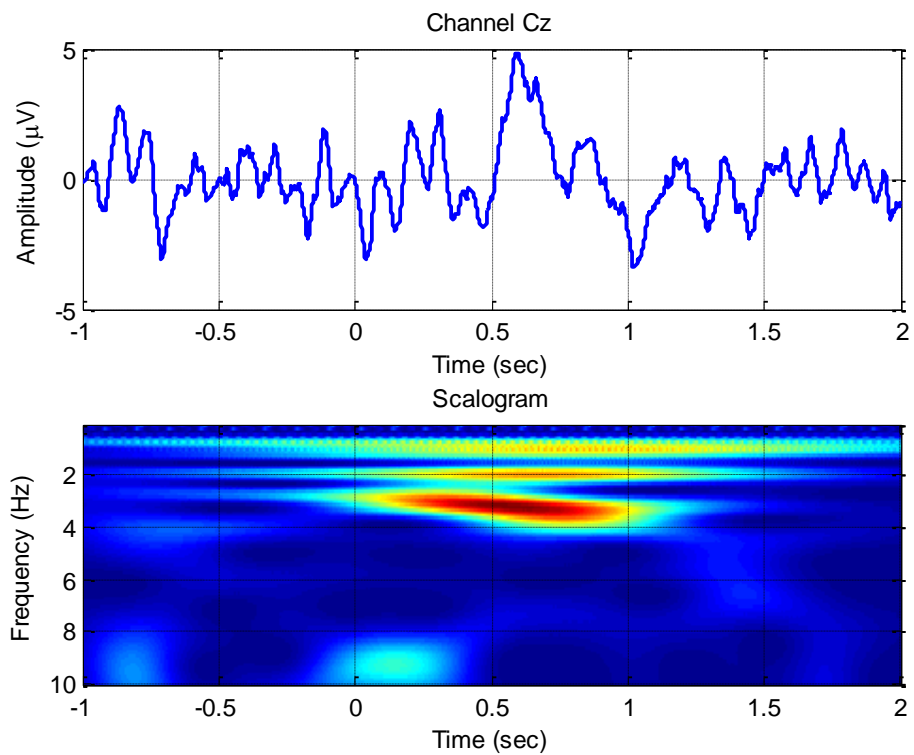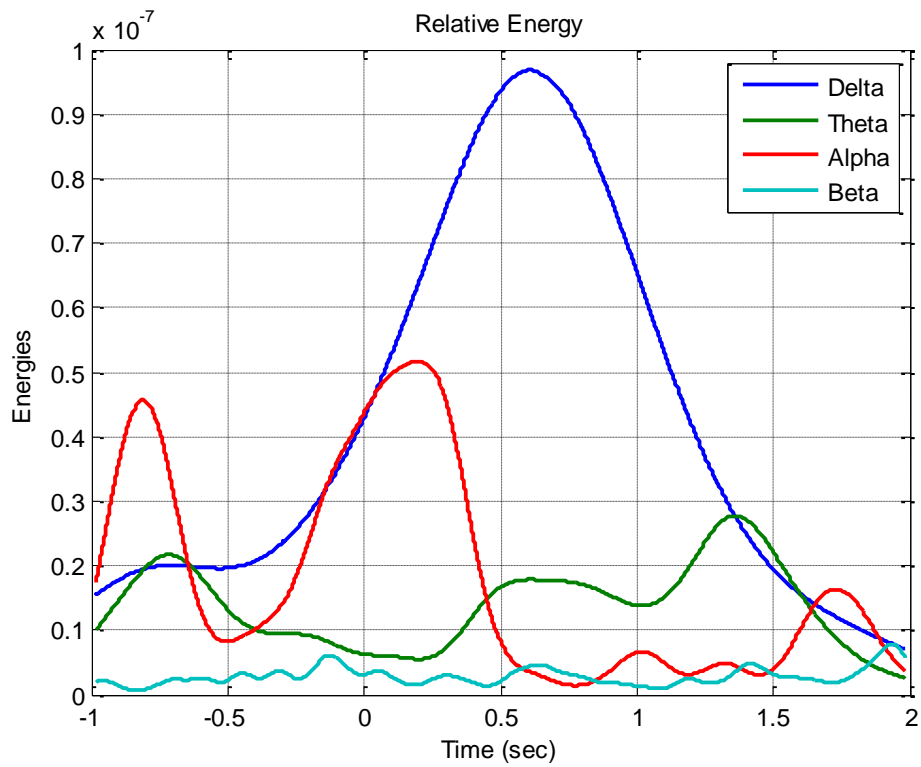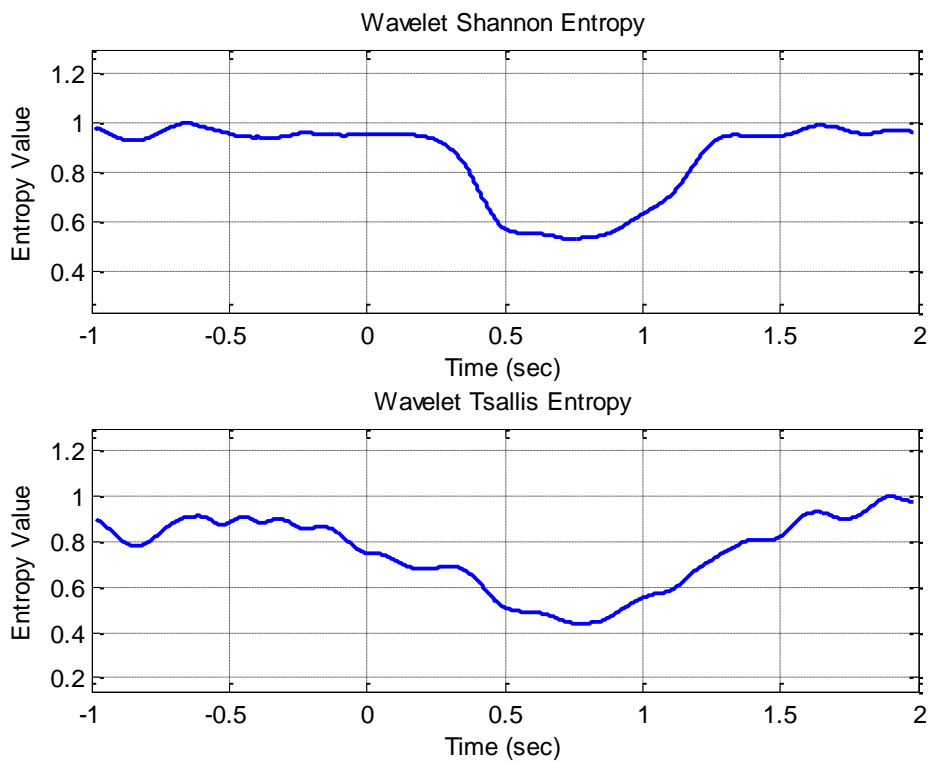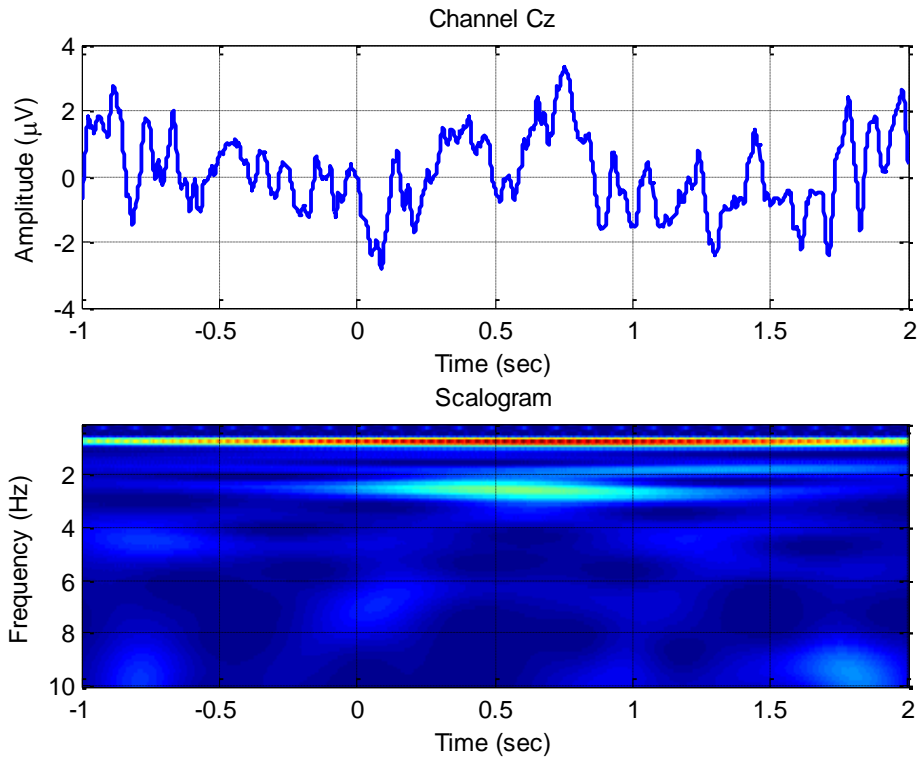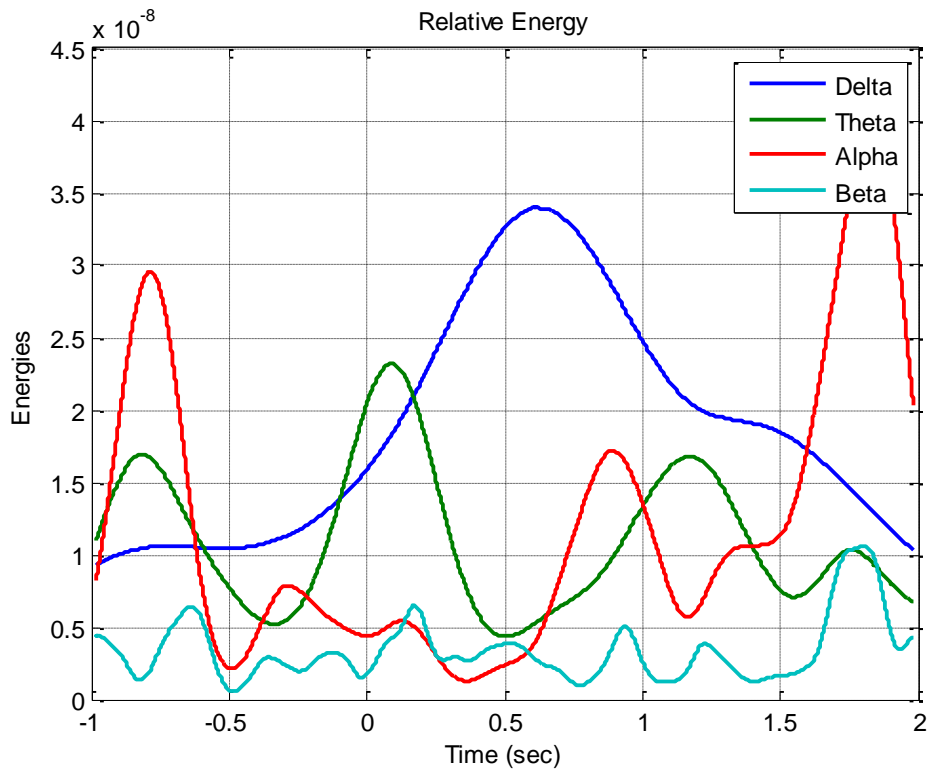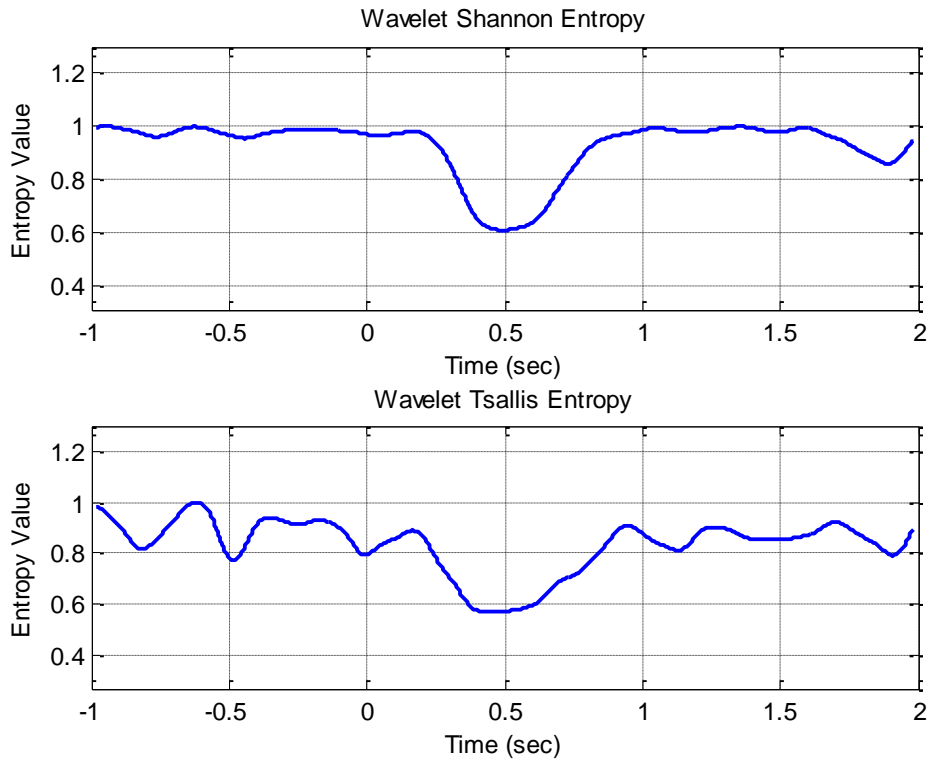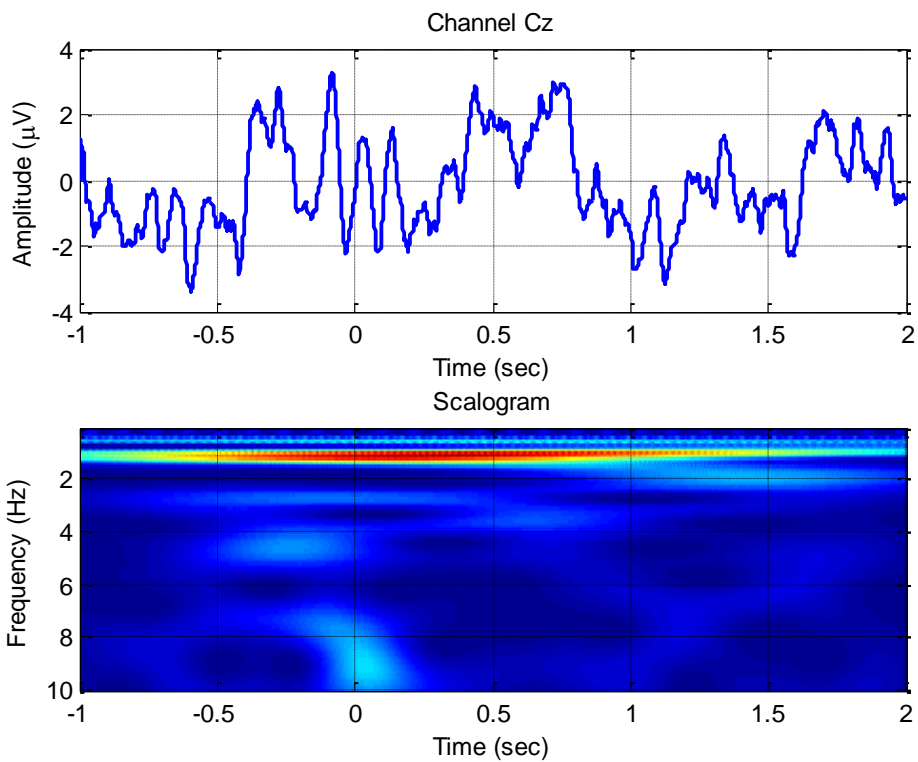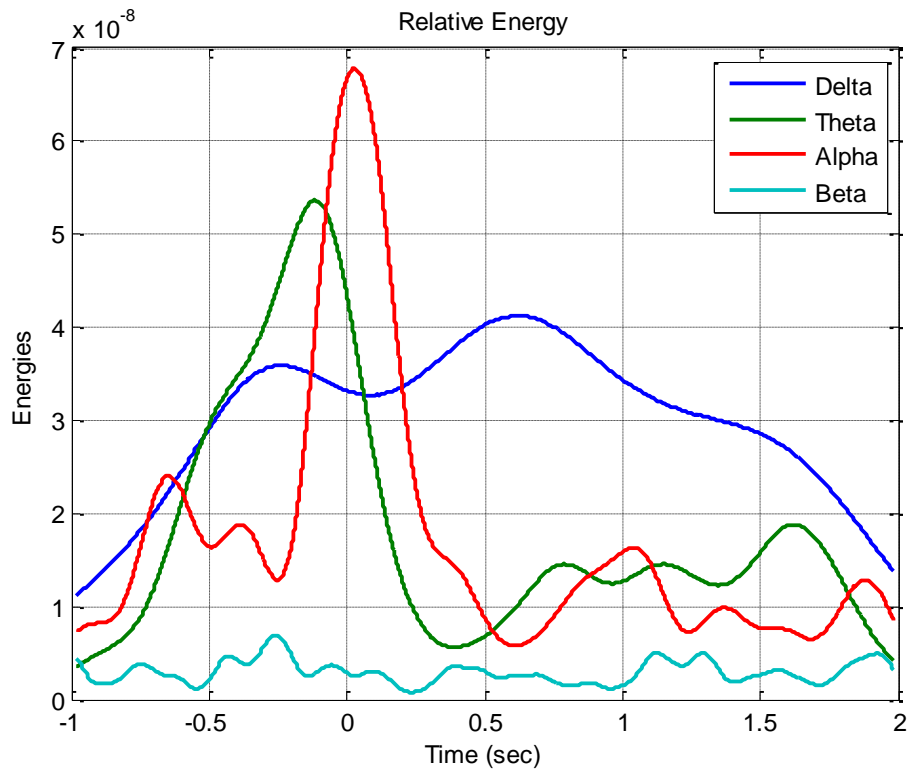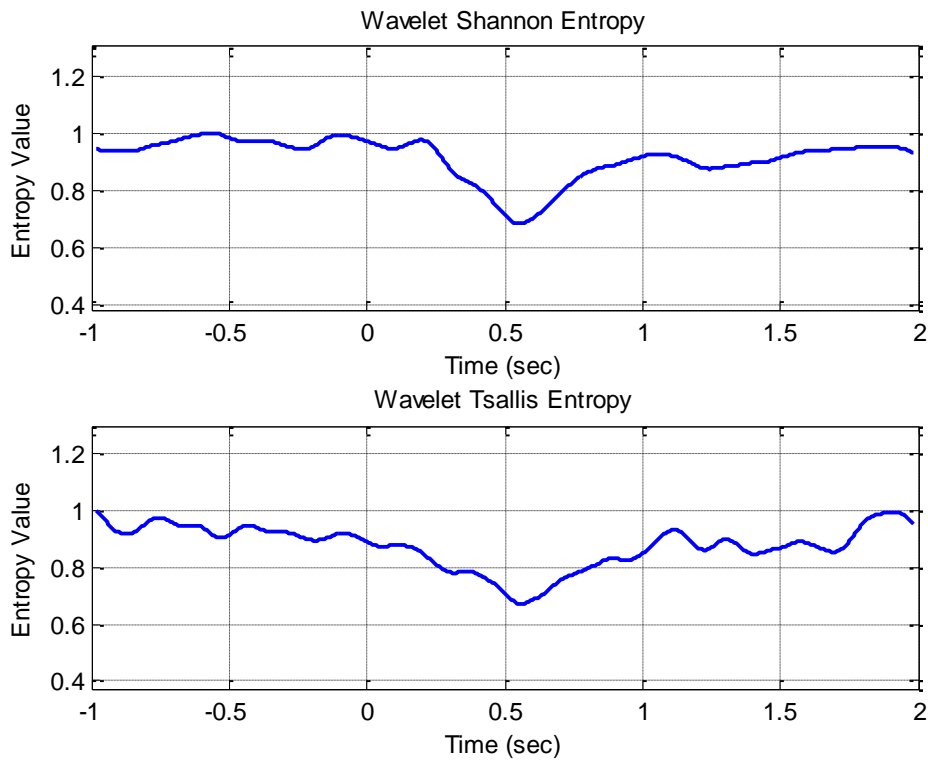Figure 40. Time evolution of normalized wavelet entropies for Subject-AP2

In Figure 32- 34, EEG signal, relative energy and wavelet entropy for subject-1 CO_2 stimuli is given and in Figure 35-37 and also in Figure 38-40 subject-2 CO_2 and PEA stimuli single trials, relative energies and wavelet entropy results are given respectively.

By looking at the relative energies which is depicted in Figures 30, 33, 36 and 39, energy of delta band increases dramatically with respect to given stimuli, in post stimulus time interval. In these figures, delta band reaches its maximum value at nearly t=0.5 seconds and also there is a significant energy decrease in other frequency bands at the same time instants. Both of these energy changes in frequency bands poses an entropy decrease due to chemosensory stimuli. At the same time, it is depicted in [34] that evoked potentials reaches its maximum value against external stimuli.

This is the main reason why wavelet entropies reaches their minimum value at the same time that is shown in Figures 29, 32, 35, 38. Since entropy has been a measure of degree of disorder, it can be inferred that, brain goes to an ordered state through the instrument of given olfactory or trigeminal stimuli.

In Table 5, both single trial and averaged responses have been given. By looking at the single trial results in Table 5, mean entropy in TW-2 is the lowest among other time windows. In graphical results, as expected, entropy decrease occurs mainly at the time interval 0.5-1 second. In comparison with studies of other sensory modalities, for example in auditory, entropy decrease occurs at time interval of 50-200 ms [61]. Such a delay in decrement of entropy can be due to complex chemosensory stimulus and also due to a delay of stimulus transmission to receptors in chemosensory stimulations (i.e. sensory transduction) [112]. In this study, we employed most popular entropy tools Shannon and Tsallis entropies. Both of them are successful at demonstration of complexity of the system. Tsallis entropy with entropic index q=1.25 gives the more detailed results to results found with Shannon entropy. Increasing q results in more coarse results which is analyzed in detail in [61]. In the next section analysis results of averaged responses will be given.

3.6.1.2. Entropy Results of Averaged Trials

In this section we have analyzed single subject responses to chemosensory stimuli. For each subject totally 22-25 single trial responses have been collected and averaged. In

Figures 41-58, original averaged responses, relative energies and entropy evolutions is given respectively. For CO_2 stimulations,
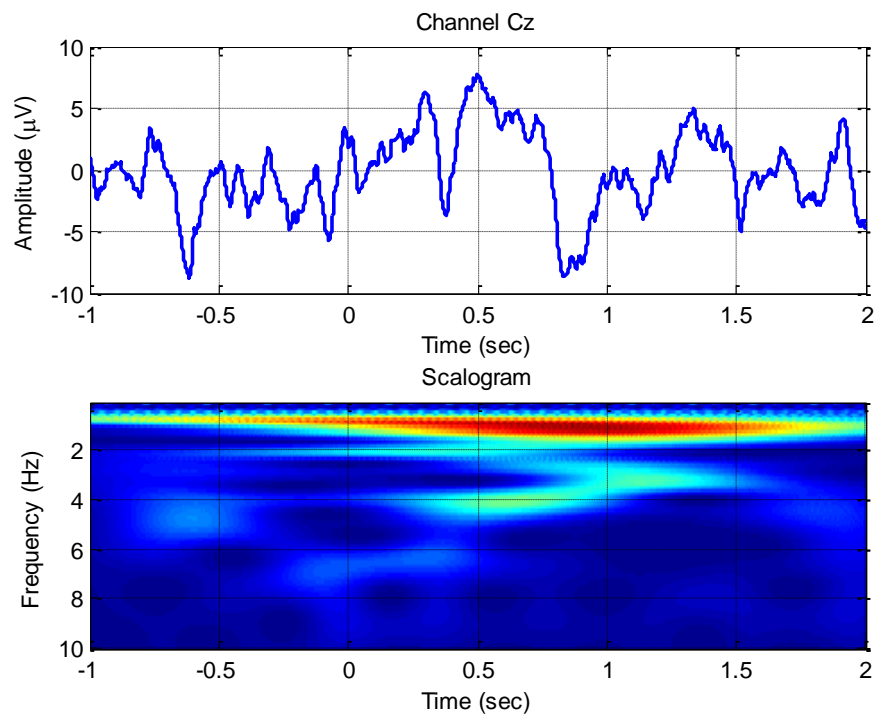
Figure 41. Subject-C1 averaged CO_2 response and computed Scalogram

Figure 42. Time evolution of relative energies for Subject-C1
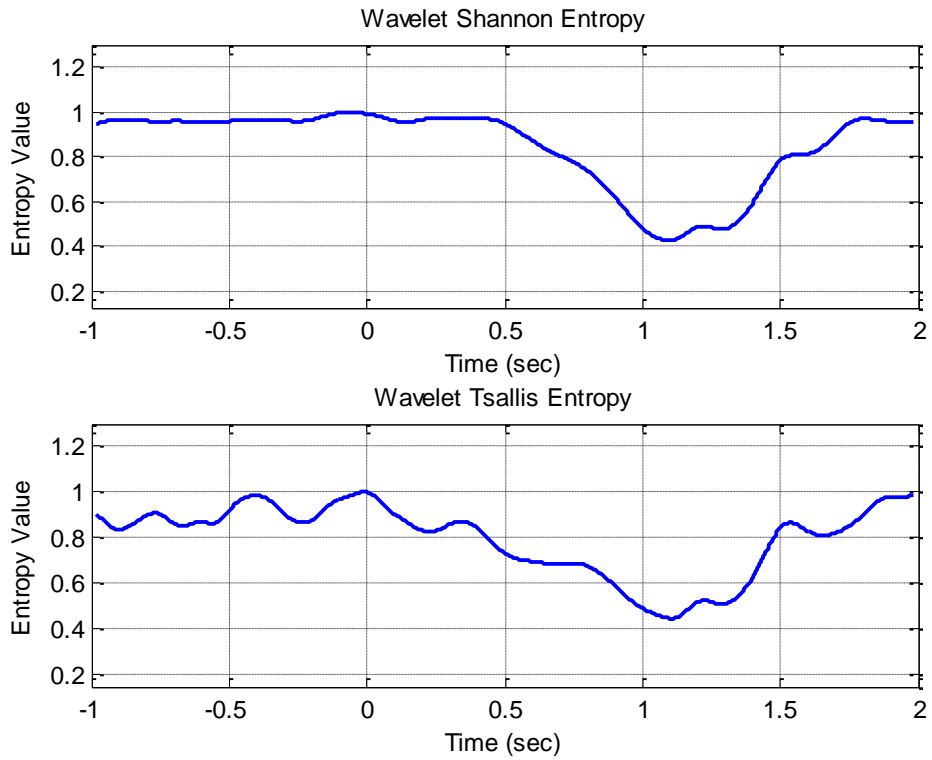
Figure 43. Time evolution of normalized wavelet entropies of Subject-C1

Figure 44. Subject-C2 averaged CO_2 response and computed Scalogram

Figure 45. Time evolution of relative energy of Subject-C2

Figure 46. Time evolution of normalized wavelet entropies of Subject-C2

Figure 47. Subject-C4 averaged CO2 response and computed Scalogram

Figure 48. Time evolution of relative energies of Subject-C4
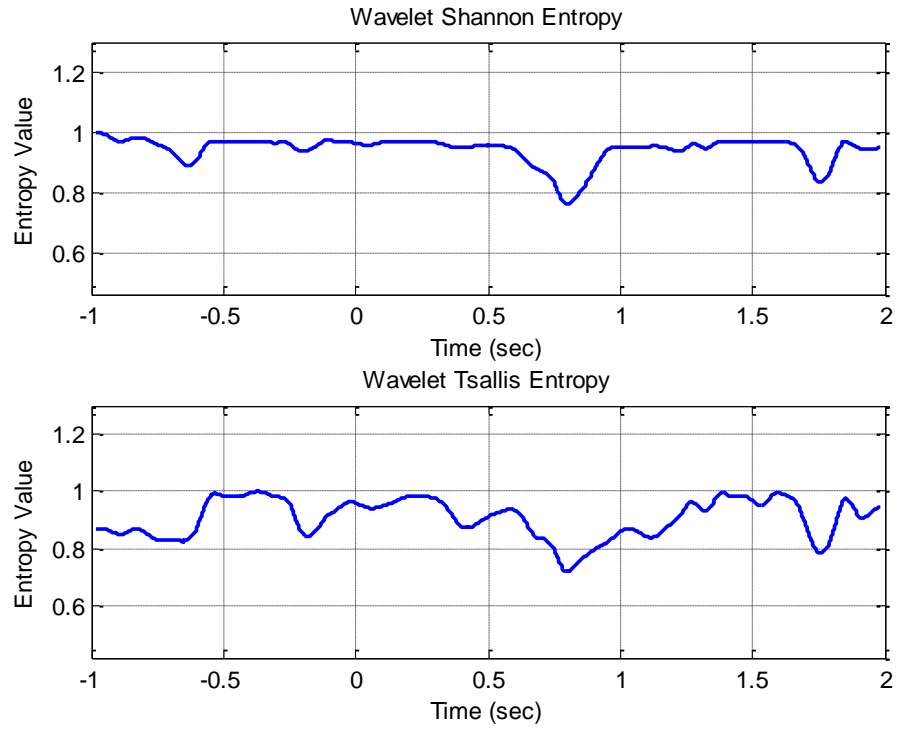
Figure 49. Time evolution of normalized wavelet entropies of Subject-C4

For the PEA stimulations,
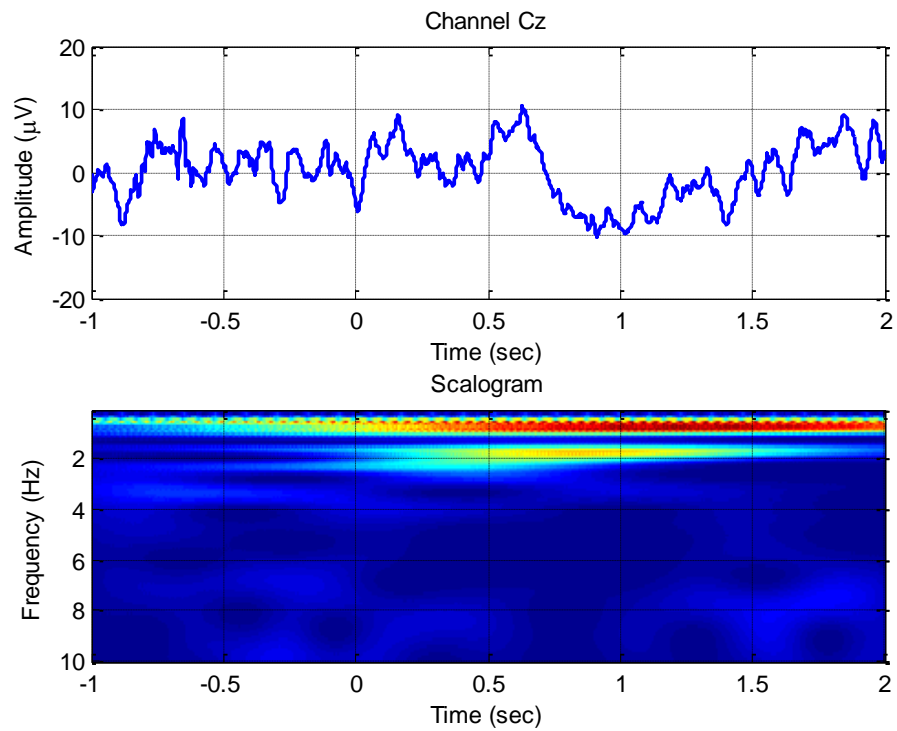
Figure 50. Averaged PEA responses of Subject-P4 and computed Scalogram
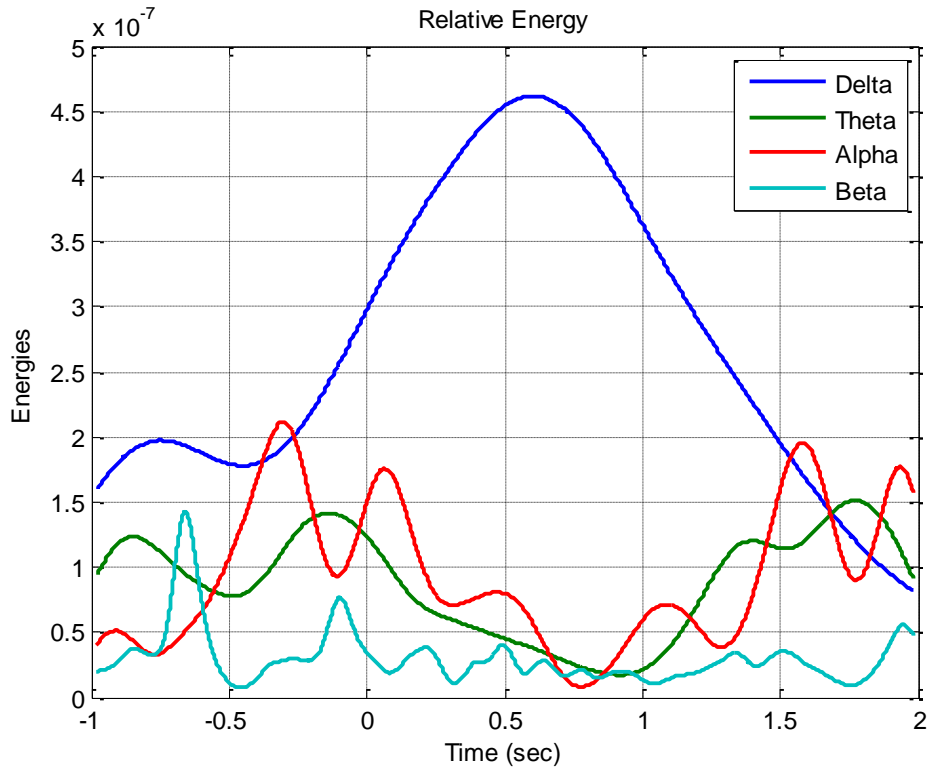
Figure 51. Time evolution of relative energies of Subject-P4
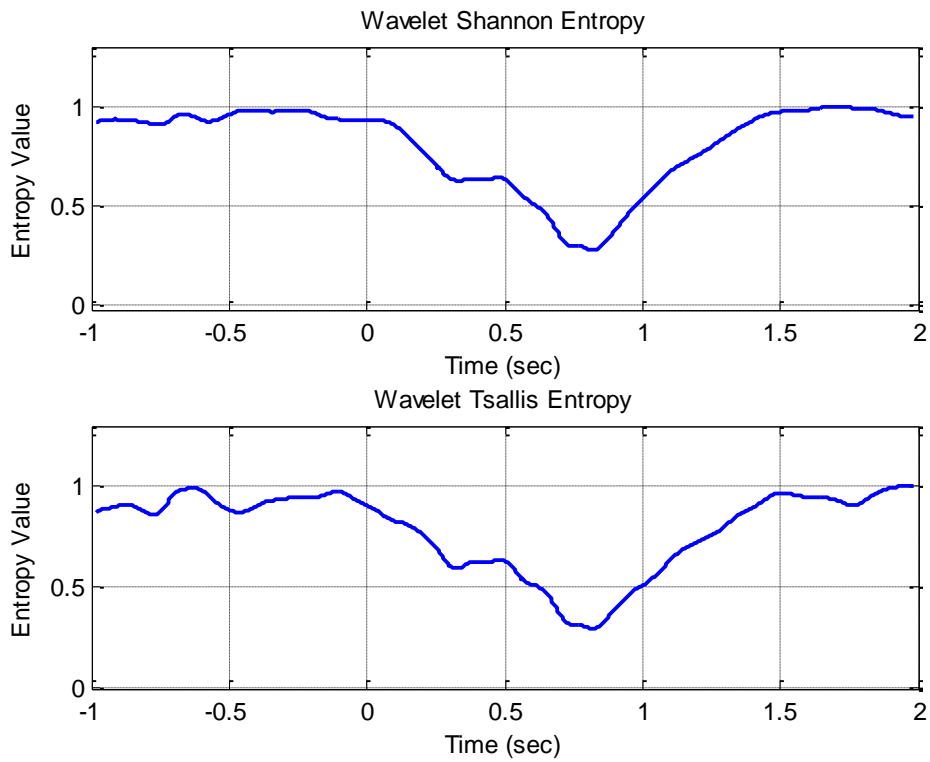
Figure 52. Time evolution of normalized wavelet entropies of Subject-P4
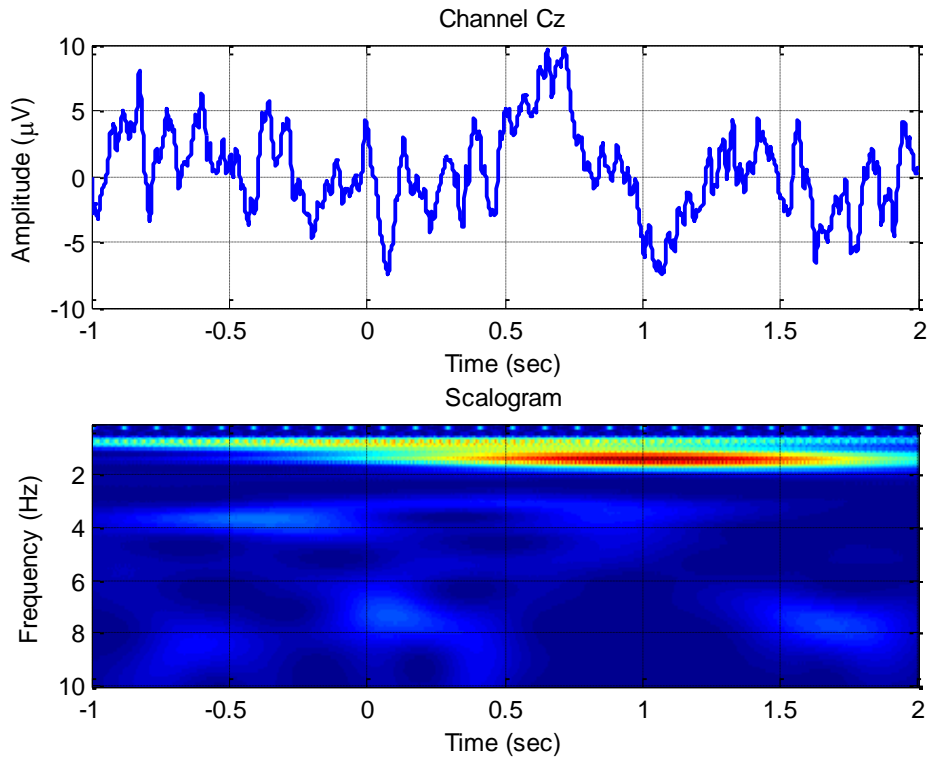
Figure 53. Averaged PEA response of Subject-P2 and computed Scalogram
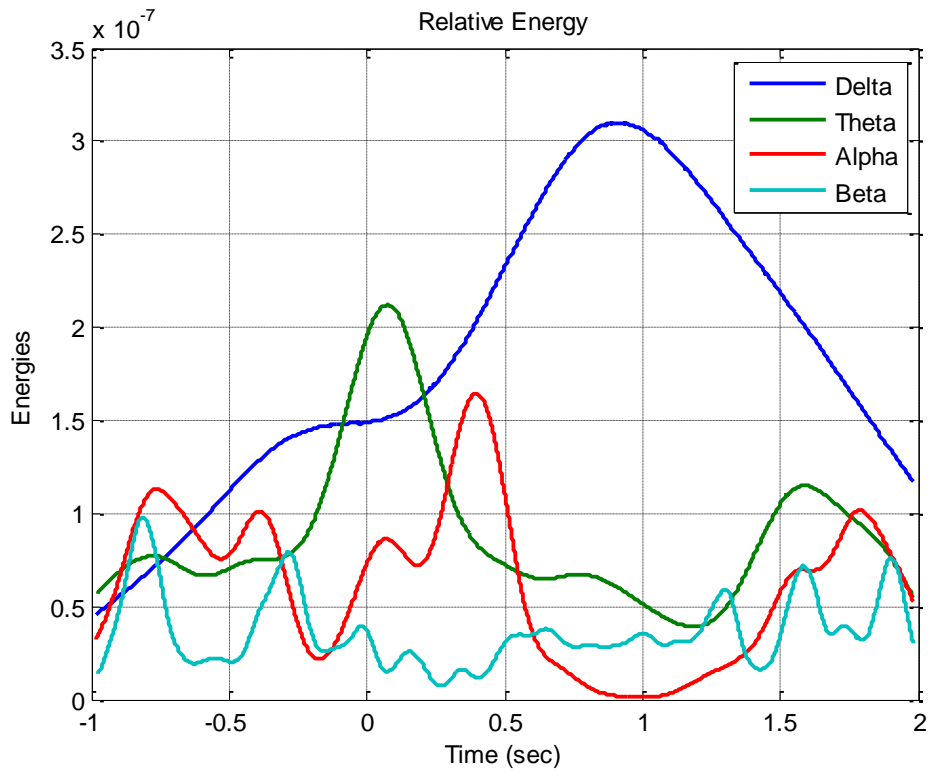
Figure 54. Time evolution of relative energies of Subject-P2
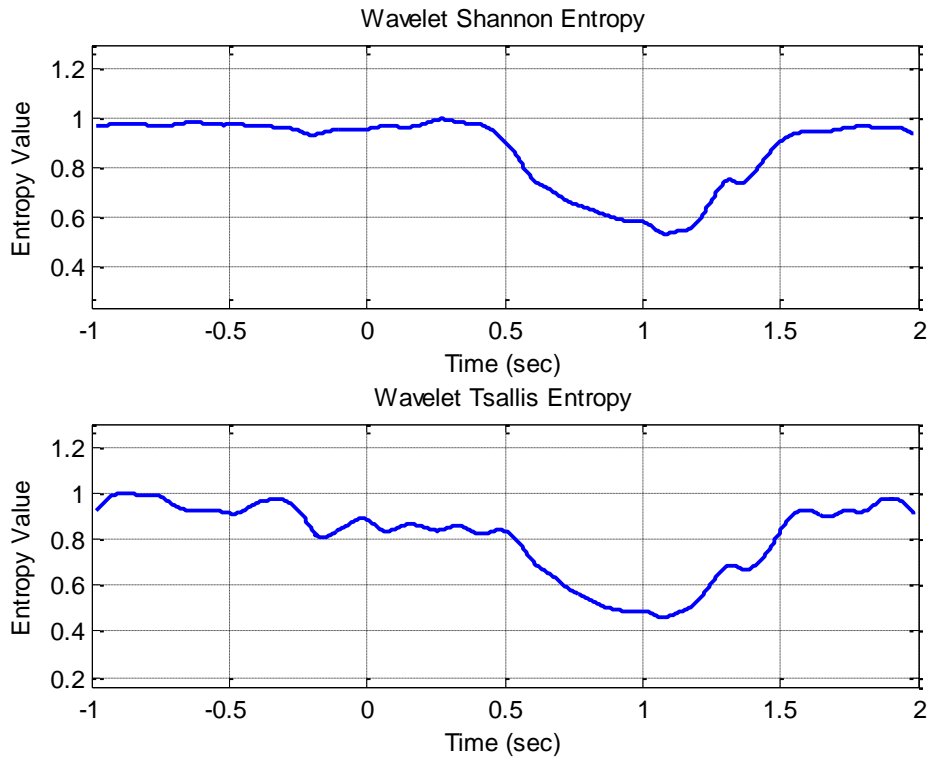
Figure 55. Time evolution of normalized wavelet entropies of Subject-P2
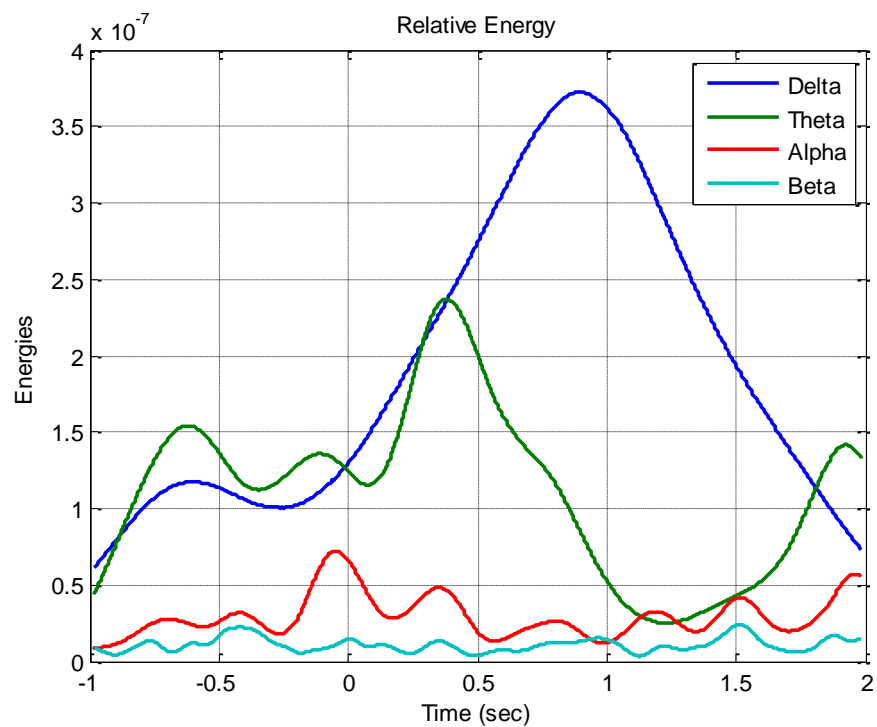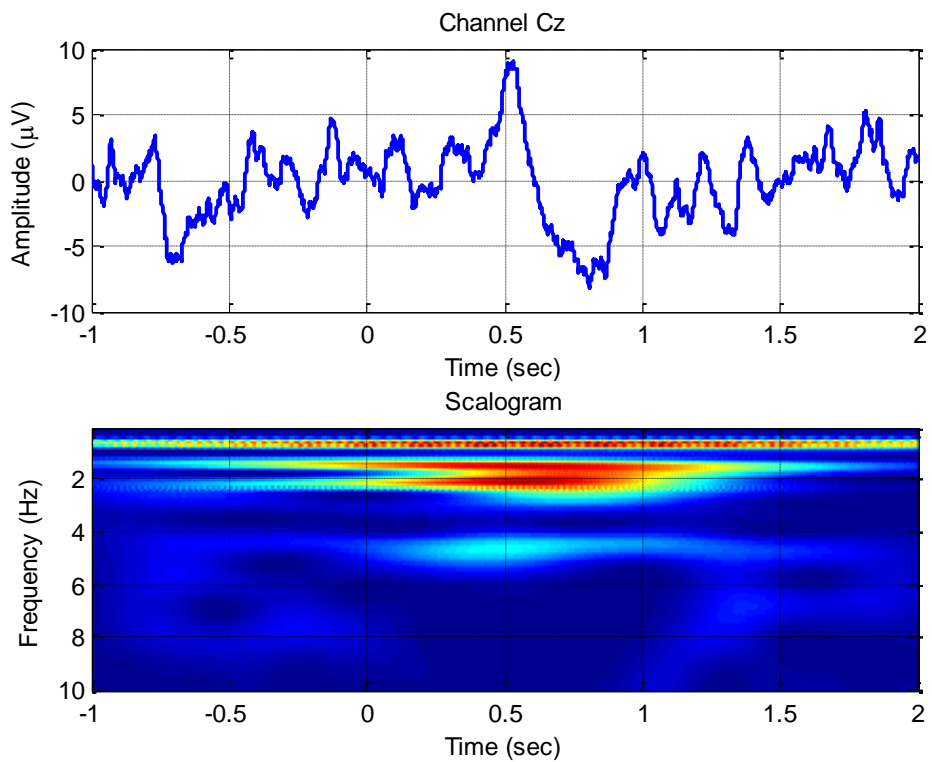

Figure 56. Averaged PEA response of Subject-P3 and computed Scalogram
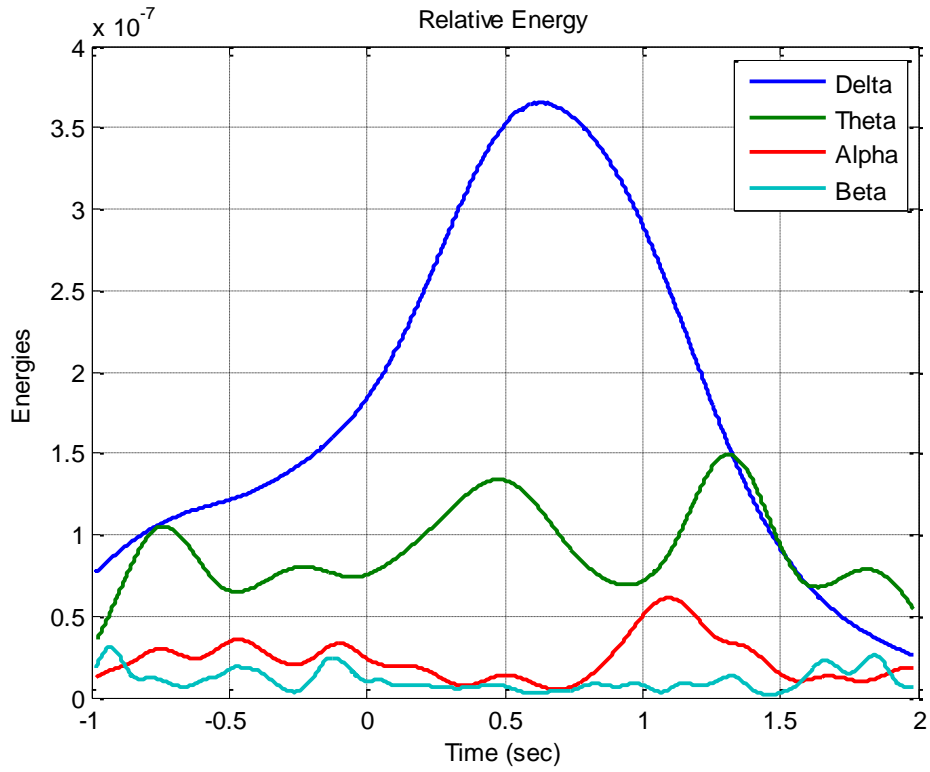
Figure 57. Time evolution of relative energies of Subject-P3

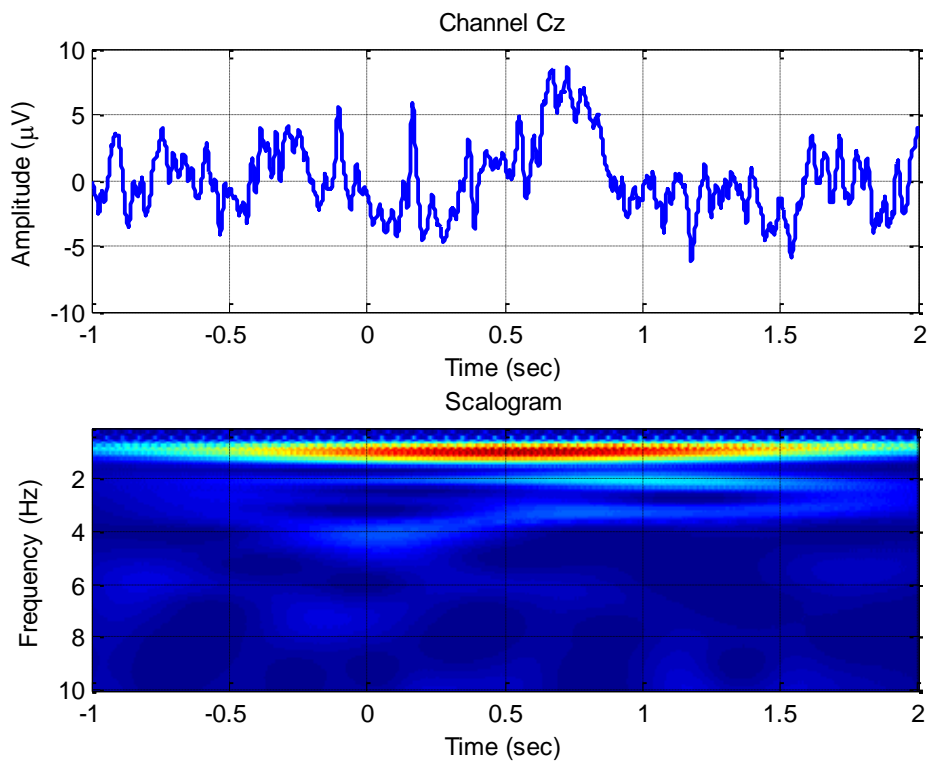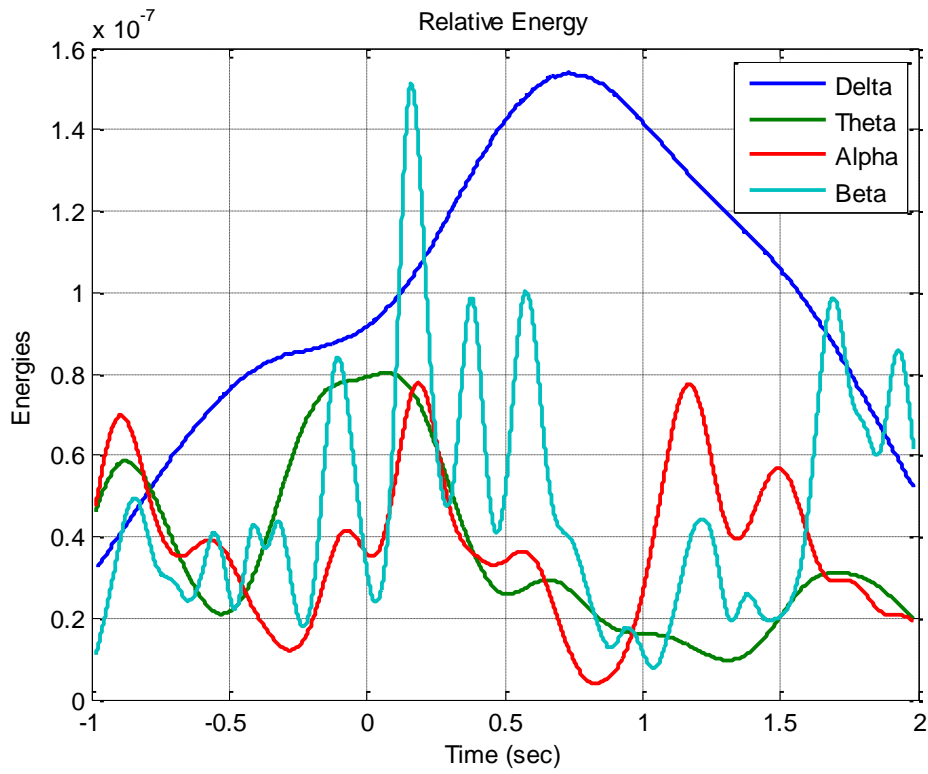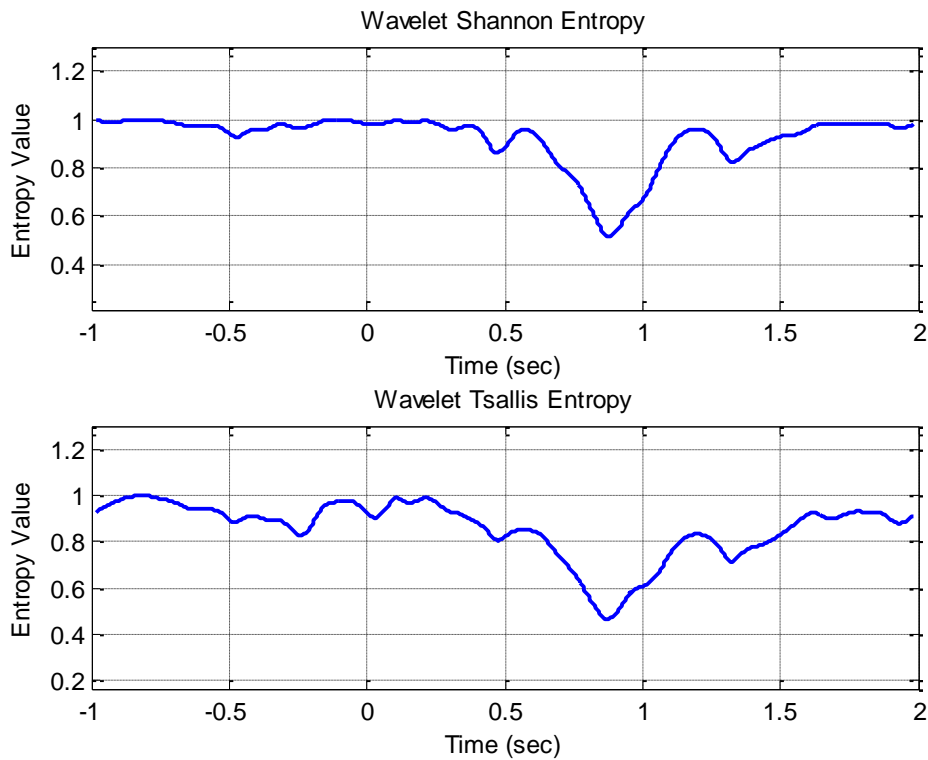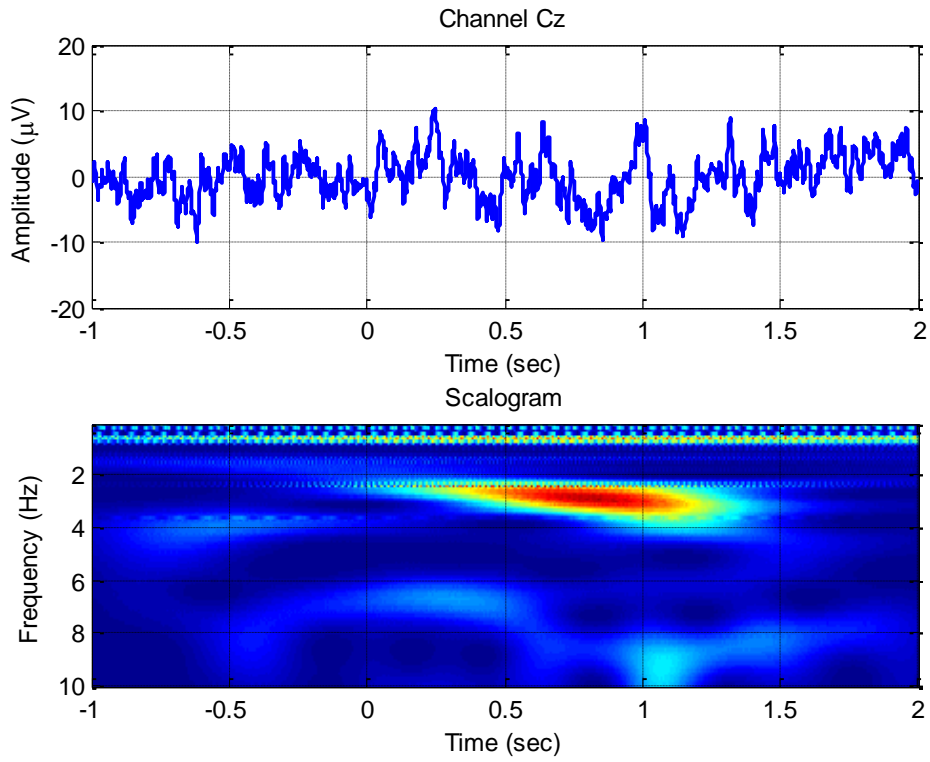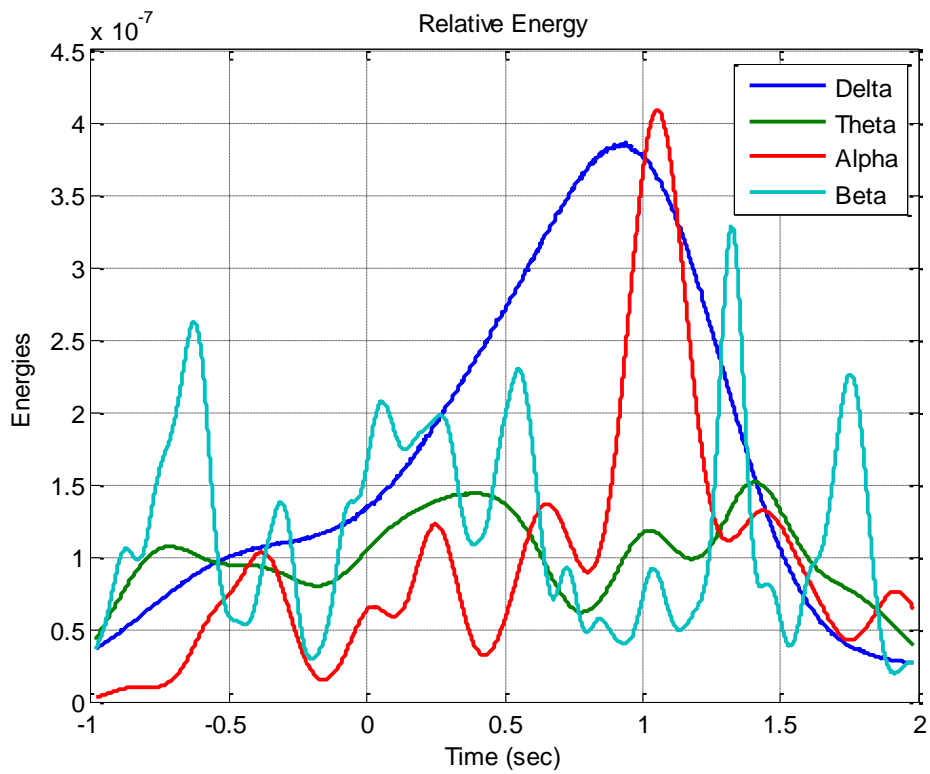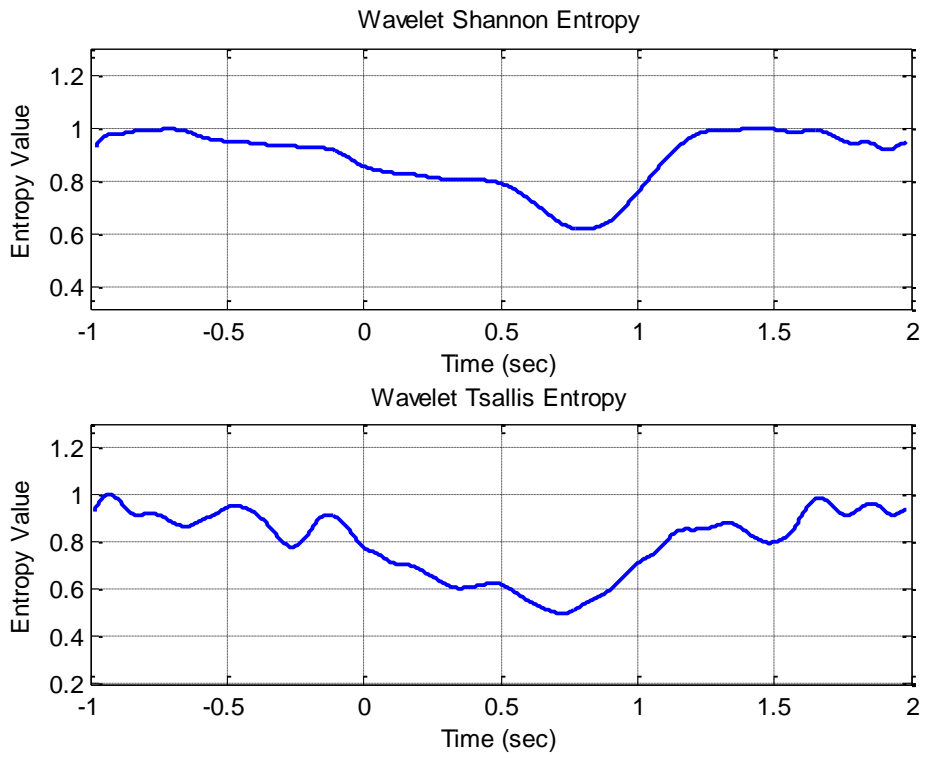Figure 58. Time evolution of normalized wavelet entropies of Subject-P3

Table 5. Mean wavelet Shannon entropy values for different time windows

Single Trial	Time Window-1	Time Window-2	Time Window-3
Subject-A(P1)	0.9757	0.7438	0.8179
Subject-A(C1)	0.9504	0.5542	0.9668
Subject-A(P2)	0.9697	0.8068	0.9277
Subject-A(C2)	0.9778	0.8161	0.9706
Single Subject (CO$_2$)			
Subject-C1	0.9729	0.7519	0.8215
Subject-C2	0.9725	0.7474	0.9507
Subject-C3	0.9385	0.8416	0.9611
Subject-C4	0.9633	0.8841	0.9386
Subject-C5	0.9216	0.7299	0.9142
Subject-C6	0.9374	0.6706	0.7205
Subject-C7	0.4957	0.3940	0.8313
Subject-C8	0.8645	0.5873	0.7792
Subject-C9	0.8452	0.5506	0.8850
Subject-C10	0.7748	0.6270	0.8953
Single Subject (PEA)			
Subject-P1	0.9748	0.9120	0.9580
Subject-P2	0.9606	0.6868	0.9230
Subject-P3	0.9239	0.6833	0.9822
Subject-P4	0.9617	0.4173	0.9795
Subject-P5	0.9157	0.7246	0.7707
Subject-P6	0.6957	0.4963	0.9168
Subject-P7	0.8680	0.8261	0.9817
Subject-P8	0.9948	0.9865	0.9741
Subject-P9	0.9640	0.9622	0.9223

Like in section 3.6.1.1, relative energy, Scalogram and wavelet entropy results have been given for averaged responses in this section. Calculation of relative energy and wavelet entropy was same in previous section. Results show that, wavelet entropy reaches its minimum value in time interval 0.5-1 seconds. The reason why entropy reaches its minimum value is the same which has detailed in results section of single trial entropy analysis. However, for Subject-P2, relative energy of delta band reaches maximum value at nearly t=1 sec. by looking at computed Scalogram, it is clearly seen that red area which denotes the higher energy, is mainly located at delta band and time interval [0 1.2] seconds. For this reason, entropy reaches its minimum value nearly at [0 1.2] sec.

Results in Table 5 were conveyed to statistical analysis. We utilized non parametric K-related sample test (Friedman test) which is able to demonstrate the meaningful alterations (i.e. variance) within TW-1, 2 and 3. Results of this test is given

in Table 6. Briefly, Friedman test is a non-parametric test that measures the analysis of variance between two or more variables which are assumed to be fully or partially related.

Statistical analyses for PEA stimuli confirmed that, wavelet Shannon entropy values are changing between three time windows and this change is statistically significant and also meaningful.

Table 6. Friedman test for PEA results

Test Statistics	
N	9
Chi-Square	8,667
df	2
Asymp. Sig.	,013

After finding the significance rate as 0.013 from Friedman test for PEA, we have analyzed pairwise meaningfulness of time windows to present the significance of the change of wavelet entropy with Wilcoxon signed rank test. Results of pairwise Wilcoxon test for PEA is demonstrated in Table 7.

Table 7. Wilcoxon test results for PEA

Ranks		N	Mean Rank	Sum of Ranks
TW3 – TW1	**Negative Ranks**	5[a]	4,20	21,00
	Positive Ranks	4[b]	6,00	24,00
	Ties	0[c]		
	Total	9		
TW2 – TW1	**Negative Ranks**	9[d]	5,00	45,00
	Positive Ranks	0[e]	,00	,00
	Ties	0[f]		
	Total	9		
TW3 – TW2	**Negative Ranks**	2[g]	1,50	3,00
	Positive Ranks	7[h]	6,00	42,00
	Ties	0[i]		
	Total	9		

Test Statistics

	TW3 – TW1	TW2 – TW1	TW3 – TW2
Z	-,178[b]	-2,666[c]	-2,310[b]
Asymp. Sig. (2-tailed)	,859	,008	,021

According to the outcomes of statistical test result, Wilcoxon test has found a significant meaningfulness between TW-2 and TW-3, and also TW-1 and TW-2. However, there hasn't been any meaningful correlation for mean entropy values found in between TW-1 and TW-3 for PEA stimuli. According to these findings, the time interval, where evoked potentials reaches their maximum peak value, wavelet Shannon entropy shrinks as expected. And this shrinkage is statistical meaningful according to statistical tests. Such a decrement in entropy can be the result of state transition of neuronal activity from disordered to more ordered as previously depicted in single trial entropy results.

Same statistical tests have been applied to CO_2 results. In Table 8, Friedman test results is given for CO_2 responses.

Table 8. Friedman test results for CO2

Test Statistics[a]

N	10
Chi-Square	15,200
df	2
Asymp. Sig.	,001

a. Friedman Test

After that, pairwise correlation of mean entropy in time windows has been analyzed with Wilcoxon test. Table 9 demonstrates the Wilcoxon test results for pairwise correlation of CO_2 of two distinct time windows. As a short information, Wilcoxon test is an alternative method to measured t-test, and it demonstrates the meaningfulness of the source of variation of entropy between two distinct time windows for each participant.

Table 9. Wilcoxon test results for CO2

Ranks

		N	Mean Rank	Sum of Ranks
TW2 – TW1	**Negative Ranks**	10[a]	5,50	55,00
	Positive Ranks	0[b]	,00	,00
	Ties	0[c]		
	Total	10		
TW3 – TW1	**Negative Ranks**	6[d]	5,00	30,00
	Positive Ranks	4[e]	6,25	25,00
	Ties	0[f]		
	Total	10		
TW3 – TW2	**Negative Ranks**	0[g]	,00	,00
	Positive Ranks	10[h]	5,50	55,00
	Ties	0[i]		
	Total	10		

Test Statistics[a]

	TW2- TW1	TW3- TW1	TW3- TW2
Z	-2,803[b]	-,255[b]	-2,803[c]
Asymp. Sig. (2-tailed)	,005	,799	,005

a. Wilcoxon Signed Ranks Test

b. Based on positive ranks.

c. Based on negative ranks.

As expected, there is a meaningful relationship between TW-2 and TW-3 and also TW-1 and TW-2, however, results shows there is not a meaningful relationship between mean entropy values found in TW-1 and TW-3. Statistical results display that the decrease of wavelet entropy is significant while transition from window-1 to window-2 where transition from a disordered state to a more ordered state and also, there is a significant entropy increase while transition from TW-2 to TW-3. Demonstration of relative energies for each averaged and single trial response suggest that, the state transition is governed by energy enhancement in delta band. Unlike the information depicted in [116], chemosensory evoked responses is shaped by means of delta oscillations in our findings.

It can be inferred that, decrease in complexity in brain functions might be the result of frequency stabilization through the instrument of given stimulus. Frequency stabilization or frequency tuning means that neural ensembles which participates in generation of evoked potentials, begin to oscillate in coherent way [116].

3.6.2. Wavelet Denoising Results

The fact that single trial activities contain both ongoing EEG oscillations and stimulus related activities together, it's hard to observe olfactory/trigeminal stimulus related potentials due to ongoing EEG oscillations. For this purpose, a common approach, conventional time domain averaging is applied to observe the modality dependent ERP/EP. However, averaging of many trials may not be a proper solution to acquire stimulus-specific oscillatory activities due to temporal jitter and many other reasons such as motor artifacts. In this sense, wavelet denoising (shrinkage) has been applied to averaged and single trial responses to obtain stimulus specific oscillations.

As a first step, we have obtained subject average responses for both olfactory (PEA) stimulations and trigeminal (CO_2) stimulations for denoising single trial responses. Denoising the average responses by using technique given in [119] also reveals the wavelet coefficients which carries stimulus related information in single trials responses. Our findings suggest that, stimulus related wavelet coefficients mostly locates in time interval 0-1.2 sec and 0-4 Hz. frequency band which corresponds to delta band. By using this set of wavelet coefficients helps to extract stimulus related oscillatory activity from single trial responses. For our analysis, we have adopted the automatic denoising technique given in [51, 119] to obtain stimulus related activity in single trial responses.

In second step, we tried to denoise subject average responses with the same technique detailed in [119]. We have employed biorthogonal spline 5.5 as recommended in [121] for wavelet denoising operation in both single trial and average responses. After the selection of mother wavelet, we have applied the algorithm which has been discussed in section 3.5. In sections 3.6.2.1 and 3.6.2.2, wavelet denoising results of both single trial and averaged activities will be given.

And finally, performance test of the wavelet denoising will be discussed by means of Spearman rank order correlation test.

In the final section, we have employed two subjects who are assumed to be hyposmic/anosmic due to their low TDI scores obtained from Sniffin' Stick test. Our aim is to demonstrate the robustness of the wavelet denoising for both EP+ and EP- case.

3.6.2.1. Single Trial Wavelet Denoising Results
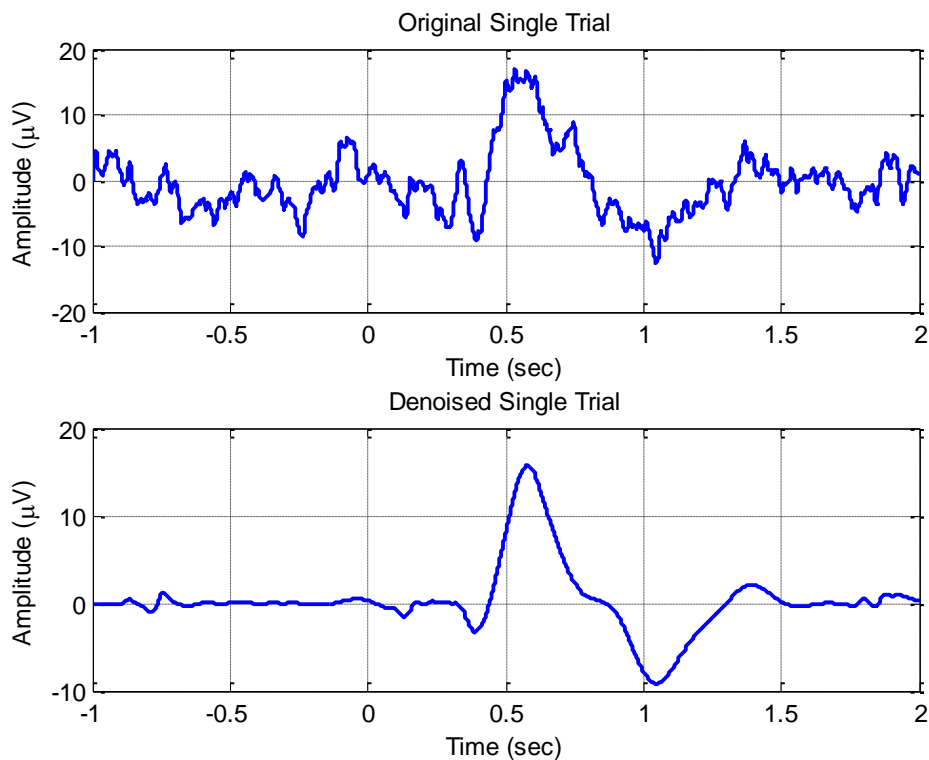
Figure 59. Original and Wavelet Denoised single trial-1 TEP of Subject-A

For single trial denoising, we have used totally 17 single trials for trigeminal and 14 single trials for olfactory responses. In Figures 59-62, 2 trigeminal and 2 olfactory original and denoised signals of Subject-A have been displayed. Graphical results shows that, wavelet denoising achieves to extract stimulus related activity with minimum amplitude degeneration. However in Figure 59, there is a small activity observed in prestimulus region for single trial-1. Such an activity might be due to movement artifact that exceeds the threshold level in denoising operation.
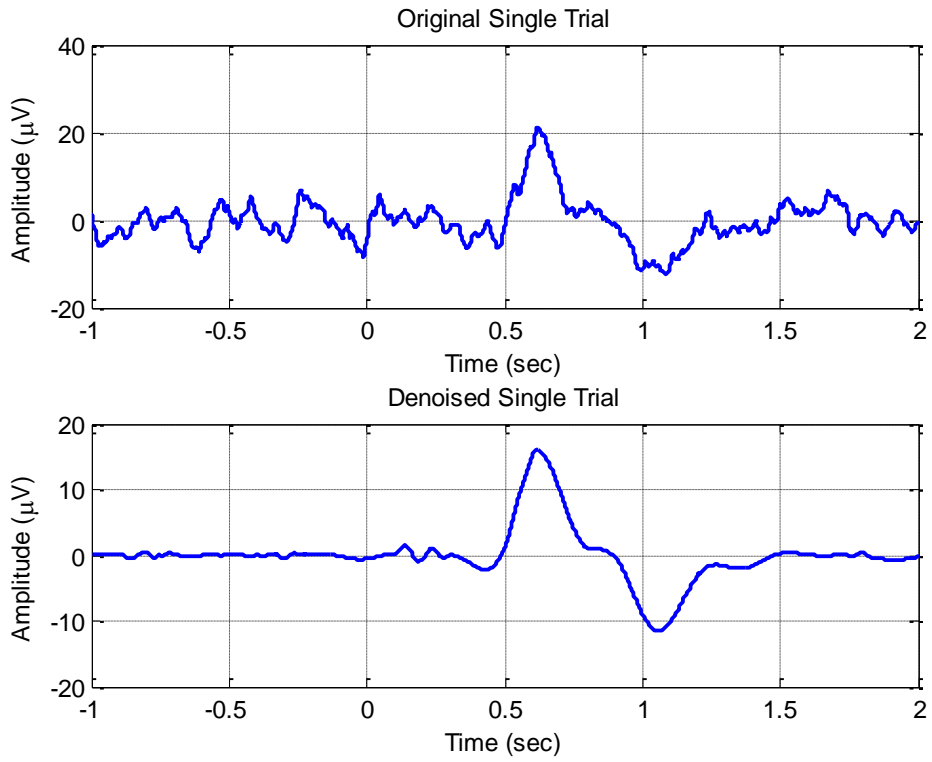
Figure 60. Original and Wavelet Denoised single trial-3 TEP of Subject-A
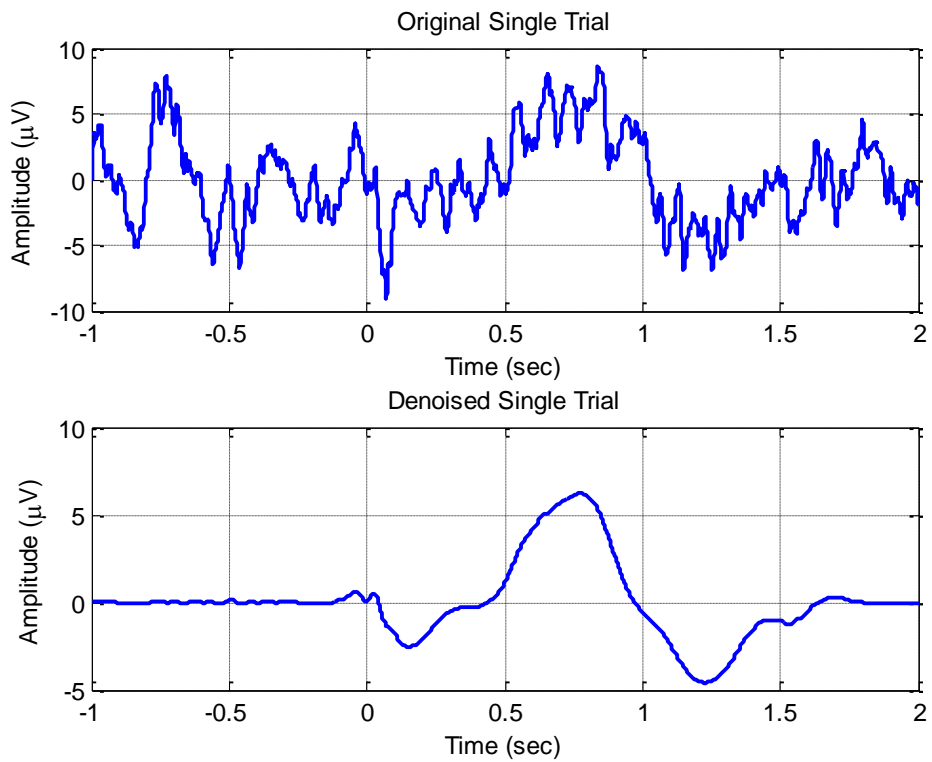
Figure 61. Original and Wavelet Denoised single trial-1 OEP of Subject-A
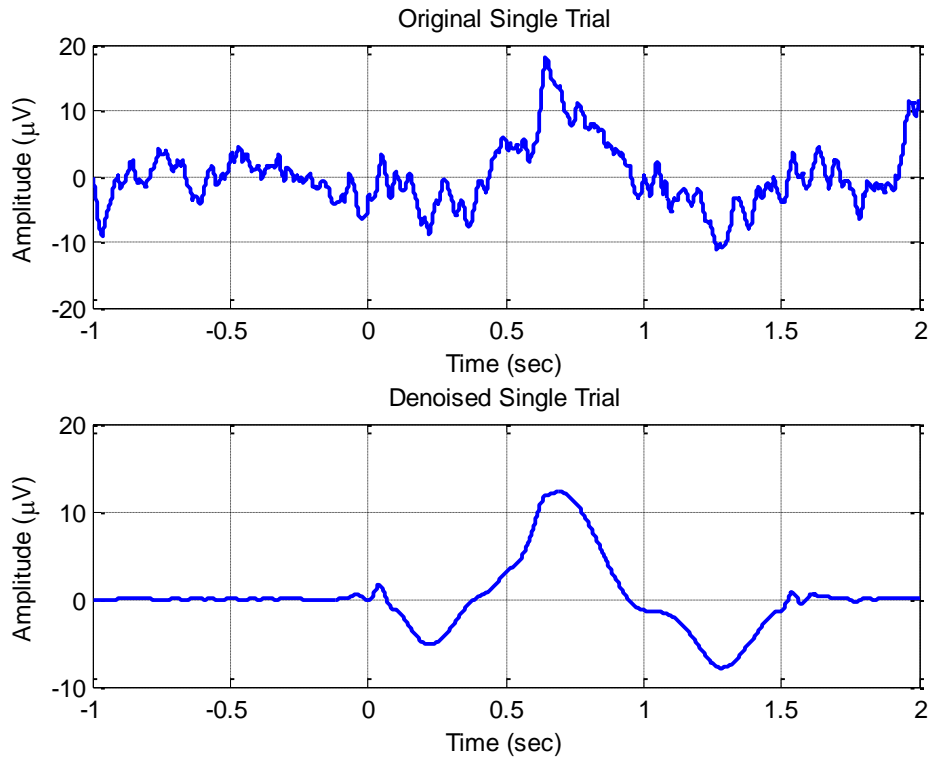
Figure 62. Original and Wavelet Denoised single trial-12 OEP of Subject-A

3.6.2.2. Wavelet Denoising Results of Averaged TEP/OEP

Besides the single trial, wavelet denoising is applicable to the averaged EP/ERP responses for both olfactory and trigeminal stimuli. Totally 24 participants average responses were used. For olfactory/trigeminal responses 12 subjects' average responses were collected. For each subject, with an average of 15 single trials have been recorded. Average of single trials have been demonstrated at upper side of figures.

In Figures 63-70, original and denoised responses has been given together to observe the alterations in signal after the denoising operation. At the end of this section, we have given the RMS values of time interval [0 1.2] seconds for original and resulting signal (see Table 10). And as a final step, to demonstrate the reliability of wavelet denoising, we have evaluated the denoising algorithm on two anosmic subjects' average PEA responses who don't have any ability to sense the smells.
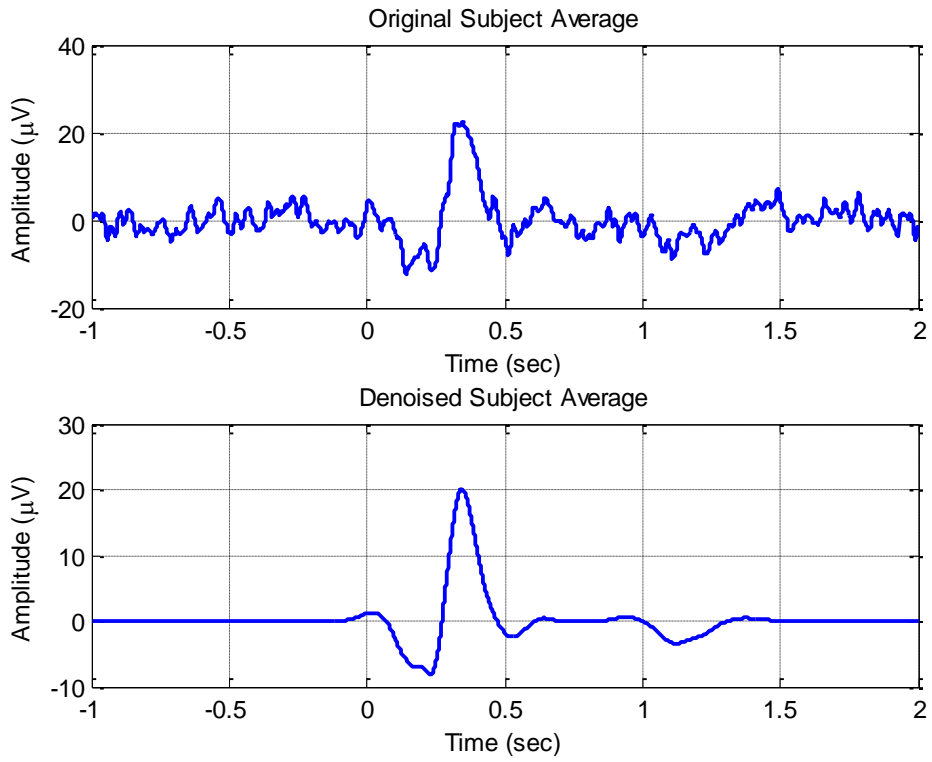
Figure 63. Original and Wavelet Denoised average TEP of Subject-1
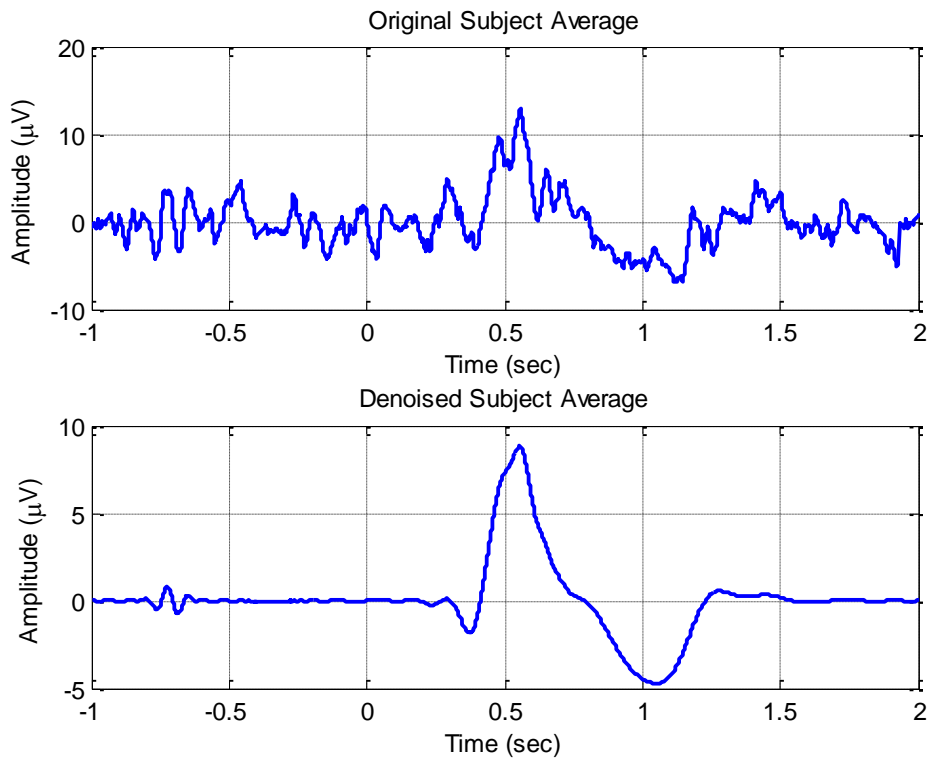
Figure 64. Original and Wavelet Denoised average TEP of Subject-11
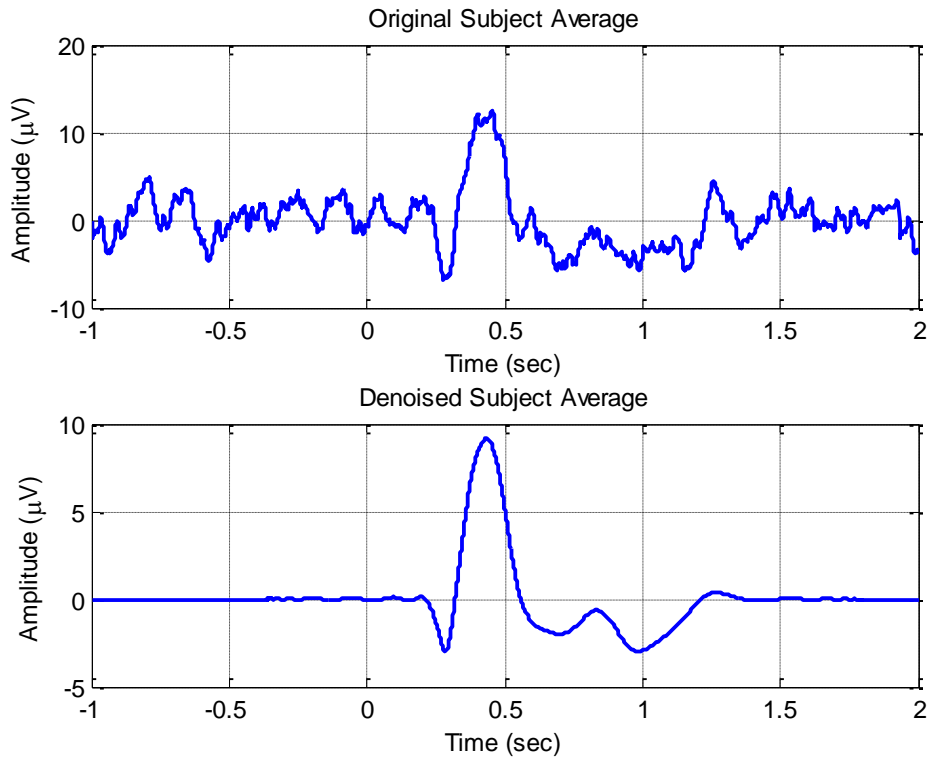
Figure 65. Original and Wavelet Denoised average TEP of Subject-2
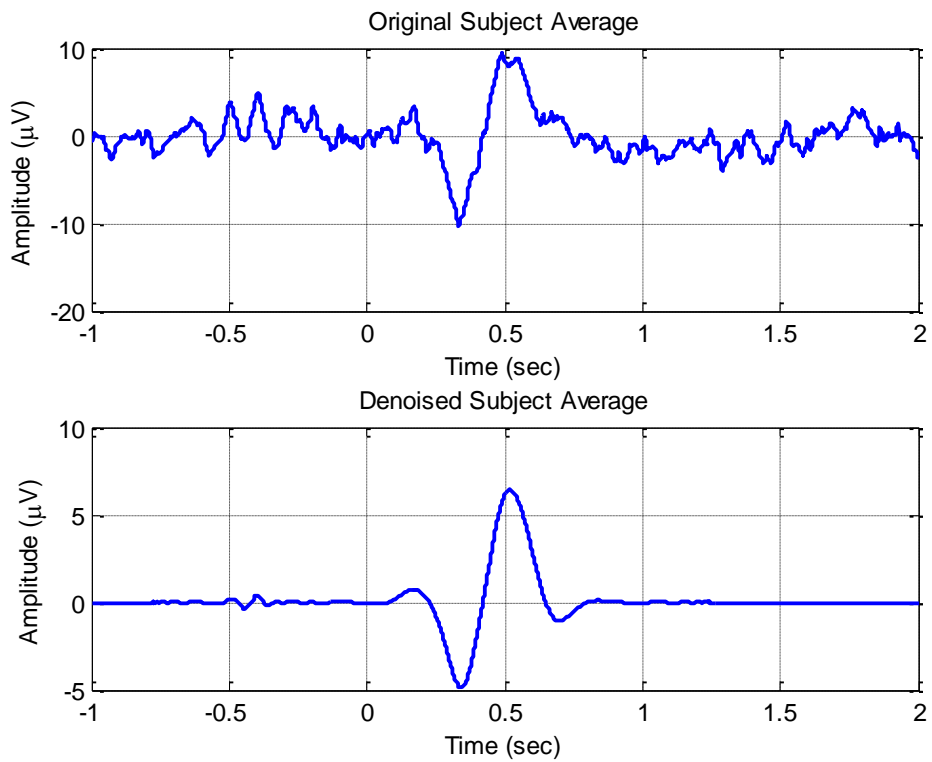
Figure 66. Original and Wavelet Denoised average TEP of Subject-7

For the averaged OEP, denoising results are given as follows,
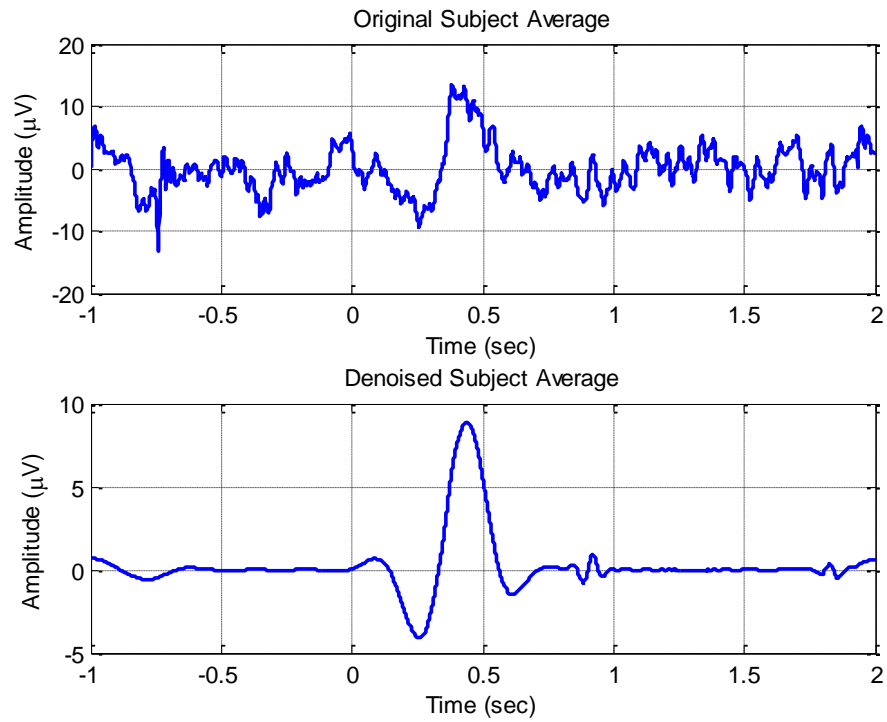
Figure 67. Original and Wavelet Denoised average OEP of Subject-13
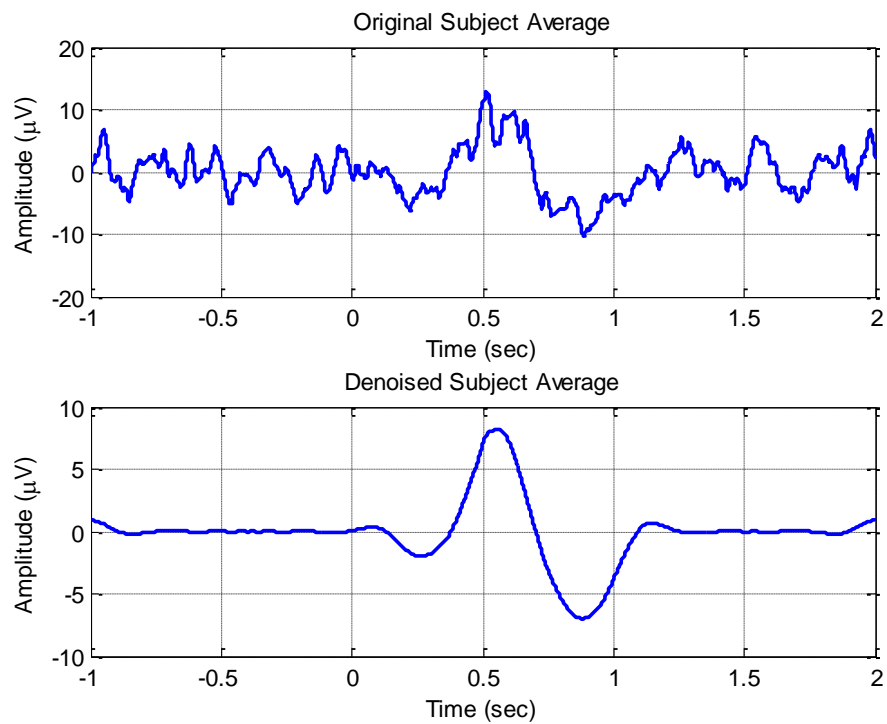
Figure 68. Original and Wavelet Denoised average OEP of Subject-16
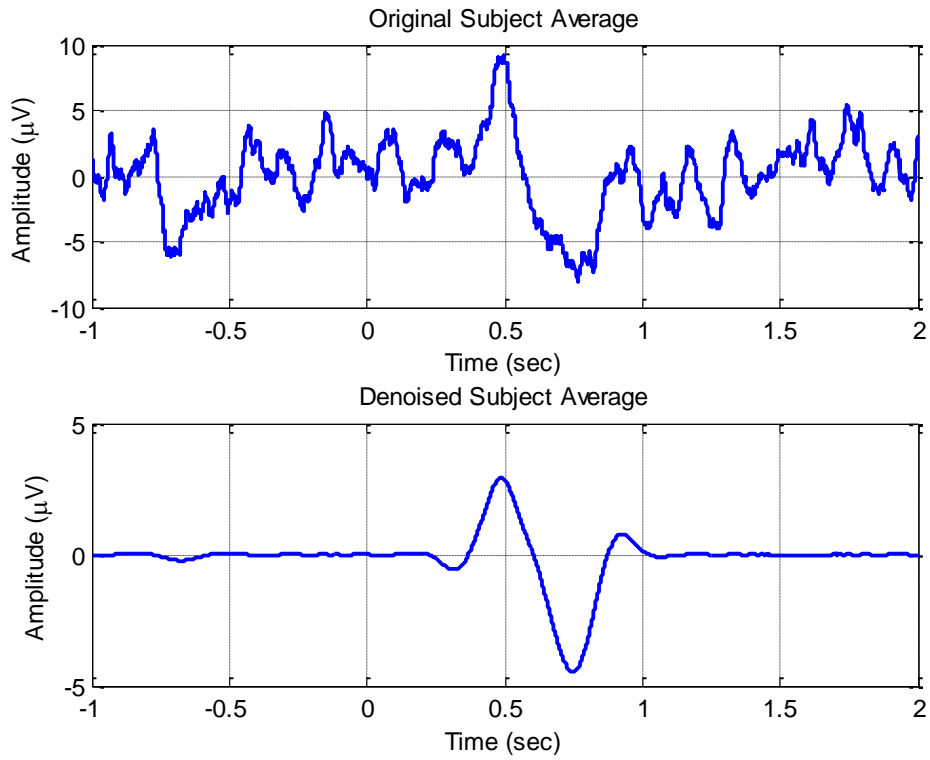
Figure 69. Original and Wavelet Denoised average OEP of Subject-17
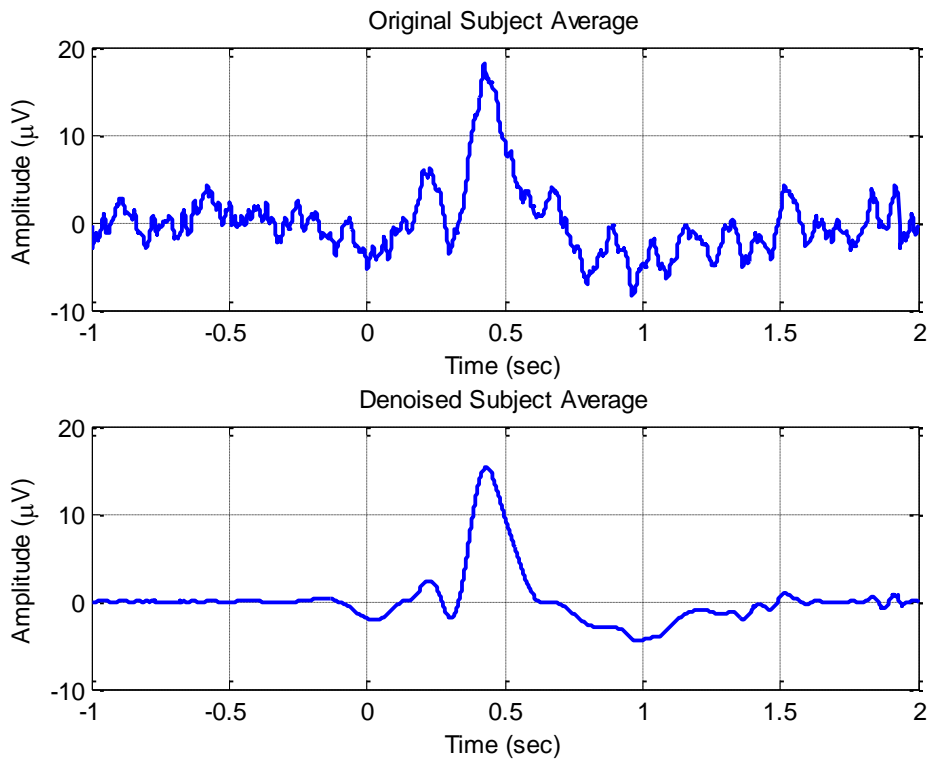
Figure 70. Original and Wavelet Denoised average OEP of Subject-15

Table 10. RMS values of original and wavelet denoised responses in time interval [0 1.2]

| Subject name	Original RMS [0 1.2]	De-noised RMS [0 1.2]
Subject-A		
Average of RMS values of 17 single trials for CO_2 response	5.3623	4.3690
Average of RMS values of 14 single trials for PEA response	5,0958	4.1807
Single Subject (CO_2)		
Subject-1	7.1915	5.7916
Subject-2	4.6576	3.1948
Subject-3	7.2328	6.4706
Subject-4	4.1226	2.3246
Subject-5	5.3681	1.9256
Subject-6	3.4068	2.2641
Subject-7	3.8270	2.3249
Subject-8	6.4893	5.3788
Subject-9	4.3037	3.0570
Subject-10	5.7642	3.1648
Subject-11	4.3308	3.4537
Subject-12	4.0132	2.9822
	Average=5.0590	*Average=3.5280*
SINGLE SUBJECT (PEA)		
Subject-13	4.8394	2.9350
Subject-14	3.6007	2.3527
Subject-15	5.8693	5.0898
Subject-16	5.1713	4.0904
Subject-17	3.6971	1.6666
Subject-18	6.3455	2.3527
Subject-19	7.0072	6.008
Subject-20	4.5985	3.1177
Subject-21	7.1465	6.0998
Subject-22	8.0462	6.2693
Subject-23	4.9371	3.2048
Subject-24	5.4672	4.8595
	Average=5.5605	*Average=4.0028*

For detailed analysis, calculated RMS values in time interval 0-1.2 sec in original and wavelet denoised signals have been analyzed by means of nonparametric Spearman rank order correlation test for both CO_2 and PEA stimulants separately. The reason of choosing the time interval 0-1.2 sec is, there will not be any stimulus related potentials found in posterior time instants. In Table 11 and Table 12, spearman rank order

correlation coefficient test results is given for PEA and CO_2 respectively. According to the PEA results, there is a very strong correlation have been found between RMS values of original and wavelet denoised signals for PEA stimuli ($p<0.01$, $r=.813$).

By looking at CO_2 results, Spearman rank order correlation test found quite strong correlation about .741 and also this correlation is nearly same as correlation found in PEA ($p<0.01$, $r=.741$). As a consequence, wavelet denoising is reasonably successful at both estimation of subject's PEA and CO_2 response.

Table 11. Spearman rank order correlation test result for PEA stimuli

Correlations

			Original RMS	Denoised RMS
Spearman's rho	**Original RMS**	Correlation Coefficient	1,000	,813**
		Sig. (1-tailed)	.	,000
		N	12	12
	Denoised RMS	Correlation Coefficient	,813**	1,000
		Sig. (1-tailed)	,001	.
		N	12	12

**. Correlation is significant at the 0.01 level (1-tailed).

Table 12. Spearman rank order correlation test results for CO2 stimuli

Correlations

			Original RMS	Denoised RMS
Spearman's rho	**Original RMS**	Correlation Coefficient	1,000	,741**
		Sig. (1-tailed)	.	,000
		N	12	12
	Denoised RMS	Correlation Coefficient	,741**	1,000
		Sig. (1-tailed)	,003	.
		N	12	112

**. Correlation is significant at the 0.01 level (1-tailed).

In the light of these results, it is fair to infer that, wavelet denoising is able to filter out the noisy component from signal with a minimum level of degeneration in amplitude and shape. By considering the property of time variant estimation of wavelet denoising, makes it a useful tool for stationary and nonstationary time series estimation.

To demonstrate the reliability of wavelet denoising, we employed two anosmic subjects who couldn't exactly sense the given n-butanol in Sniffin' Stick tests. Applying wavelet denoising to their averaged PEA response elicited no significant chemosensory evoked potentials.
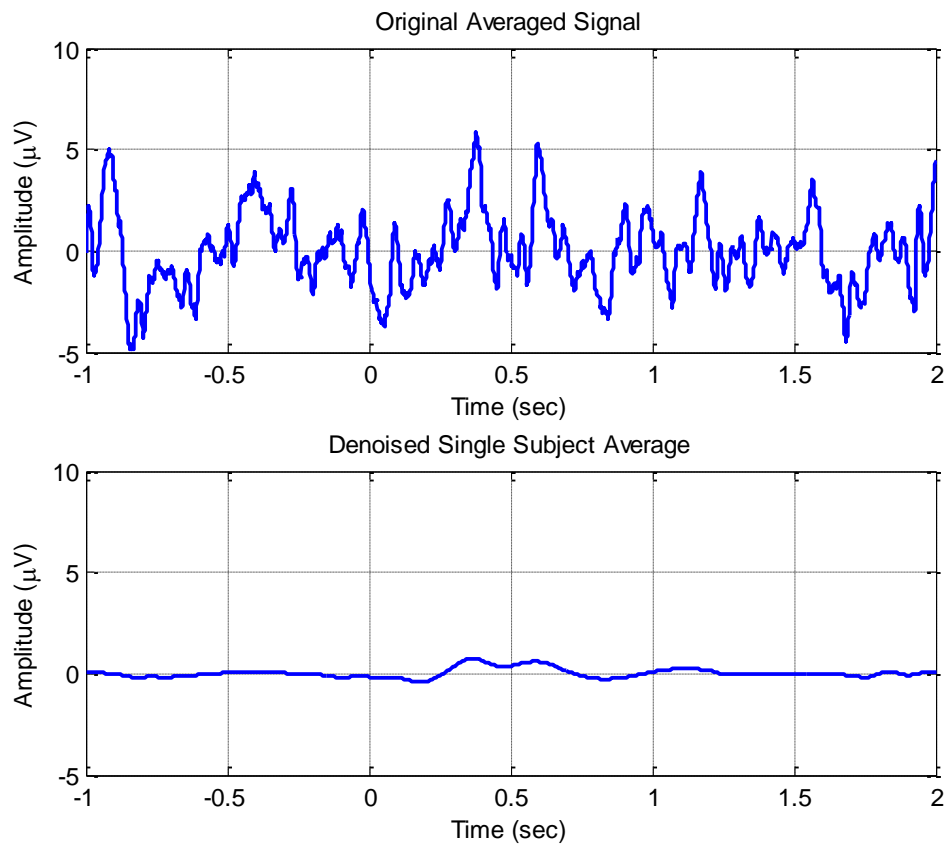
Figure 71. Original and Wavelet Denoised average OEP of Subject-K1
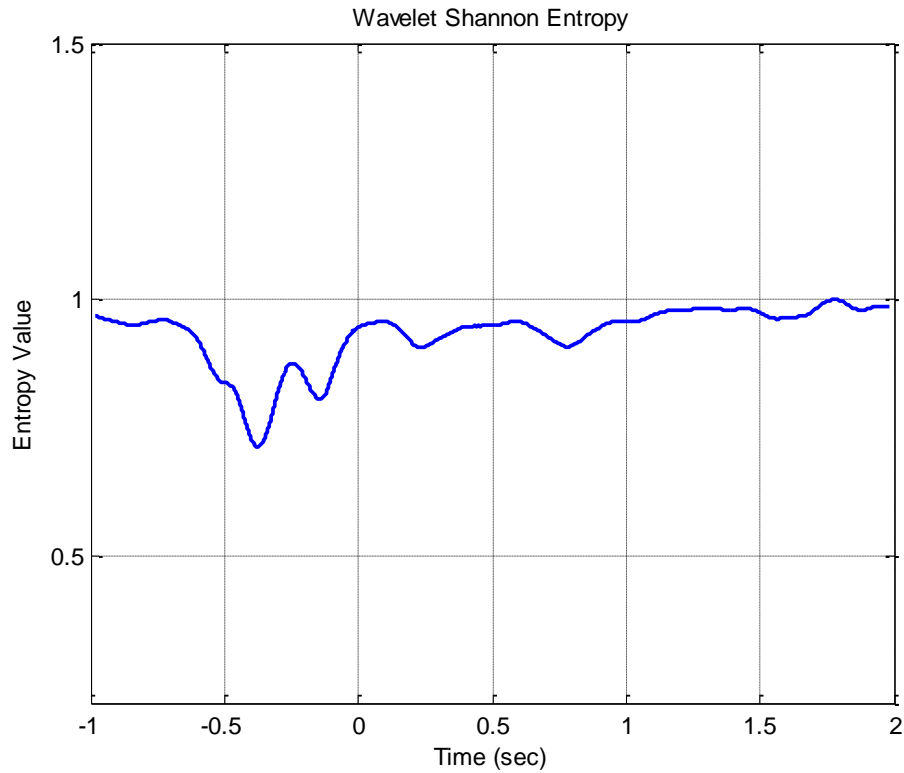
Figure 72. Time evolution of wavelet Shannon entropy result of Subject-K1

By looking at the Figure 71, there is an extremely small activity observed in the time interval between 0-1.2 seconds. And also, we have applied wavelet Shannon entropy to observe the degree of disorder between regions of prestimulus, stimulus onset and post stimulus. There is a significant entropy decrease in prestimulus region in Figure 72. We are ensure that, such a decrease is not related with chemosensory stimuli. Looking at the post stimulus region, no significant entropy decrease have been found for Subject-K1.
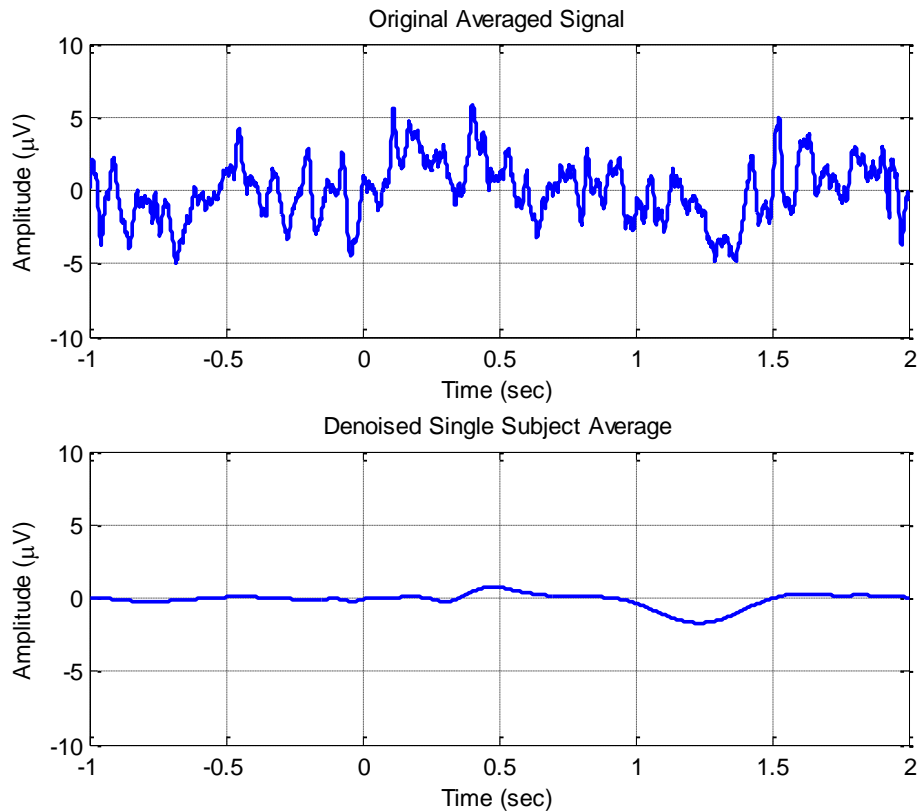
Figure 73. Original and Wavelet Denoised average OEP of Subject-K2

In Figure 73 and Figure 74, averaged and denoised PEA response and wavelet entropy result of Subject-K2 is given respectively. Same as the findings obtained from Subject-K1, there is no significant evoked potentials and no meaningful entropy decrease have been obtained through the instrument of wavelet denoising. Like in Figure 71, Figure 73 displays a small activity observed in Subject-K2 in time interval 0-1.2 seconds.

Wavelet entropy results displays that there is no significant power enhancement in any frequency band and/or there is no frequency stabilization between neural structures. In the light of these findings, it can be inferred that, both of two subjects might be suffers from an olfactory dysfunction or sino-nasal pathologies.
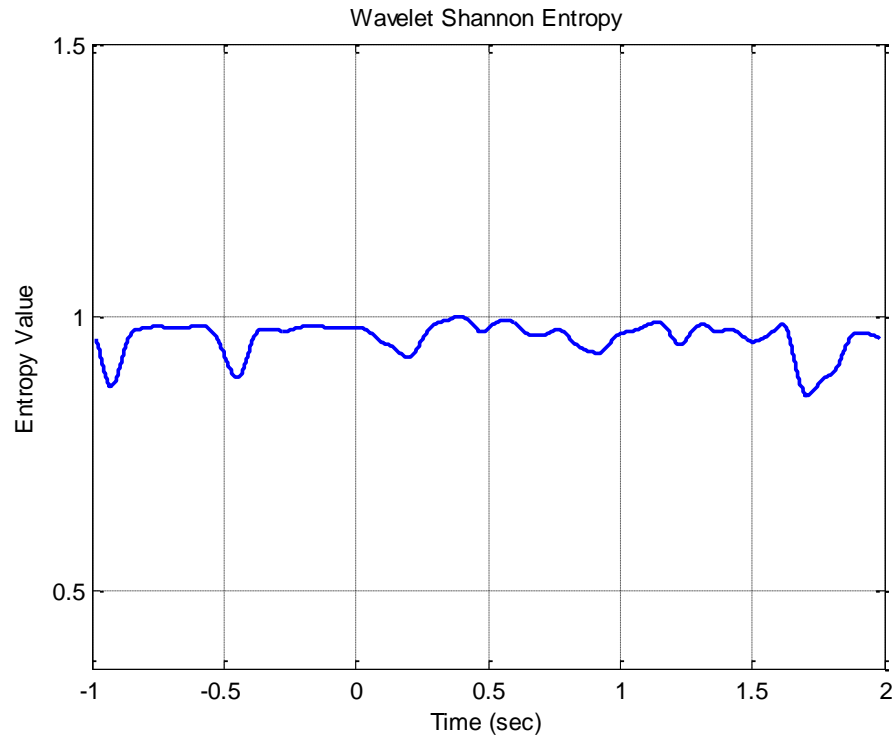
Figure 74. Time evolution of wavelet Shannon entropy result of Subject-k2

In the next chapter, we will demonstrate how wiener filter extracts evoked potentials from averaged and single trial EEG responses and success rate will be discussed by means of comparing the findings with wavelet denoising.

CHAPTER 4

WIENER FILTER

Wiener filters are known as class of optimum linear filters which is developed by Norbert Wiener in 1949 [122]. Wiener filters can be used in noise filtering, channel equalization, joint process estimation, and smoothing and echo cancelation.

In theory, Wiener filters regard the corresponding input signal as Wide Sense Stationary (WSS) process. A useful approach for optimal filter design is minimization of mean square error signal that is defined as the difference between target response and actual response of the filter. In particular, two main restrictions have been placed so far,

1. Assuming the filter is linear, however, it makes easier to analyze with mathematical operations.

2. Operation of the filter is in discrete time. It is possible to realize it using digital hardware and software.

4.1. Minimum Mean Square Error Estimation

Filter coefficients are represented by w that takes input signal $u(n)$ and estimates the output signal $y(n)$.
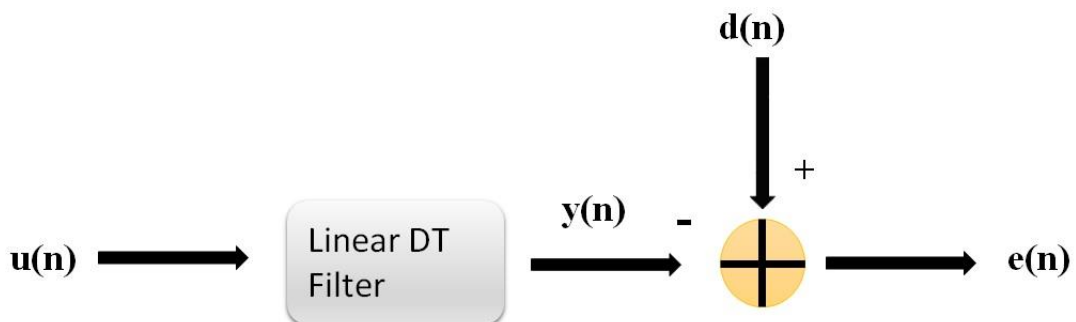
Figure 75. Block diagram of linear discrete time filter [123]

In Figure 75, $y(n)$ is actual output and $d(n)$ is target response of the filter. Input-output relation for an FIR filter is given in eq. (4.1),

$$y(n) = \sum_{k=0}^{M-1} w_k^* \, u(n-k) \tag{4.1}$$

where $y(n) \in \mathbb{R}^N$ is the actual output, w_k's are the filter coefficients and * denotes the complex conjugate. Equation (4.1) can be written in more compact form,

$$Y = w^T U \tag{4.2}$$

In equation (4.2), Y and U represents the vectorial demonstration of output $y(n)$ and delayed input $u(n-k)$, w^T is the filter coefficients. Main purpose is to minimize the estimation error as much as possible. In this manner, error signal $e(n)$ is defined as follows,

$$
\begin{aligned}
e(n) &\triangleq d(n) - y(n) \\
&= d(n) - w^T U
\end{aligned}
\tag{4.3}
$$

Equation (4.3) can be written in a more detailed form in order to demonstrate the relation between error signals and filter coefficients,

$$
\begin{pmatrix} e(0) \\ e(1) \\ e(2) \\ \vdots \\ e(N-1) \end{pmatrix} = \begin{pmatrix} d(0) \\ d(1) \\ d(2) \\ \vdots \\ d(N-1) \end{pmatrix} - \begin{pmatrix} u(0) & \cdots & u(1-P) \\ u(1) & \cdots & u(2-P) \\ \vdots & \cdots & \vdots \\ u(N-1) & \cdots & u(N-P) \end{pmatrix} \begin{pmatrix} w_0 \\ w_1 \\ \vdots \\ w_{P-1} \end{pmatrix} \tag{4.4}
$$

In equation (4.3), $d(n)$ is defined as the desired (target) response. Equation (4.4) gives the matrix representation of equation (4.3). In here, number of signal samples and number of filter coefficients are demonstrated with N and P. If N=P, we have a square signal matrix and there exists unique solution with zero estimation error $e(n)$, if $N < P$, there exists infinite number of solutions with zero estimation error and such an equation is said to be underdetermined. In case of over-determined, number of samples N is greater than number of filter coefficients P (N>P).

Optimization of the filter coefficients is achieved by minimum mean square value estimation of error signal. Selection of the criterion function is thought as,

$$J = E[e(n)\, e^*(n)] \tag{4.5}$$

where $E\{.\}$ denotes the expected value. Thus, problem is converted to search of conditions by which the cost function J reaches its minimum value. Let the filter coefficients are consist of real and imaginary part as follows,

$$w_k = a_k + jb_k \qquad k = 0,1,2,\dots \tag{4.6}$$

Utilizing the gradient operator, we can obtain the stationary points of the cost function. At these specific points, real and imaginary components of gradient vector ∇J is equal to zero.

$$\nabla_k J = \frac{\partial J}{\partial a_k} + j\frac{\partial J}{\partial b_k} = 0 \quad for\ k = 0,1,2,\dots \tag{4.7}$$

Under such condition, the filter is said to be optimal in sense of mean square error [124]. By substituting (4.5) into (4.7) we get,

$$\nabla_k J = E\left[\frac{\partial e(n)}{\partial a_k}e^*(n) + \frac{\partial e^*(n)}{\partial a_k}e(n) + j\frac{\partial e(n)}{\partial b_k}e^*(n) + j\frac{\partial e^*(n)}{\partial b_k}e(n)\right] \tag{4.8}$$

After performing the partial derivatives with respect to filter parameters a_k and b_k, equation (4.8) becomes,

$$\nabla_k J = -2E[u(n-k)\, e^*(n)] \tag{4.9}$$

The equation (4.9) is obtained in the following form by using the optimum error signal that can be obtained by when the filter operates at optimal conditions and is denoted by,

$$\nabla_k J = E[u(n-k)\, e_o^*(n)] = 0 \tag{4.10}$$

In other words, for the requirement of optimality, the error signal should be orthogonal to filter input described by $u(n)$. This constitutes the principle of

orthogonality for the conditions of optimal filtering. Equation (4.10) can be rearranged as,

$$E\left[\sum_{k=0}^{\infty} w_k^* \, u(n-k)e_o^*(n)\right] = E[y(n) \, e_o^*(n)] \qquad (4.11)$$

and as a natural result of (4.11), the following equation can be obtained by using the linearity property of expected value operator, we will obtain,

$$E[y(n) \, e_o^*(n)] = 0 \qquad (4.12)$$

By looking at equations (4.11) and (4.12), it can be easily seen that, the optimal error signal $e_o(n)$ is also orthogonal to actual response of the filter $y(n)$ as filter input $u(n)$ given in equation (4.10).

4.2. Wiener-Hopf Equations

In the section 4.1, the sufficient and necessary conditions for optimal filtering. By utilizing the eq. (4.1) and (4.3) into (4.10) we obtain,

$$E\left[u(n-k)\left(d^*(n) - \sum_{m=0}^{\infty} w_{0m} \, u^*(n-m)\right)\right] = 0 \qquad (4.13)$$

Reorganization of equation (4.13) yields

$$\sum_{m=0}^{\infty} w_{om} \, E[u(n-k) \, u^*(n-m)] = E[u(n-k) \, d^*(n)] \qquad (4.14)$$

The above equation is rearranged as follows by using the autocorrelation function of delayed input with a lag of $k - m$, $E[u(n-k) \, u^*(n-m)]$ in the left hand-side and the cross correlation function of the filter input and target output in the right hand-side, the Wiener-Hopf equation is given as,

$$\sum_{m=0}^{\infty} w_{om} \, R_{uu}(k-m) = R_{ud}(-k) \tag{4.15}$$

Vector notation of Wiener-Hopf equation is given as,

$$R_{uu} w_o = R_{ud} \tag{4.16}$$

where $R_{uu} \in \mathbb{R}^{MxM}$ is the autocorrelation matrix of input of the filter and it is demonstrated as,

$$R_{uu} = \begin{bmatrix} r_{uu}(0) & r_{uu}(1) & \dots & r_{uu}(M-1) \\ r_{uu}(-1) & r_{uu}(0) & \dots & r_{uu}(M-2) \\ \vdots & \vdots & \dots & \vdots \\ r_{uu}(1-M) & r_{uu}(2-M) & \dots & r_{uu}(0) \end{bmatrix} \tag{4.17}$$

And $R_{ud} \in \mathbb{R}^M$ is the vector of the cross-correlation between filter input and desired response,

$$R_{ud} = [r_{ud}(0), r_{ud}(-1), \dots, r_{ud}(1-M)]^T \tag{4.18}$$

Finally w_o is the optimal filter weight vector can be obtained by solving the equation (4.16),

$$w_o = R_{uu}^{-1} \, R_{ud} \tag{4.19}$$

4.3. Error-Performance Surface

Estimation error for the FIR case that is given in eq. (4.3),

$$e(n) = d(n) - \sum_{k=0}^{M-1} w_k^* \, u(n-k) \tag{4.20}$$

Putting the eq. (4.20) into (4.5), it yields,

$$J = E[|d(n)|^2] - \sum_{k=0}^{M-1} w_k^* \, E[u(n-k) \, d^*(n)] - \sum_{k=0}^{M-1} w_k \, E[u^*(n-k) \, d(n)]$$

$$+ \sum_{k=0}^{M-1}\sum_{i=0}^{M-1} w_k^* \, w_i \, E[u(n-k)u^*(n-i)] \qquad (4.21)$$

By considering the equivalent form of expectation values in (4.21), we can reorganize this equation as,

$$J = \sigma_d^2 - \sum_{k=0}^{M-1} w_k^* \, R_{ud}(-k) - \sum_{k=0}^{M-1} w_k^* \, R_{ud}^*(-k) + \sum_{k=0}^{M-1}\sum_{i=0}^{M-1} w_k^* \, w_i \, R_{uu}(i-k) \quad (4.22)$$

where σ_d denotes the variance of desired response whose mean value equals to zero. For the minimum point of the error performance surface, the cost function J takes its minimum value which is denoted by J_{min}. At this specific point, the gradient of the cost function equals to zero,

$$\nabla_k J = 0 \qquad for \; k = 0,1,2, \dots \qquad (4.23)$$

By inserting the equation (4.22) into (4.23), we can obtain,

$$\nabla_k J = -2R_{ud}(-k) + 2 \sum_{i=0}^{M-1} w_i \, R_{uu}(i-k) = 0 \qquad (4.24)$$

$$R_{ud}(-k) = \sum_{i=0}^{M-1} w_i \, R_{uu}(i-k) \qquad (4.25)$$

Finally, taking into consideration of the optimal filtering requirements, we can denote the transversal filter with optimum weights,

$$\sum_{i=0}^{M-1} w_{oi} \, R_{uu}(i-k) = R_{ud}(-k) \qquad (4.26)$$
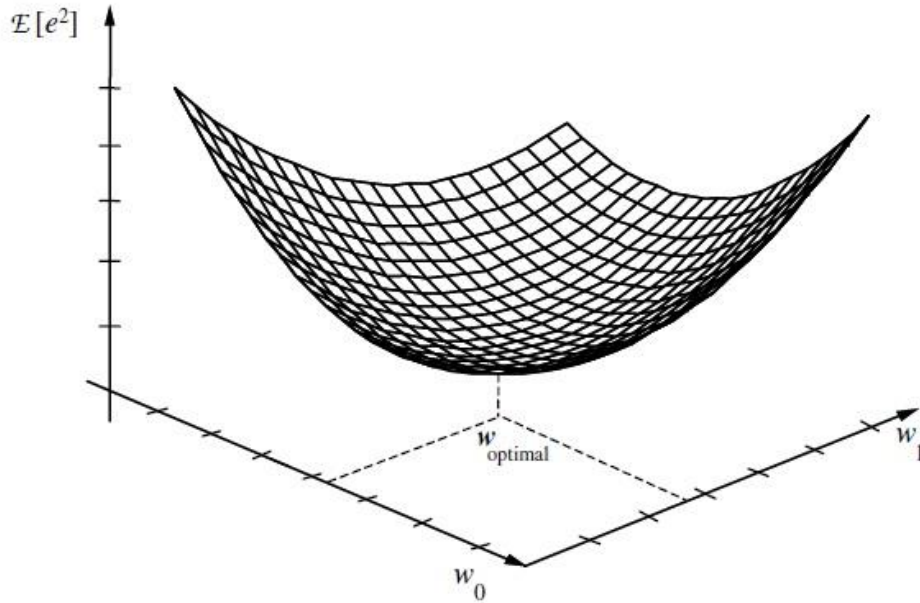
Figure 76. Error-Performance Surface of two dimensional filter [123]

4.4. Formulation of Wiener Filters in Frequency Domain

Consider a situation where $y(n)$ is the summation of target output $x(n)$ and noise $\Gamma(n)$.

$$y(n) = x(n) + \Gamma(n) \tag{4.27}$$

In frequency domain, relation between the filter's actual output $\hat{x}(n)$ and observation $y(n)$ can be represented as [123],

$$\hat{X}(f) = W(f)Y(f) \tag{4.28}$$

where $W(f)$ denotes the filter transfer function in frequency domain. The estimation error in frequency domain $E(f)$ is the difference between frequency domain representations of target response $X(f)$ and actual response $\hat{X}(f)$.

$$E(f) = X(f) - \hat{X}(f) \tag{4.29}$$

$$E(f) = X(f) - W(f)Y(f) \tag{4.30}$$

And also, mean square error is defined in frequency domain is as follows,

$$E[|E(f)|^2] = E[(X(f) - W(f)Y(f))^*(X(f) - W(f)Y(f))]$$ (4.31)

Attainment of the least square error achieved by differentiation of the mean square error with respect to $W(f)$,

$$\frac{\partial E[|E(f)|^2]}{\partial W(f)} = 2W(f)S_{yy}(f) - 2S_{xy}(f)$$ (4.32)

In equation (4.32), $S_{yy}(f)$ and $S_{xy}(f)$ are spectral and cross-power spectrum of $X(f)$ and $Y(f)$ respectively. At the minimum point, partial derivative is equal to zero.

$$2\big(W(f)S_{yy}(f) - S_{xy}(f)\big) = 0$$ (4.33)

By rearranging the equation (4.33) we can obtain the filter transfer function as follows,

$$W(f) = \frac{S_{xy}(f)}{S_{yy}(f)}$$ (4.34)

Since noise and the signal are assumed to be uncorrelated (i.e. $R_{x\Gamma}(n) = 0$ and $R_{xy} = R_{xx}$), we can obtain,

$$R_{yy}(n) = R_{xx}(n) + R_{\Gamma\Gamma}(n)$$ (4.35)

Thus, filter transfer function becomes

$$W(f) = \frac{S_{xx}(f)}{S_{xx}(f) + S_{\Gamma\Gamma}(f)}$$ (4.36)

4.5. Results

In this section, we have utilized wiener filters to obtain stimulus related oscillatory activities which is embedded in ongoing EEG. For this purpose, we have considered grand average as target response for both single trial and single subject (i.e. averaged) analysis.

4.5.1. Single Trial OEP/TEP Extraction by Using Wiener Filters

Figure 77. Original and Wiener filtering result of single trial-1 TEP of Subject-A

Figure 78. Original and Wiener filtering result of single trial-3 TEP of Subject-A

Figure 79. Original and Wiener filtering result of single trial-1 OEP of Subject-A
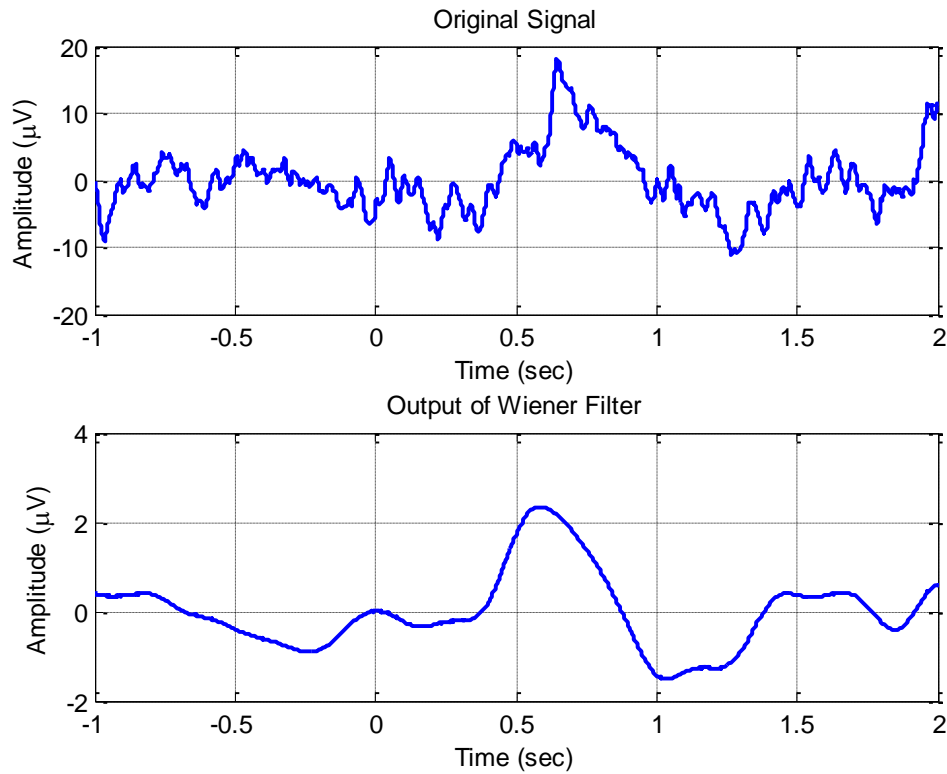
Figure 80. Original and Wiener filtering result of single trial-12 OEP of Subject-A

In order to extract single trial responses of subjects, we have utilized grand average of responses as desired (i.e. target) response. Briefly, grand average is the average of all subjects' average responses. In Figures 77-80, original and filtering results can be seen together and it can be seen in Table 13, average of 17 CO_2 single trial RMS values between 0-1.2 second is 5.3623 and wiener filtered signals RMS value is 0.7938. It can be fair to say that Wiener filter eliminates the huge amount of signal power. And for the PEA case, average RMS value of 14 single trial between 0-1.2 second is 5.0958 and filtered single trial RMS value is 0.9614 which is slightly higher than CO_2 case. To sum up, it can be inferred that, Wiener filter is more successful at filtering of brain's PEA responsiveness than CO_2. But when considering the RMS results of both PEA and CO_2 case, there is a dramatic power loss when eliminating the noise (i.e. stimulus unrelated activity). In the literature, there is not any recent study that have utilized Wiener filters so that we couldn't have any chance to compare our findings. In the next section, we have tried to filter subjects' averaged TEP/OEP responses.

4.5.2. Extraction of Average OEP/TEP by Using Wiener Filters
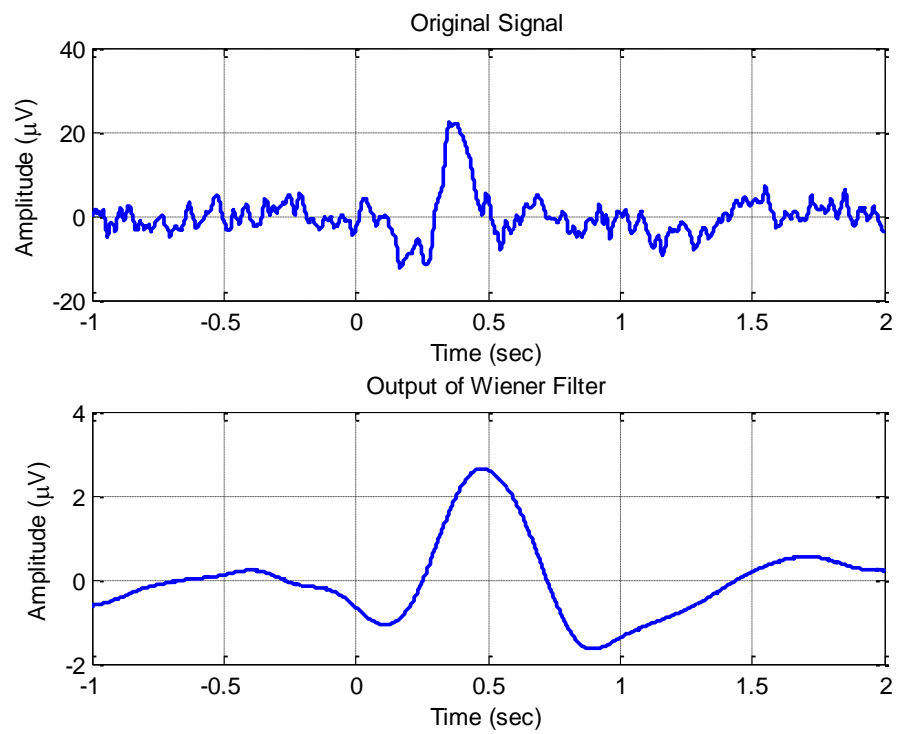
Figure 81. Original and Wiener filtering result of average TEP of Subject-1
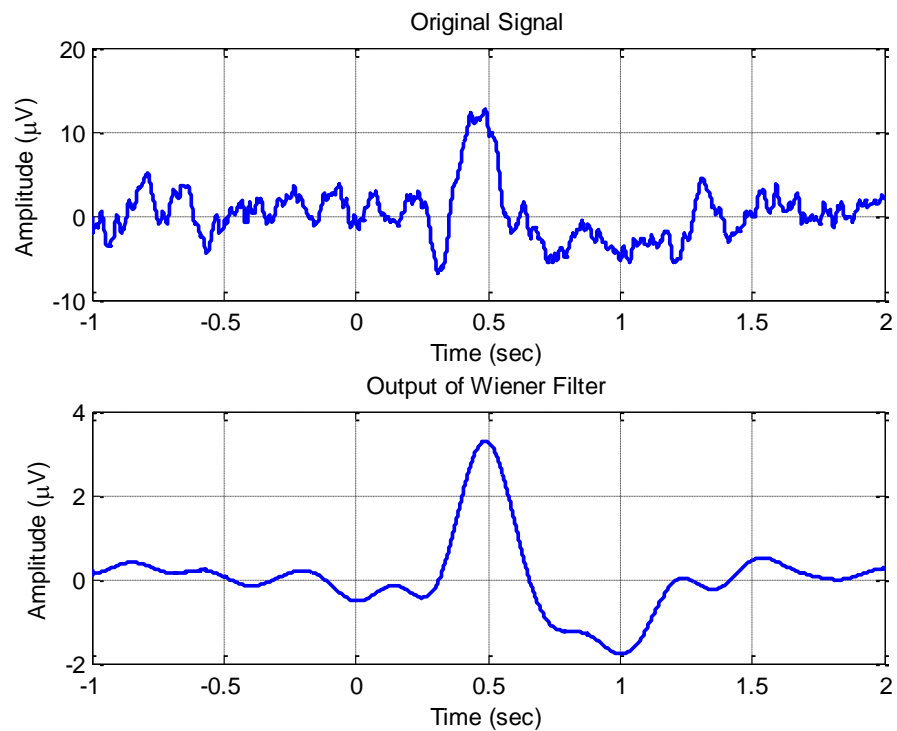
Figure 82. Original and Wiener filtering result of average TEP of Subject-2
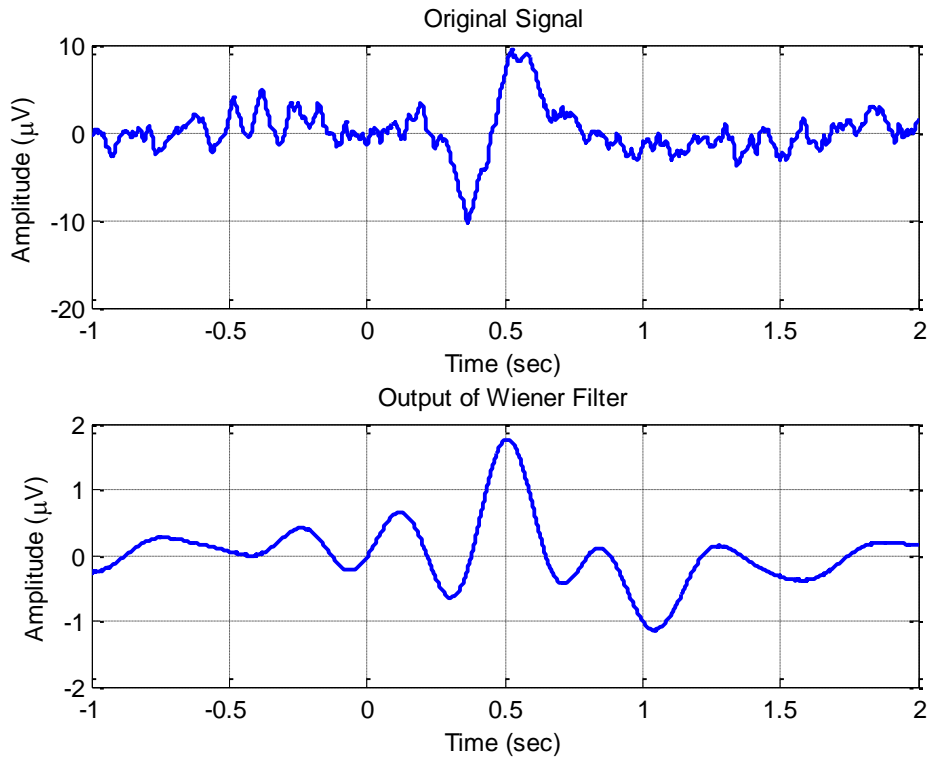
Figure 83. Original and Wiener filtering result of average TEP of Subject-7
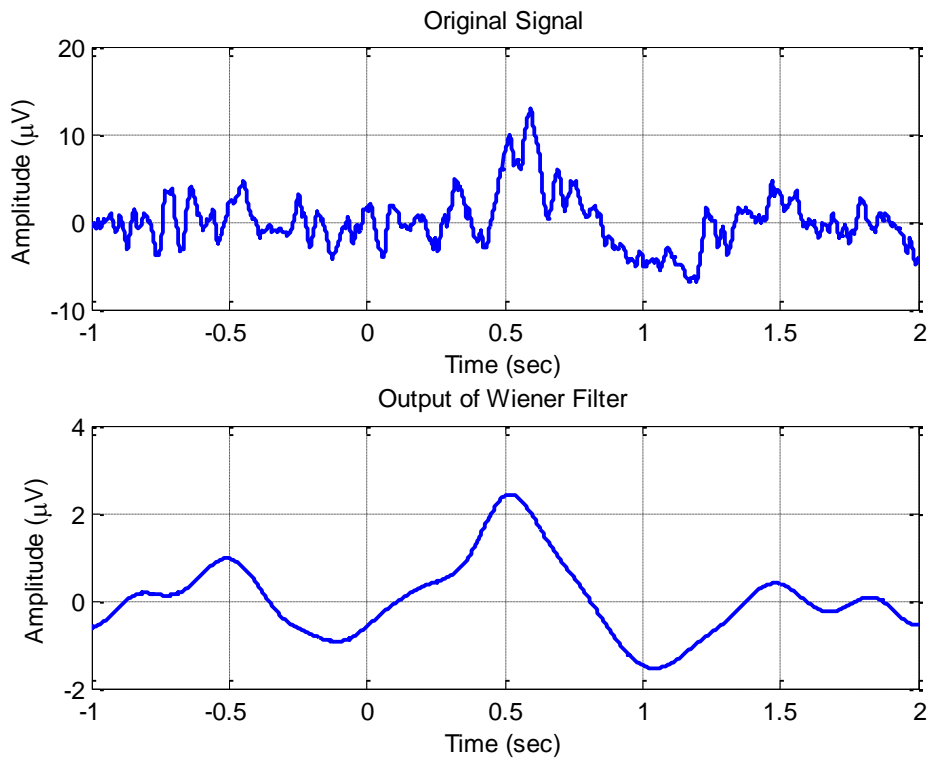
Figure 84. Original and Wiener filtering result of average TEP of Subject-11
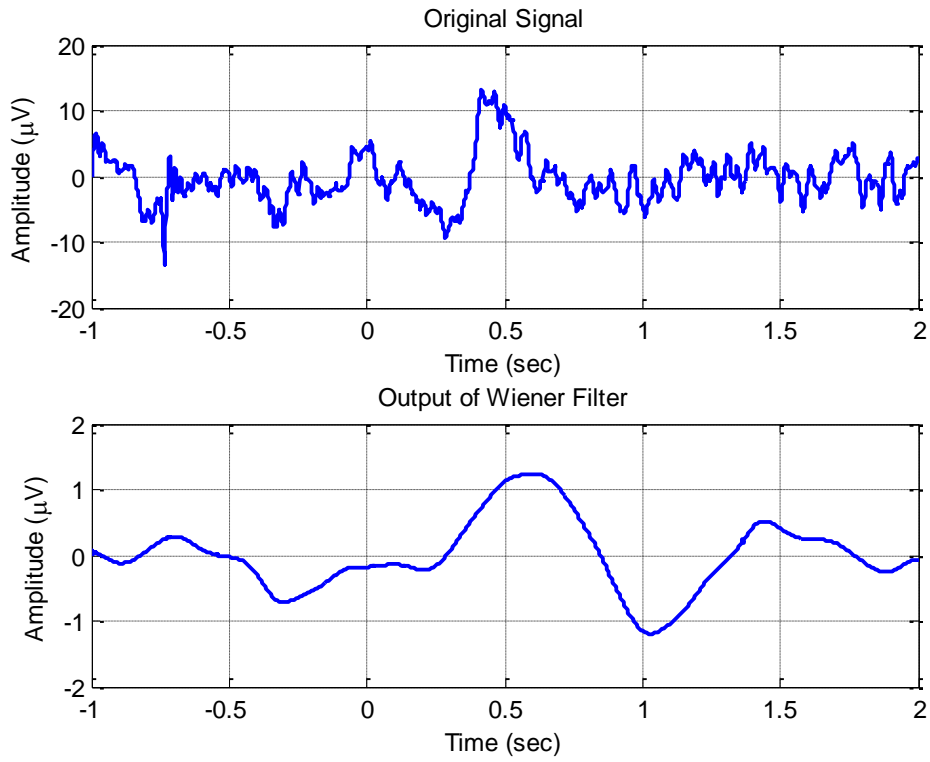
Figure 85. Original and Wiener filtering result of average OEP of Subject-13
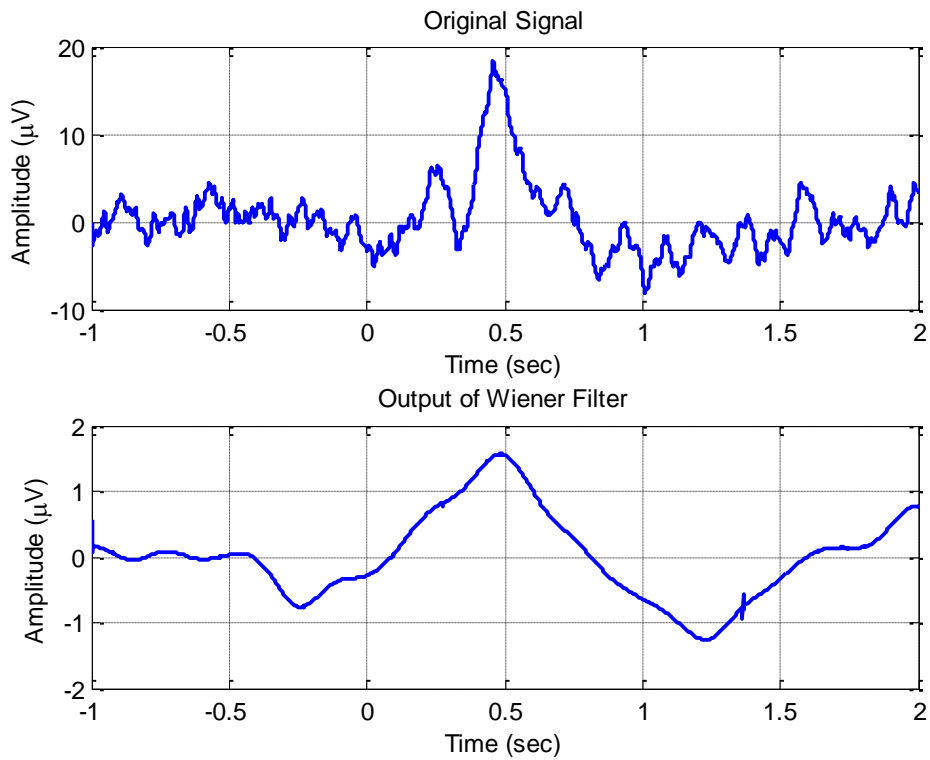
Figure 86. Original and Wiener filtering result of average OEP of Subject-15
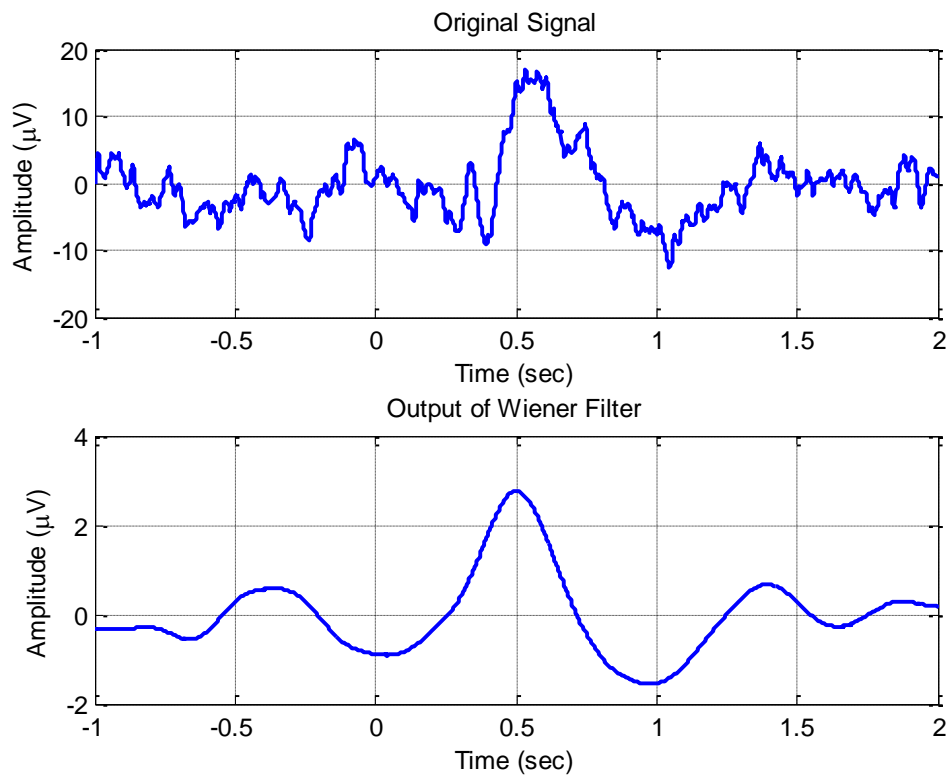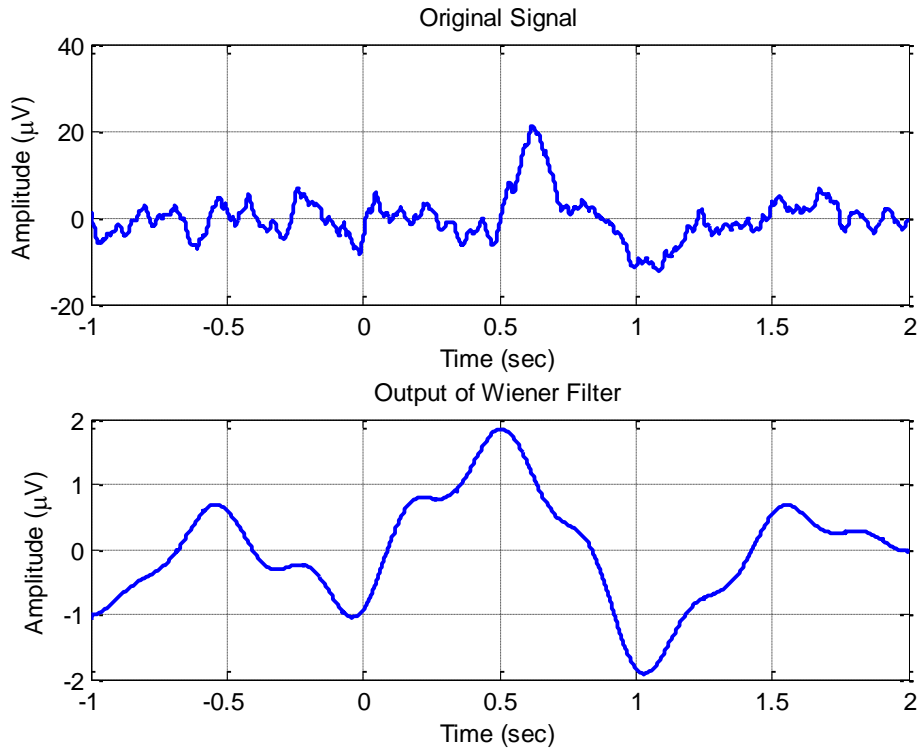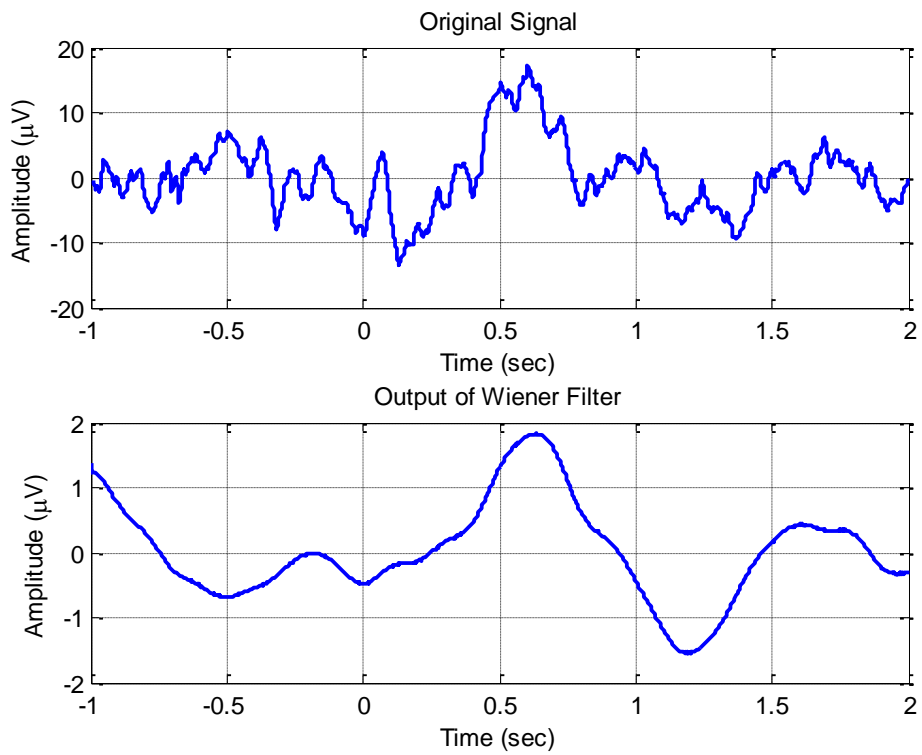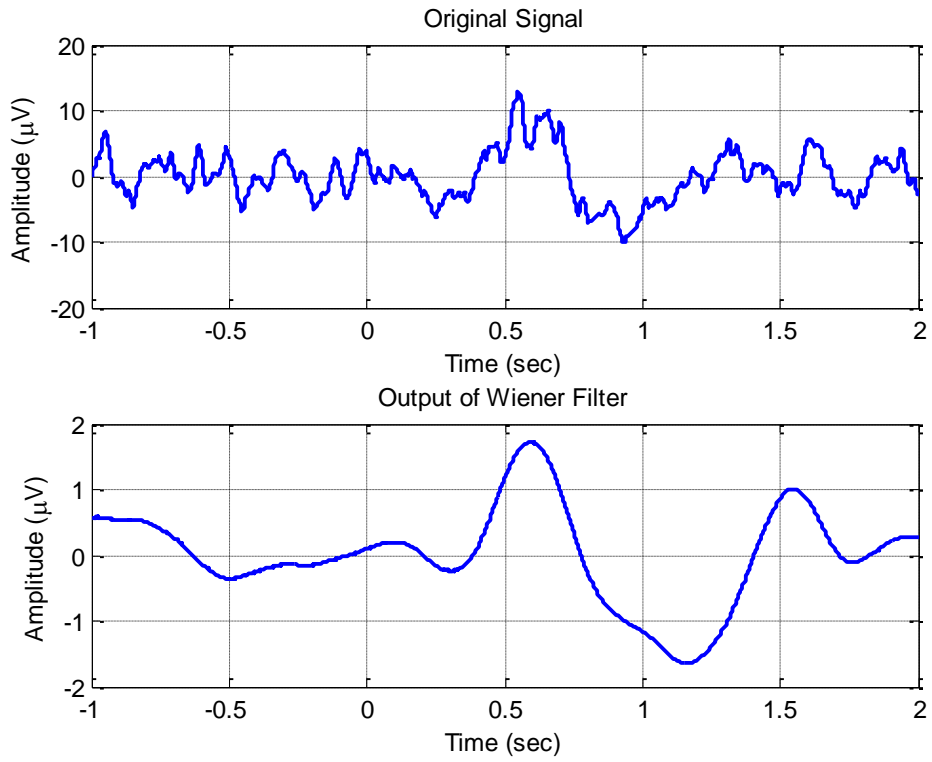
Figure 87. Original and Wiener filtering result of average OEP of Subject-16
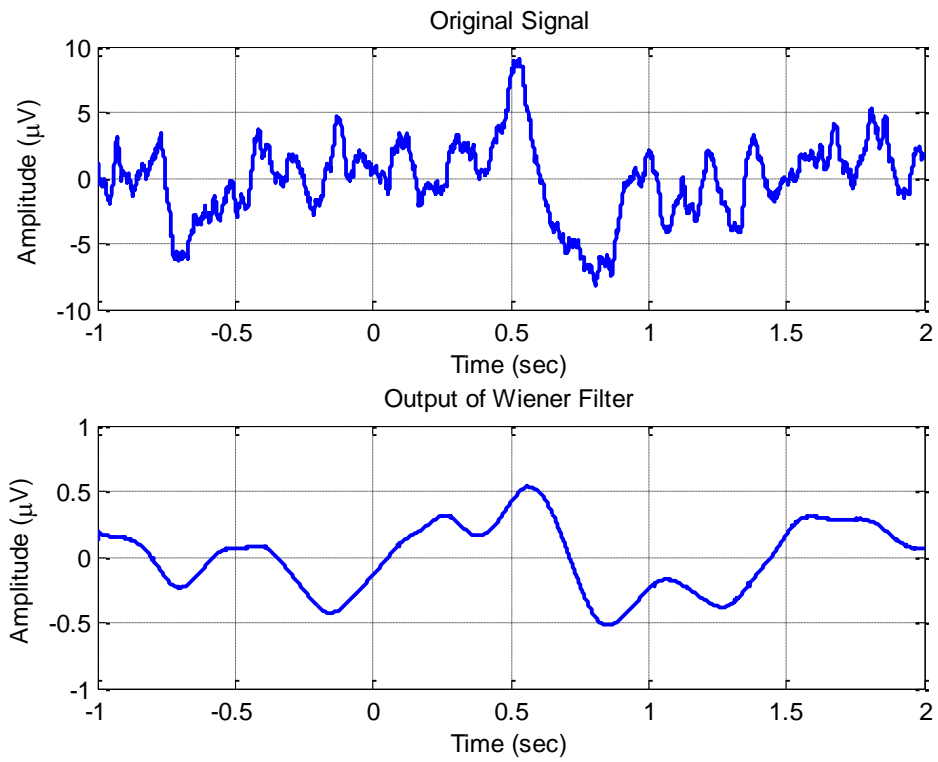
Figure 88. Original and Wiener filtering result of average OEP of Subject-17

Table 13. Original and Wiener Filtered RMS values of Subject's in time interval [0 1.2]

Single Trial	Original RMS	RMS of Filter Output
Average of 17 single trial RMS values for CO_2	5.3623	0.7938
Average of 14 single trial RMS values for PEA	5.0958	0.9614
Single Subject CO2		
Subject-1	7.1915	1.4572
Subject-2	4.6576	1.4464
Subject-3	7.2328	1.0566
Subject-4	4.1226	1.3067
Subject-5	5.3681	1.1720
Subject-6	3.4068	0.5824
Subject-7	3.8270	0.7467
Subject-8	6.4893	1.4318
Subject-9	4.3037	0.6468
Subject-10	5.7642	1.3124
Subject-11	4.3308	1.2349
Subject-12	4.0132	1.0234
	Average=5.0590	*Average=1.1181*
Single Subject PEA		
Subject-13	4.8394	0.7779
Subject-14	3.6007	0.9252
Subject-15	5.8693	0.8372
Subject-16	5.1713	0.9702
Subject-17	3.6971	0.3104
Subject-18	6.3455	0.6211
Subject-19	7.0072	0.9255
Subject-20	4.5985	1.3093
Subject-21	7.1465	0.3210
Subject-22	8.0642	0.9538
Subject-23	4.9371	1.1860
Subject-24	5.4672	1.2194
	Average= 5.5605	*Average=0.8630*

As in previous chapter, we have conveyed the RMS values of signals, calculated in time interval of 0-1.2sec, into nonparametric Spearman rank order correlation test. By looking at the results of PEA in Table 14, there is a strong correlation between original RMS value and RMS value of filtered signal (p=0.021, r=.648), but in CO_2 results, not any meaningful correlation has been found (see Table 15) (p>0.05, r=.336).

Table 14. Spearman rank order correlation test results of PEA responses

Correlations

			Original	Wiener Filter
Spearman's rho	**Original**	Correlation Coefficient	1,000	,648[*]
		Sig. (1-tailed)	.	,021
		N	12	12
	Wiener Filter	Correlation Coefficient	,648[*]	1,000
		Sig. (1-tailed)	,021	.
		N	12	12

*. Correlation is significant at the 0.05 level (1-tailed).

In the light of correlation results, Wiener filtering technique is able to denoise the averaged (i.e. single subject) PEA response with a reasonable performance but it is not as successful as wavelet denoising (see Table 11). However, for the CO_2 responses, Wiener filter is not a suitable choice. It can be seen in Table 13, Wiener filter didn't show any satisfactory performance at saving the signal power and characteristics.

Table 15. Spearman rank order correlation results for CO2 responses

Correlations

			Original	Wiener Filter
Spearman's rho	**Original**	Correlation Coefficient	1,000	,336
		Sig. (1-tailed)	.	,156
		N	12	12
	Wiener Filter	Correlation Coefficient	,336	1,000
		Sig. (1-tailed)	,156	.
		N	12	12

Although correlation test gives satisfactory result for PEA responses, there is a huge amount of amplitude decrease can be seen in Figures 77-88 for both single trial and average responses. Such a decrement makes Wiener filter non-utilizable for extraction of chemosensory stimulus related activity. Besides them, for all graphical results, there is an activity has been observed before stimulus onset. In such a case, it is fair to say that, wavelet denoising outperforms for all single trial and average responses than Wiener filters. To sum up, Wiener filtering is not an appropriate choice for SNR (signal to noise ratio) enhancement of both single subject and single trial chemosensory responsiveness.

CHAPTER 5

EMPIRICAL MODE DECOMPOSITION

The Hilbert-Huang transform was proposed by Huang et.al. in 1998 that is a method which can decompose a data or signal into limited and small number of Intrinsic Mode Functions (IMF) [55]. It was well designed for nonlinear and nonstationary data analysis. The fundamental part of this transformation is Empirical Mode Decomposition (EMD). Unlike wavelet decomposition, EMD is fully data driven tool. This method have the principle that analyzing and decomposing the signal into IMF's that they have to satisfy two important conditions as well [55, 125].

- In the whole dataset, the number of local extremes (maxima and minima) and number of zero-crossing must be equal or at most differ by one.
- At any point, mean value of the envelope that is defined by local maxima and local minima is zero.

This means that an IMF should represent one simple oscillatory function. But it is not very general and frequent condition. In general, instead of constant amplitude and frequency in an oscillatory content, an IMF should be demonstrated by varying amplitude and frequency.

By looking at condition described above, the first condition looks like narrow band requirement of a stationary Gaussian process and second criteria is the modified version of global requirement that converges to local one.

5.1. Sifting Process

Our aim is to construct a representation to given observation $x(t)$.

$$x(t) = \sum_{k=1}^{K} a_k(t)\, \varphi_k(t)$$

(5.1)

Where $a_k(t)$ is the amplitude modulation and $\varphi_k(t)$ is the oscillations. The main idea is that the fast oscillations superimposed to slow oscillations and there is a procedure that it

can be decomposed in to limited number of oscillatory components (see Figure 89) (i.e. IMF's).
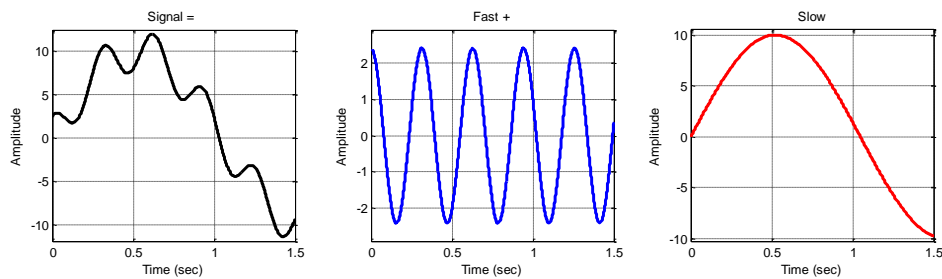
Figure 89. Fast oscillating and slow oscillating components of signal

The procedure to find and extract the so-called IMF's is the sifting process. Initial step of sifting process is the construction of upper and lower envelope by using local maxima and local minima's.
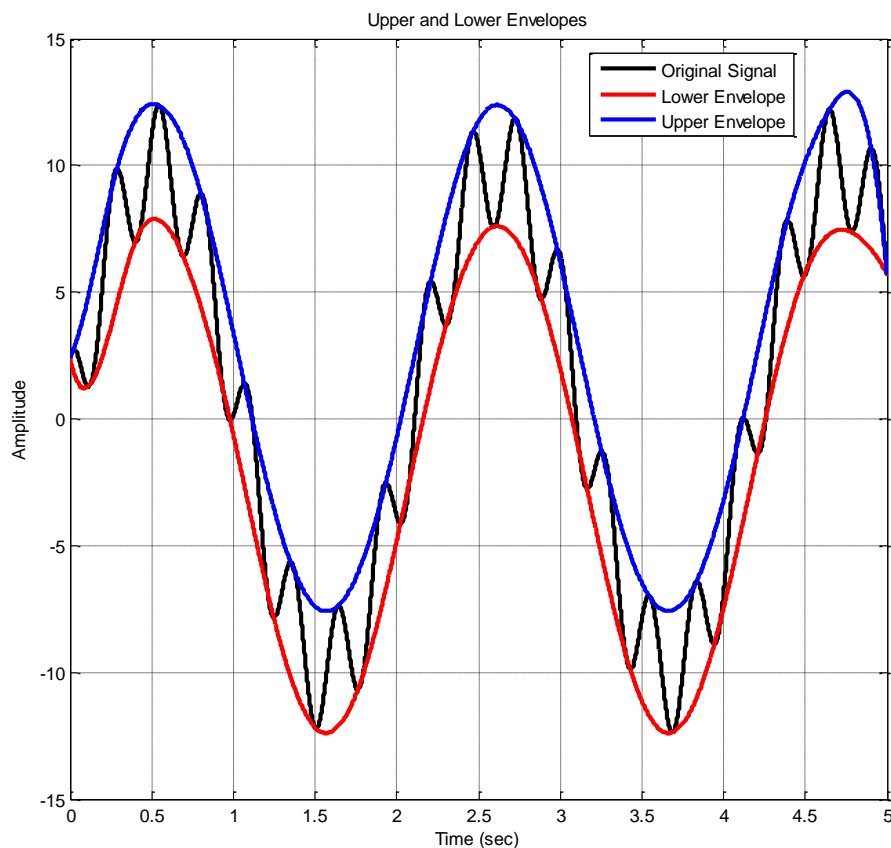
Figure 90. Upper and lower envelopes of the signal x (t)

In a signal, local maxima's and minima's can be detected by utilizing second derivative test. The test states that,

- If $\dot{x}(t) = 0$ and $\ddot{x}(t) < 0$, then x has local maximum at time t.
- If $\dot{x}(t) = 0$ and $\ddot{x}(t) > 0$, then x has local minimum at time t.
- If $\ddot{x}(t) = 0$ then test is inconclusive.

In Figure 90, blue line represents the upper envelope and red line displays the lower envelope. These envelopes are obtained by finding the local maxima and minima points of signal and interpolating them with cubic spline. Mean of these envelopes are,

$$m_1(t) = \frac{e_{upper}(t) + e_{lower}(t)}{2} \tag{5.2}$$

By subtracting the mean of envelopes from original signal we could obtain,

$$h_1(t) = x(t) - m_1(t) \tag{5.3}$$

If $h_1(t)$ does not satisfy aforementioned IMF conditions, equation (5.2) and (5.3) has to be repeated. Instead of $x(t)$, $h_1(t)$ has to be considered for further progress.

$$h_{11}(t) = h_1(t) - m_{11}(t) \tag{5.4}$$

Where $m_{11}(t)$ is the mean value of upper and lower envelope of the $h_1(t)$. This procedure should be repeated k times until $h_{1k}(t)$ satisfies the IMF conditions [56, 126].

$$h_{1k}(t) = h_{1(k-1)}(t) - m_{1k}(t) \tag{5.5}$$

$$c_1(t) = h_{1k}(t) \tag{5.6}$$

where $c_1(t)$ is the first IMF extracted from observation. For further investigation residual signal should be considered as main signal and above processes must be evaluated step by step. The residual signal $r_1(t)$,

$$r_1(t) = x(t) - c_1(t) \tag{5.7}$$

After extraction n IMF, residual function $r_n(t)$ becomes monotonic means that no further information can be extracted. As a result, we can represent the initial signal $x(t)$ by means of summation of extracted IMF's and residual $r_n(t)$ (see Figure 91),

$$x(t) = r_n(t) + \sum_{j=1}^{n} c_j(t)$$

(5.8)
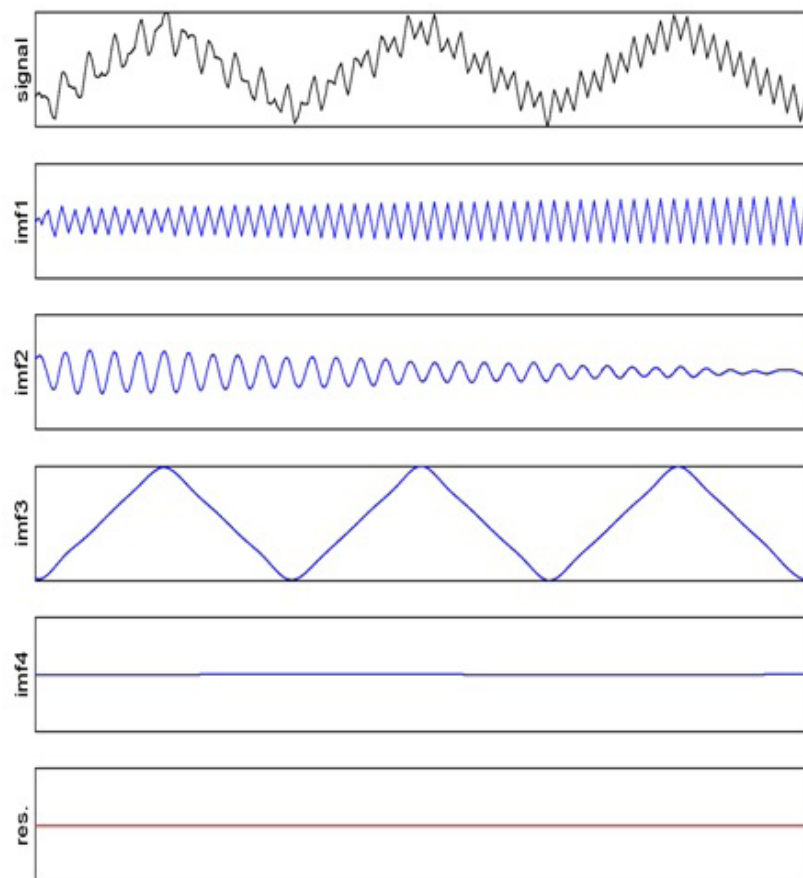
Figure 91. Set of IMF's and residual of the multi component signal x (t).

(Source: Patrick Flandrin Lecture Notes for EMD)

5.2. Single Trial Estimation with EMD-Based Approach

Since EMD has come up as a fully data-driven time series analysis tool, we have evaluated the algorithm which is given in [56] to extract chemosensory stimulus related oscillations. In order to achieve this, first, we have calculated the frequency spectra of the average of single trial EP, recorded from CZ channel. Discrete Fourier transform has been applied to averaged EP to detect the OEP/TEP laden frequency band. Frequency components, which carry the power greater than mean plus two times of standard deviation of averaged response, constitutes the EP Laden frequency band. After that, each single trial decomposed into their IMFs. IMFs, whose mean frequency which is depicted in equation (5.9), falls inside of the laden frequency band, has been summed to reconstruct the stimulus related single trial response as described in equation (5.10).

$$f_{mean} = \frac{\sum_{i=1}^{N} I_i \cdot f_i}{\sum_{i=1}^{N} I_i} \tag{5.9}$$

$$x_{recon} = \sum_j c_j \tag{5.10}$$

For this study, we have utilized 17 single trials for trigeminal stimuli and 14 single trials for olfactory stimuli of only one subject. Average of 17 single trials for CO_2 stimuli of subject-1 can be seen in below Figure 92. After averaging all CO_2 single trials, we have found the subject-specific trigeminal EP laden frequency band by utilizing DFT of averaged response that power greater than mean plus two times standard deviation through average TEP spectrum (see Figure 93). Consequently, we have found the trigeminal laden frequency band between 0.3827-9.521 Hz.

After that, all CO_2 single trials have been decomposed into their IMF's. IMF's of second single trial is demonstrated in Figure 94 and Figure 95. Totally nine IMF have been obtained from this single trial. In single trial-2, IMFs, whose mean frequency satisfy the laden frequency band criterion are IMF-5, 6 and 7. These IMFs were summed to obtain stimulus related activity. In Figure 96 and Figure 97, original and reconstructed second and eighth single trials are given respectively.
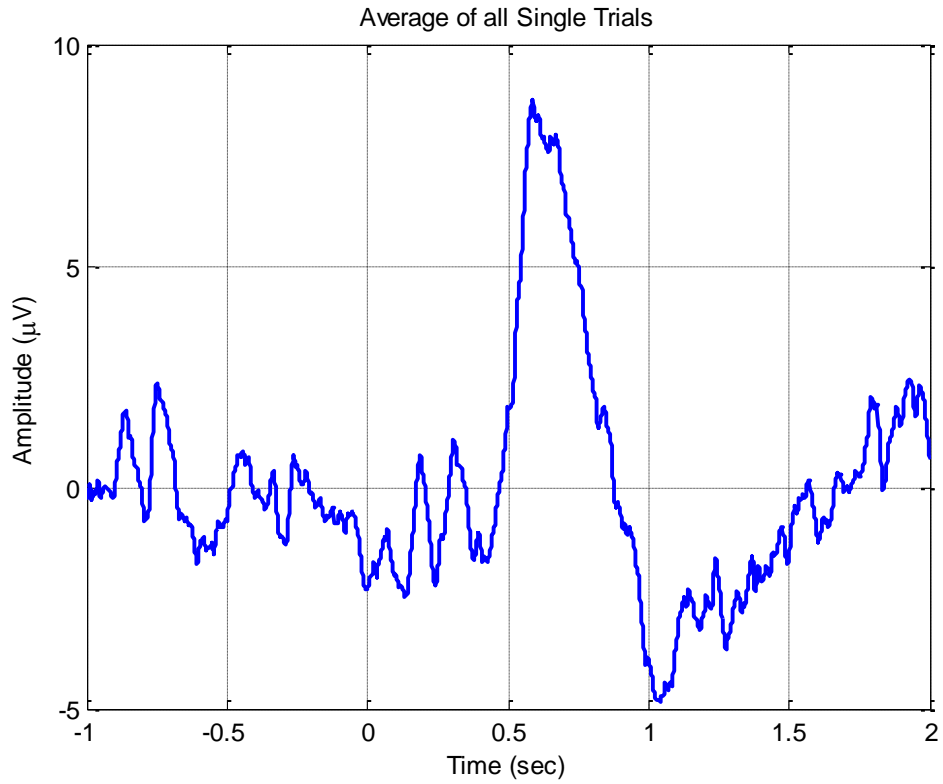
Figure 92. Average of all single trials of subject-1 for CO2 stimuli
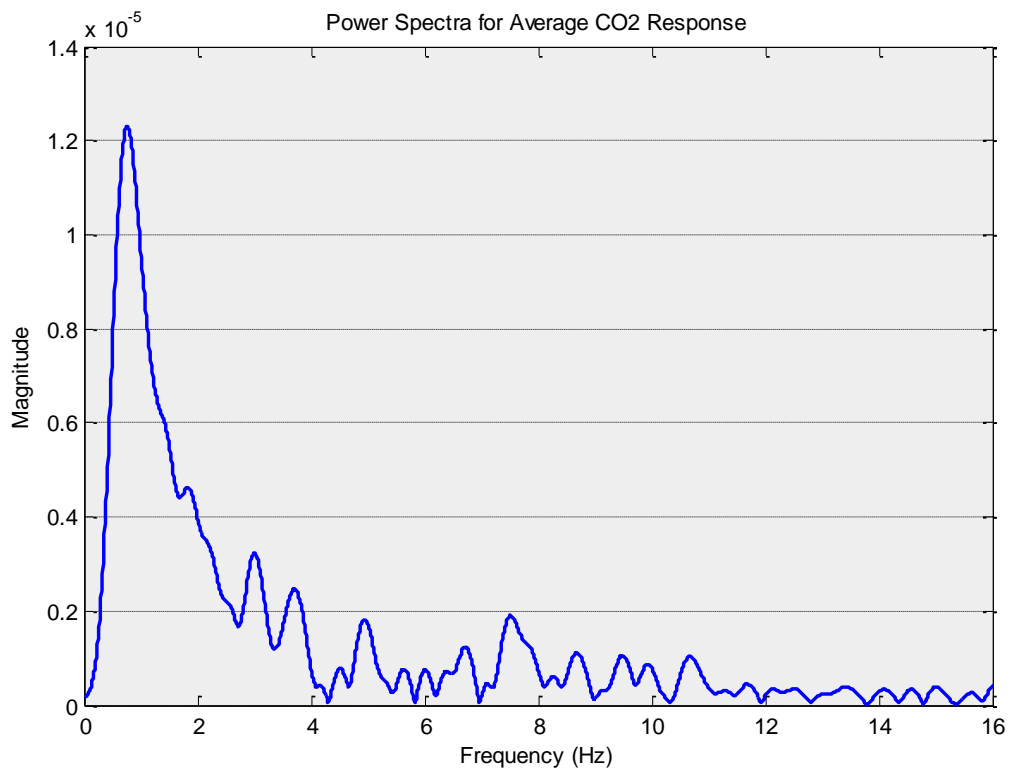
Figure 93. Power Spectrum of averaged CO_2 response
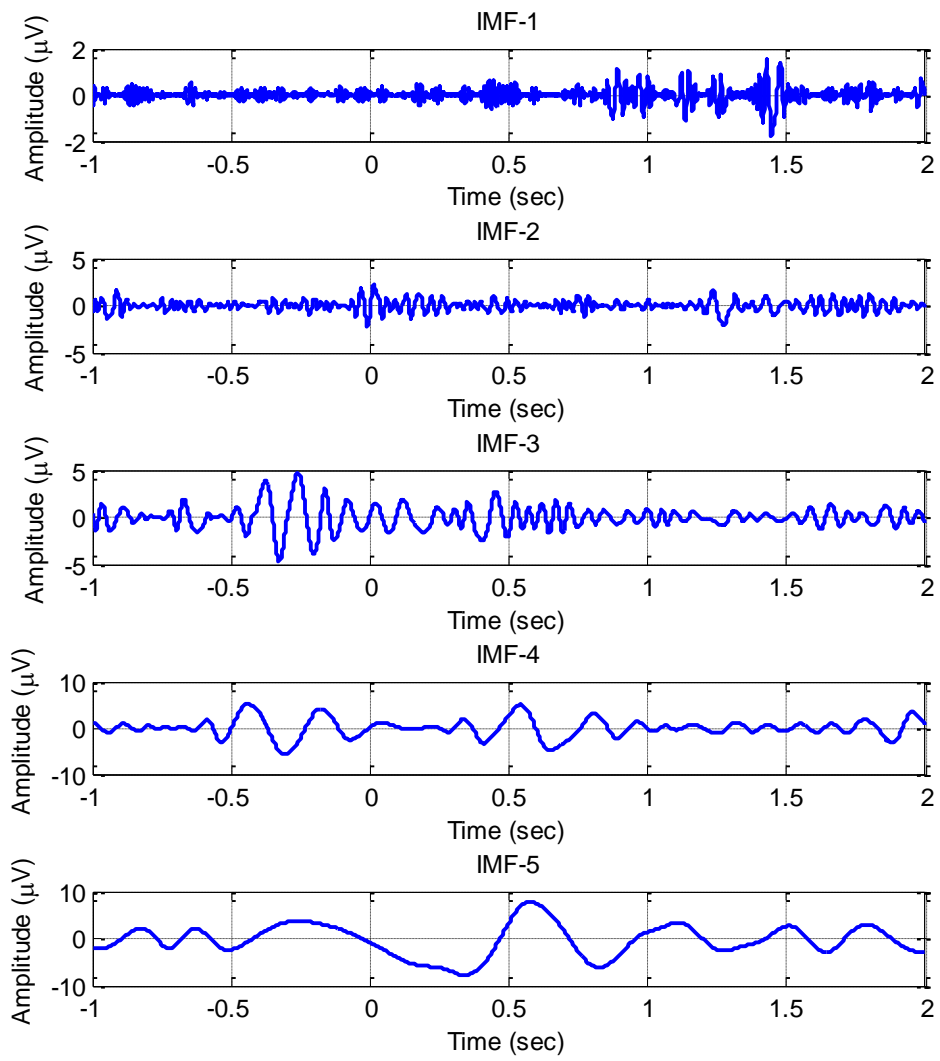
Figure 94. IMF1-5 for single trial-2 of CO_2 stimuli
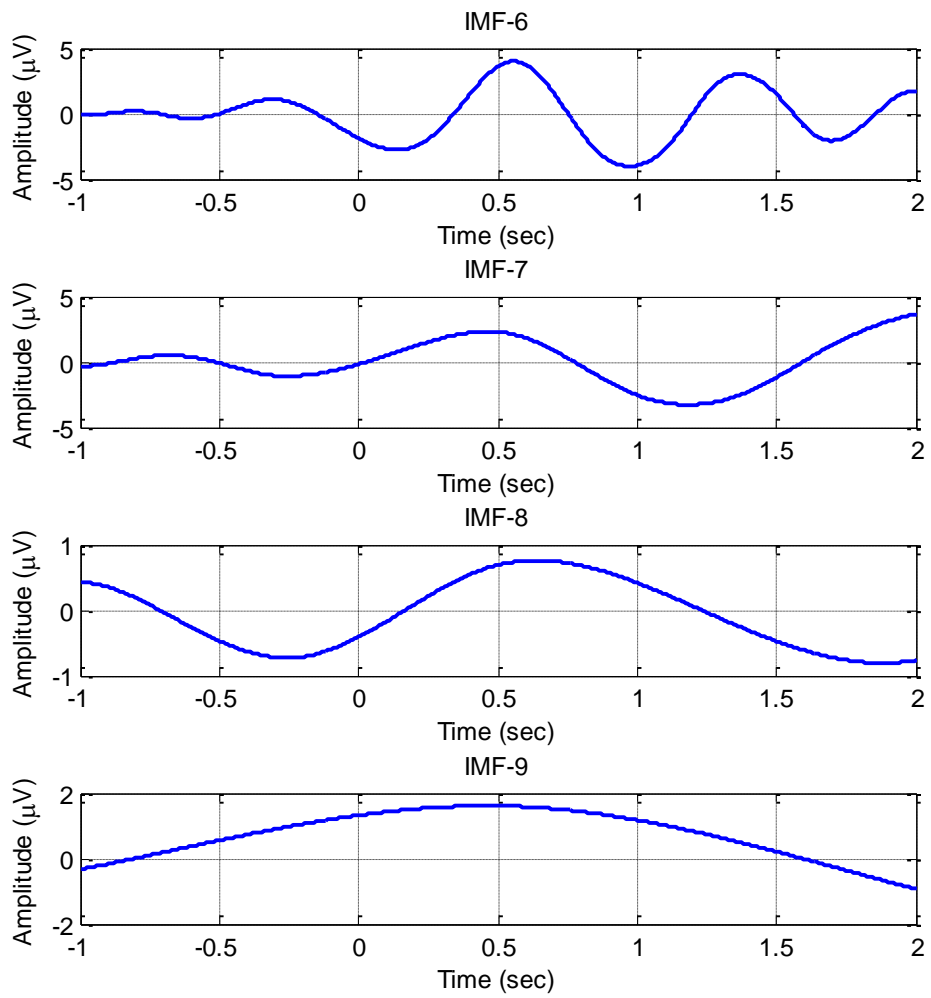
Figure 95. IMF6-9 for single trial-2 for CO_2 stimuli
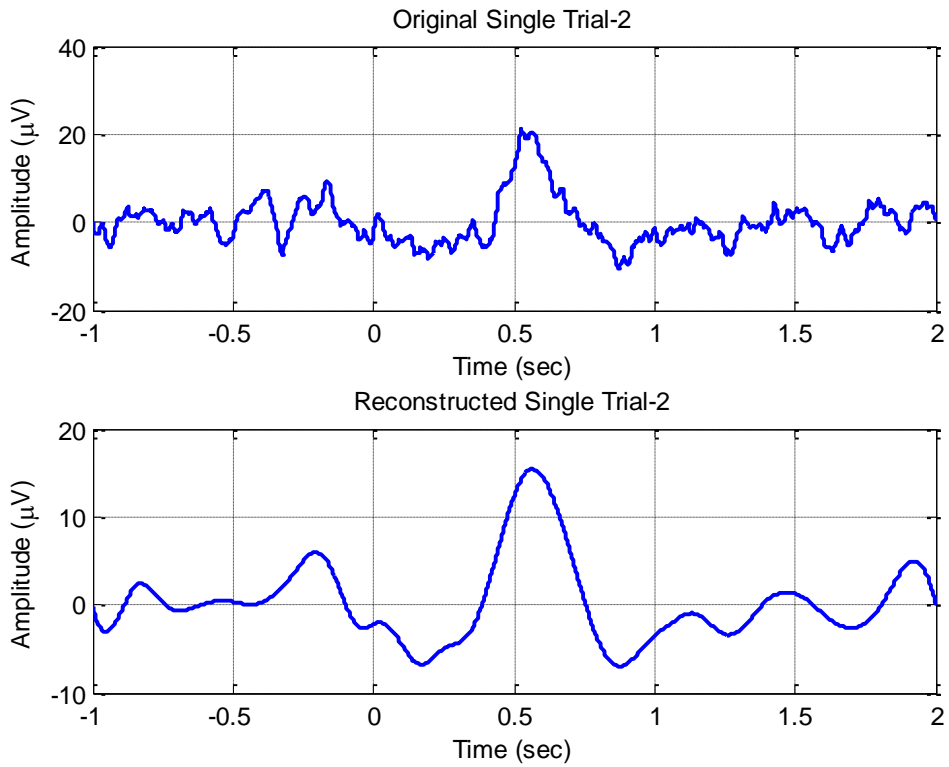
Figure 96. Original and reconstructed single trial-2 for CO2 stimuli
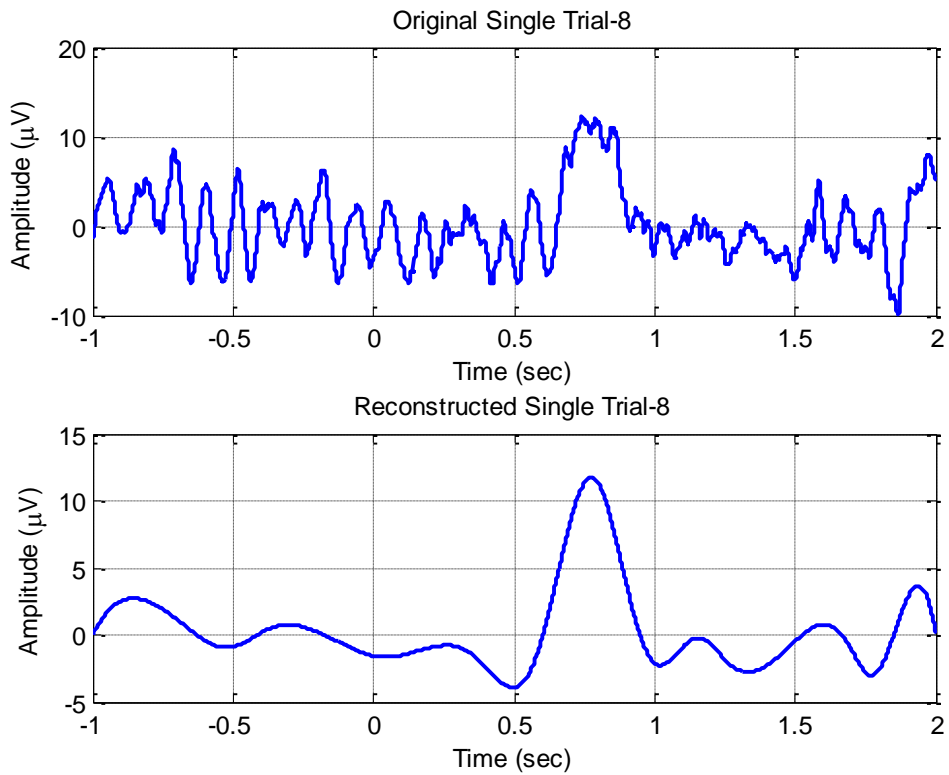
Figure 97. Original and reconstructed single trial-8 for CO2 stimuli

After completing the stimulus related activity extraction of CO_2, same procedure has been applied to single trials of olfactory (PEA) stimulation. We have found the OEP laden frequency band from average 14 single trials (see Figure 98). IMFs of single trials were selected by considering the laden frequency band. In Figure 99, power spectrum of PEA response is given.
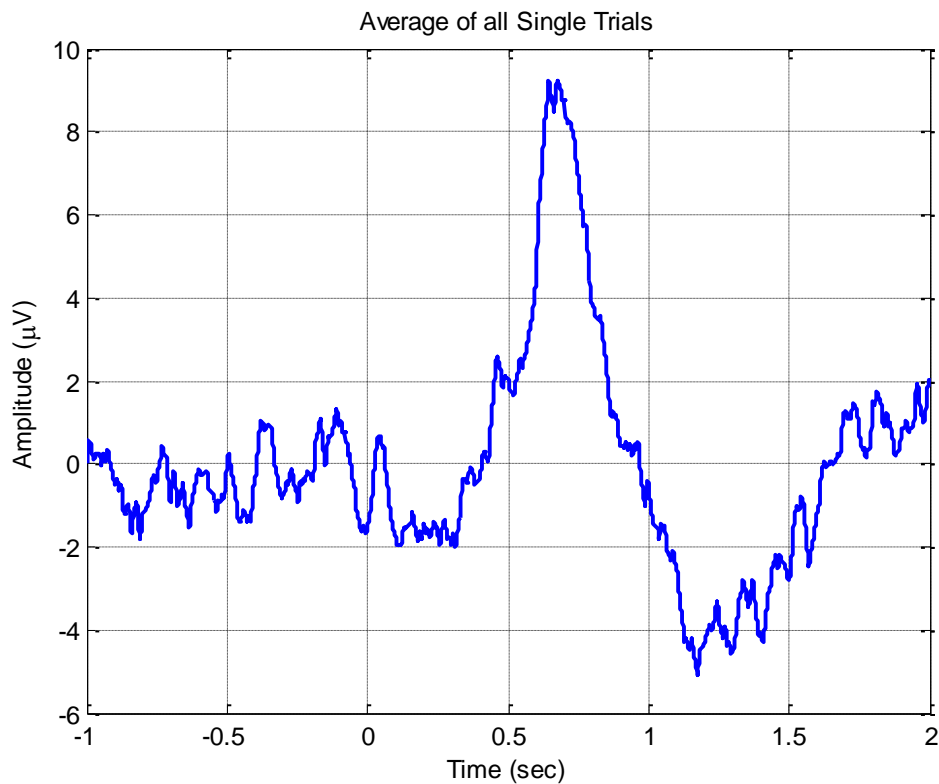
Figure 98. Average of all single trials for olfactory stimuli of Subject-1

In Figure 98, average of 14 single trials is given. By squaring all the spectral components by which has been obtained with means of DFT, we have obtained the power spectrum of the averaged PEA response. Selection of laden frequency band is achieved by same procedure as in CO_2 session. We have found the laden band 0.432-6.982 Hz. And all PEA single trials decomposed into their IMFs with EMD process. After selection of stimulus related IMFs by means of frequency band criteria, which has been extracted from single trials, each single trial reconstructed (i.e. summed) to obtain stimulus related oscillatory activities. In Figures 100 and 101, decomposed IMFs of single trial-5 for PEA stimulation is given. For reconstruction of stimulus related single trial-5, related IMFs are 5th and 6th ones.

In Figure 102 and 103, original and reconstructed single trials of 5 and 8 have been given respectively. By analyzing these figures, it is clearly seen that, reconstructed single trials shows some differences. Since EP is assumed to be stationary under constant stimulus conditions, olfactory fatigue loss of attention and many different reasons ruins this stationarity. By using EMD-Based technique, we are able to see this variability. As a consequence, it is fair to say that, this technique enables to observe the variation between single trials as previously pointed out in [56]. Since conventional averaging may abolish the important activities (i.e. ERD and ERS) which are not time-locked to stimulus onset, this approach can elicit the amplitude and latency changes between individual trials.
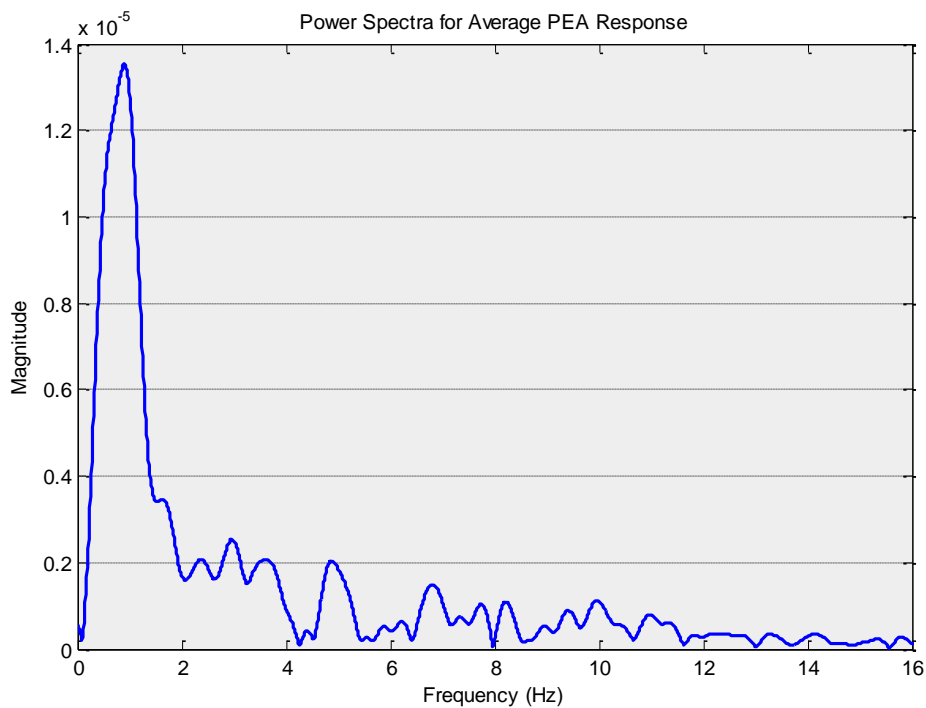
Figure 99. Power Spectrum of averaged PEA response

In this study, due to some technical troubles, we couldn't obtain 64 channel EEG recordings for all single trial recordings. Since, both frequency band and spatial criteria has been applied in aforementioned study, we couldn't apply the spatial criteria due to lack of some channel recordings.
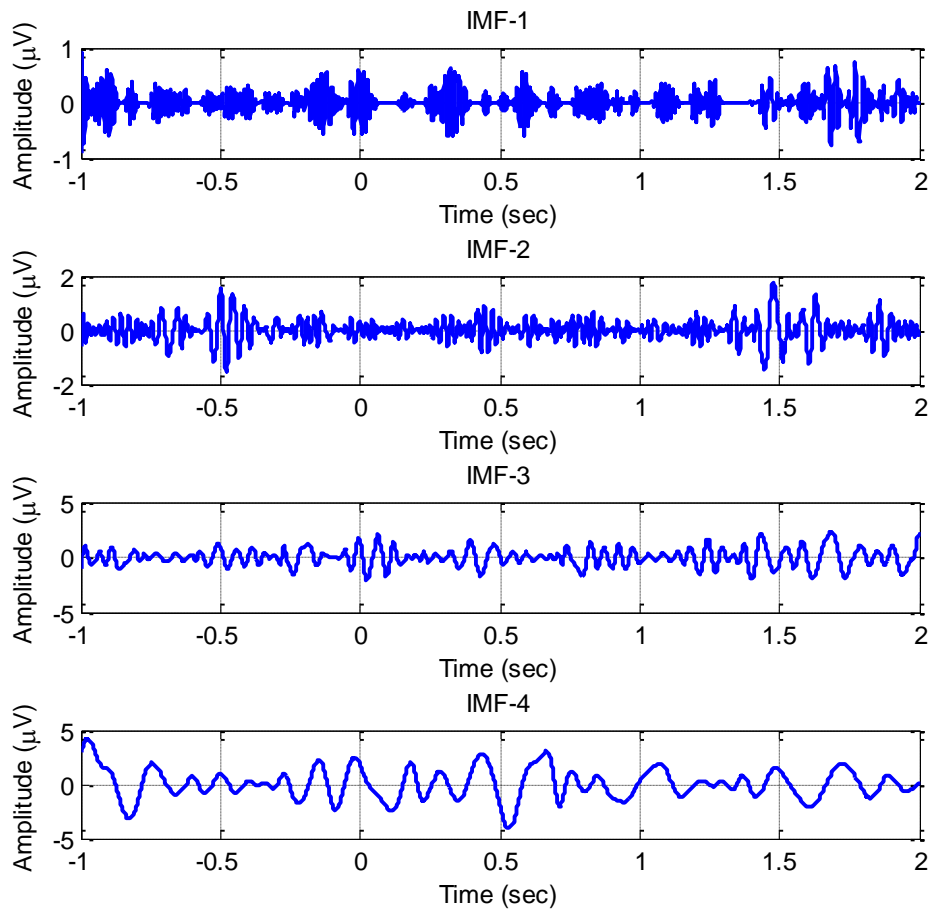
Figure 100. IMF 1-4 for single trial-5 of olfactory stimuli
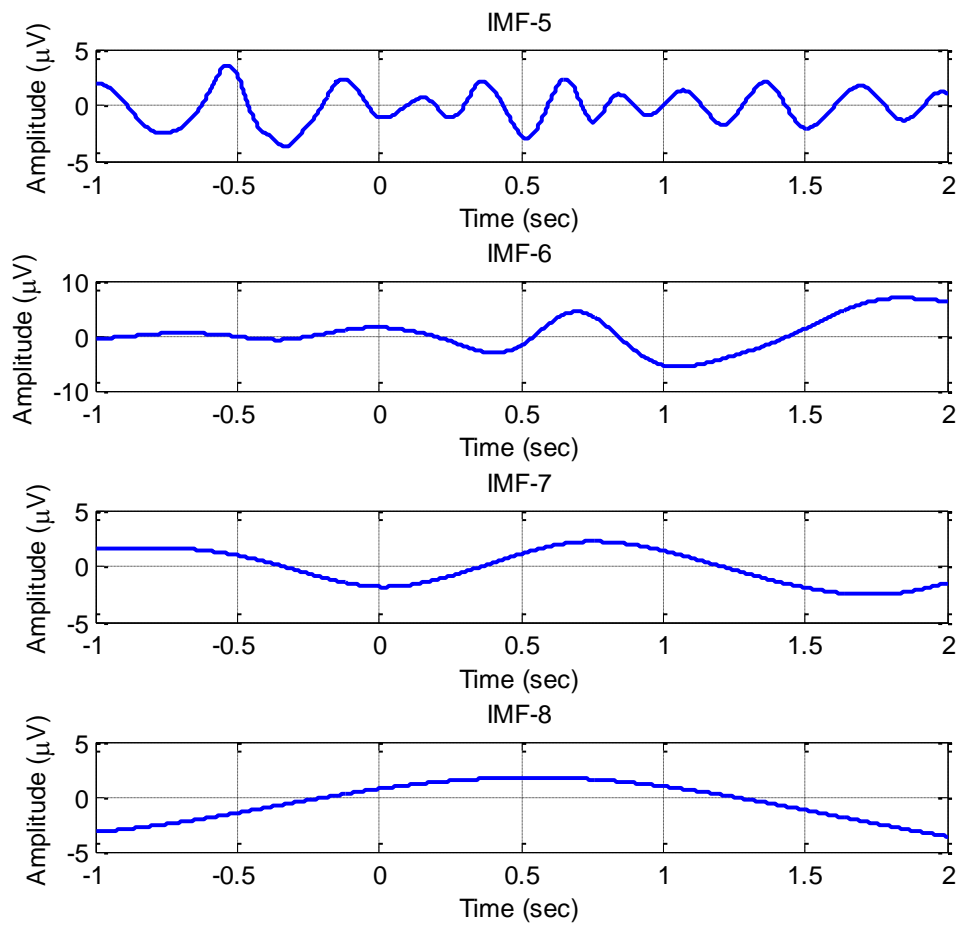
Figure 101. IMF 5-8 for single trial-5 of olfactory stimuli
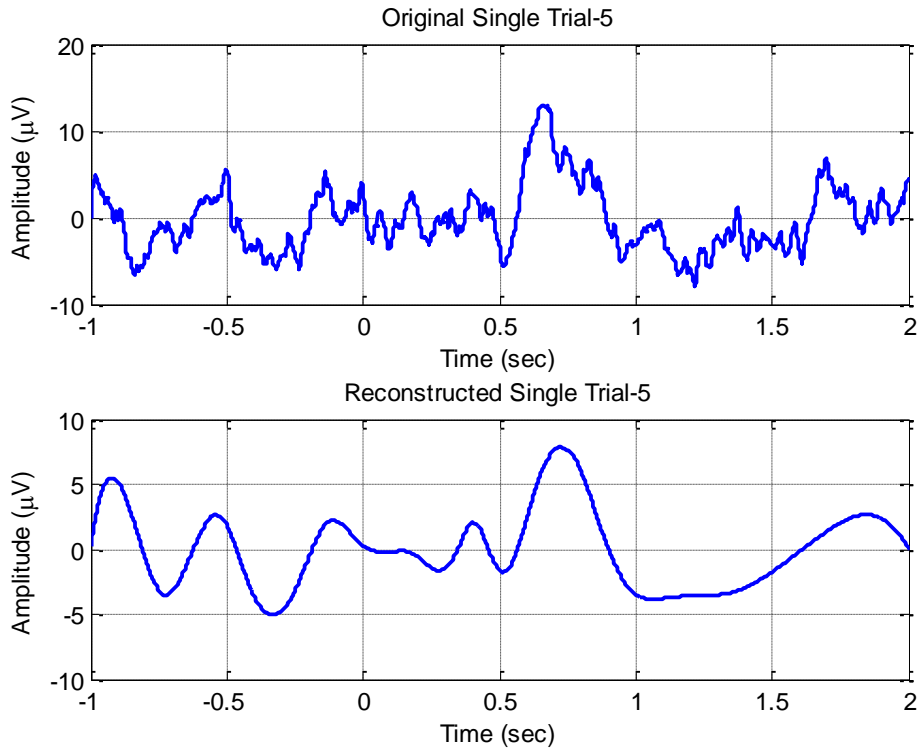
Figure 102. Original and reconstructed single trial-5 for PEA stimuli
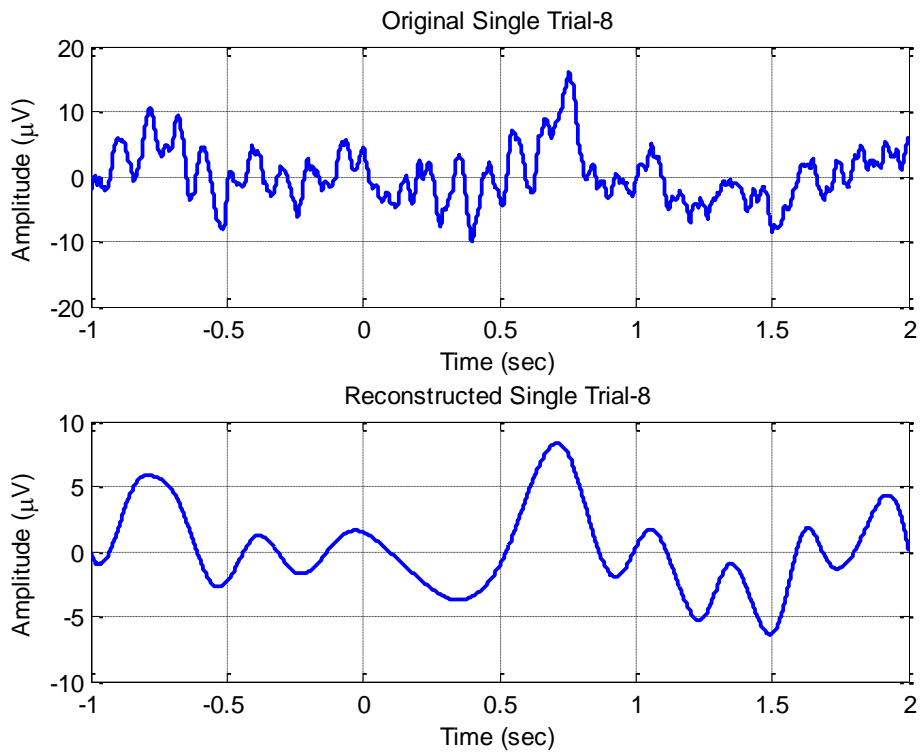
Figure 103. Original and reconstructed single trial-8 for PEA stimuli

After completing the stimulus related activity extraction with EMD-Based approach, we have compared the findings with wavelet denoising and wiener filter results. For trigeminal and olfactory EP extraction, we have compared the RMS of time interval 0-1.2sec. It can be seen from the Figure 104 and Figure 105, in comparison with other techniques, EMD based approach has given closer results in most trials to the original single trial for both olfactory and trigeminal stimuli in the sense of RMS calculated in corresponding time interval.
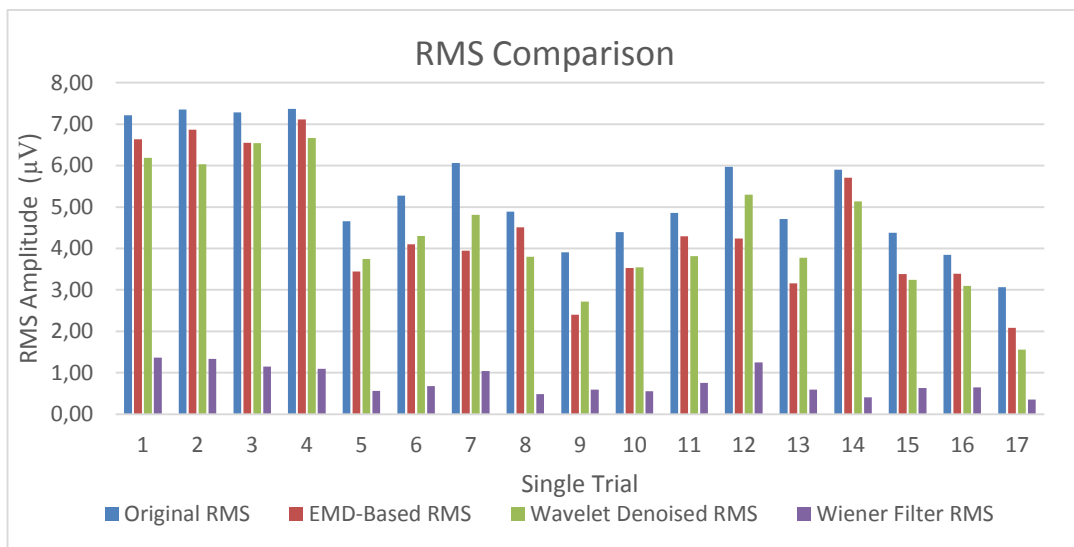
Figure 104. RMS values between 0-1.2 second for CO2 single trials
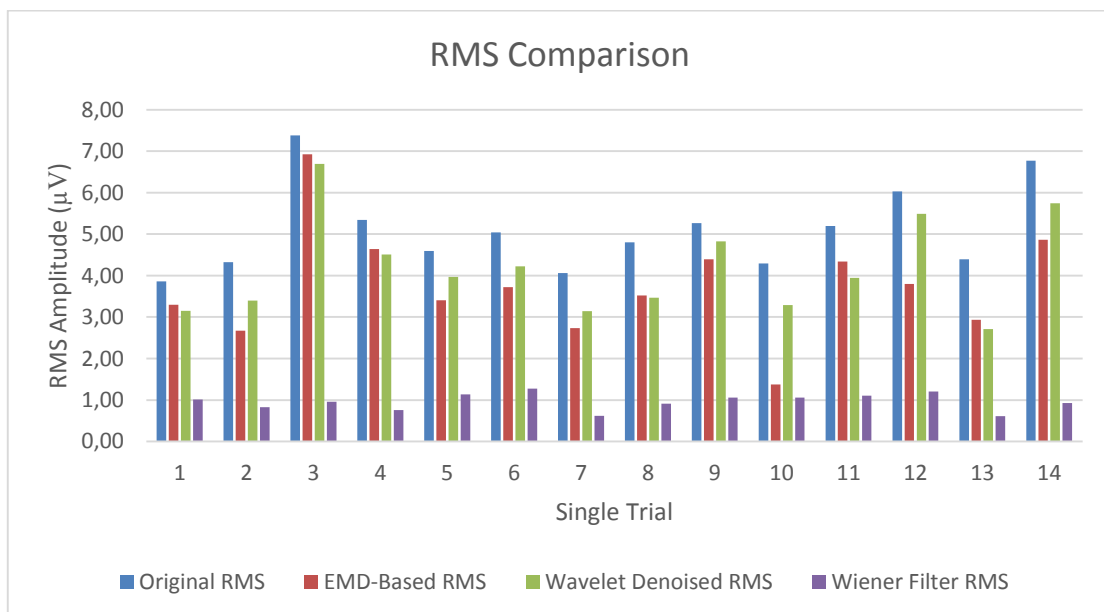
Figure 105. RMS values between 0-1.2 second for PEA single trials

Table 16. RMS amplitudes of PEA single trials

# Single Trial	EMD-Based (µV)	Wavelet Denoising (µV)	Wiener Filter (µV)	Original RMS (µV)
Single Trial-1	3,30	3,15	1,01	3,86
Single Trial-2	2,67	3,40	0,83	4,33
Single Trial-3	6,93	6,69	0,96	7,38
Single Trial-4	4,64	4,51	0,76	5,34
Single Trial-5	3,40	3,96	1,14	4,60
Single Trial-6	3,72	4,23	1,27	5,04
Single Trial-7	2,73	3,14	0,62	4,06
Single Trial-8	3,52	3,47	0,91	4,80
Single Trial-9	4,39	4,82	1,06	5,27
Single Trial-10	1,37	3,29	1,06	4,29
Single Trial-11	4,34	3,95	1,11	5,19
Single Trial-12	3,80	5,49	1,21	6,03
Single Trial-13	2,93	2,71	0,61	4,39
Single Trial-14	4,86	5,74	0,92	6,77

Table 17.RMS amplitudes of CO2 single trials

# Single Trial	EMD-Based (µV)	Wavelet Denoising (µV)	Wiener Filter (µV)	Original RMS (µV)
Single Trial-1	6,63	6,19	1,36	7.21
Single Trial-2	6,87	6,03	1,34	7.35
Single Trial-3	6,55	6,54	1,15	7.28
Single Trial-4	7,11	6,67	1,10	7,37
Single Trial-5	3,45	3,75	0,56	4,66
Single Trial-6	4,10	4,30	0,68	5,28
Single Trial-7	3,95	4,81	1,04	6,06
Single Trial-8	4,51	3,80	0,48	4,89
Single Trial-9	2,40	2,72	0,59	3,91
Single Trial-10	3,53	3,54	0,55	4.40
Single Trial-11	4,29	3,81	0,75	4,86
Single Trial-12	4,24	5,30	1,25	5,97
Single Trial-13	3,16	3,78	0,60	4,71
Single Trial-14	5,71	5,13	0,41	5,90
Single Trial-15	3,38	3,24	0,63	4,38
Single Trial-16	3,39	3,10	0,65	3,85
Single Trial-17	2,08	1,56	0,35	3,07

After their RMS amplitudes had been observed with 3 different approach, similarity between extracted activities and subject's average was examined by utilizing their cross correlations. The reason why we compared with subject's averaged response is, averaging of many trials elicits the stationary brain's chemosensory responsiveness. It is thought that, under same stimulus conditions, responsiveness of the brain remains constant in the sense of amplitude and latency.

Table 18. Cross correlation between averaged CO2 response and single trials obtained by different approaches

	Wavelet Denoising	Wiener Filter	EMD- Based
Single Trial-1	0,83	0,76	0,87
Single Trial-2	0,77	0,76	0,86
Single Trial-3	0,77	0,62	0,84
Single Trial-4	0,74	0,66	0,88
Single Trial-5	0,66	0,55	0,69
Single Trial-6	0,56	0,54	0,71
Single Trial-7	0,62	0,52	0,58
Single Trial-8	0,59	0,39	0,72
Single Trial-9	0,52	0,61	0,47
Single Trial-10	0,57	0,57	0,80
Single Trial-11	0,65	0,45	0,66
Single Trial-12	0,69	0,72	0,67
Single Trial-13	0,50	0,55	0,76
Single Trial-14	0,65	0,53	0,63
Single Trial-15	0,53	0,59	0,73
Single Trial-16	0,46	0,61	0,79
Single Trial-17	0,40	0,38	0,52

It can be seen from Table 18 and Table 19, for both CO_2 and PEA responses, EMD-based single trial extraction method is able to extract the most correlative signal among all utilized techniques within the frame of this thesis. Collaboration of two results which have obtained from comparison of RMS and cross correlation values, EMD-Based technique gives satisfactory results in estimation of chemosensory stimulus related activity. In Figure 106 and Figure 107, original and extracted single trial for CO_2 and PEA with 3 different techniques is given. It is clear that, in both stimuli type (i.e. PEA and CO_2 responses), highest amplitude and maximum similarity while extracting stimulus related activity has been obtained by EMD-Based extraction technique.

Table 19. Cross correlation between averaged PEA response and single trials obtained by different approaches

# Single Trial	Wavelet Denoising	Wiener Filter	EMD-Based
Single Trial-1	0,66	0,65	0,69
Single Trial-2	0,63	0,53	0,69
Single Trial-3	0,78	0,59	0,88
Single Trial-4	0,77	0,67	0,83
Single Trial-5	0,69	0,70	0,79
Single Trial-6	0,73	0,73	0,70
Single Trial-7	0,64	0,49	0,68
Single Trial-8	0,55	0,62	0,77
Single Trial-9	0,75	0,60	0,72
Single Trial-10	0,55	0,63	0,27
Single Trial-11	0,57	0,53	0,65
Single Trial-12	0,79	0,72	0,62
Single Trial-13	0,54	0,48	0,73
Single Trial-14	0,69	0,60	0,84

But there is a critical point we should consider. For all considered estimation/extraction (or SNR enhancement) techniques used in this thesis, our main intention is to extract only the brain activity, which is related to only chemosensory stimuli. By looking at the Figure 106 and Figure 107, outcomes of EMD-based and Wiener filter display some oscillatory activity before the stimulus onset which is not related to given external stimuli. It's the fact that, while brain processes the chemosensory information, ongoing cognitive, memory and other external/internal stimulus/information processing also continues in brain and also, as a natural result, these processes can enhance/deplete the power of related/unrelated frequency band/bands. In line with our request, we want to consider only chemosensory stimulus related activity. As can be seen from Figures 106 and 107, unlike EMD-Based method and Wiener filtering technique, wavelet denoising eliminates most of stimulus unrelated activity before the stimulus onset (i.e. t=0) and after t=1.2 seconds. Besides this, wavelet denoising has gave satisfactory result at cross-correlation and RMS results (see Table 16-19). For these reasons, wavelet denoising can be thought as the best choice in light of our intention. Despite the pre-stimulus activity observed in EMD-based technique, this approach can be used as an alternative tool for SNR enhancement of chemosensory stimulus related brain activity due to our findings.
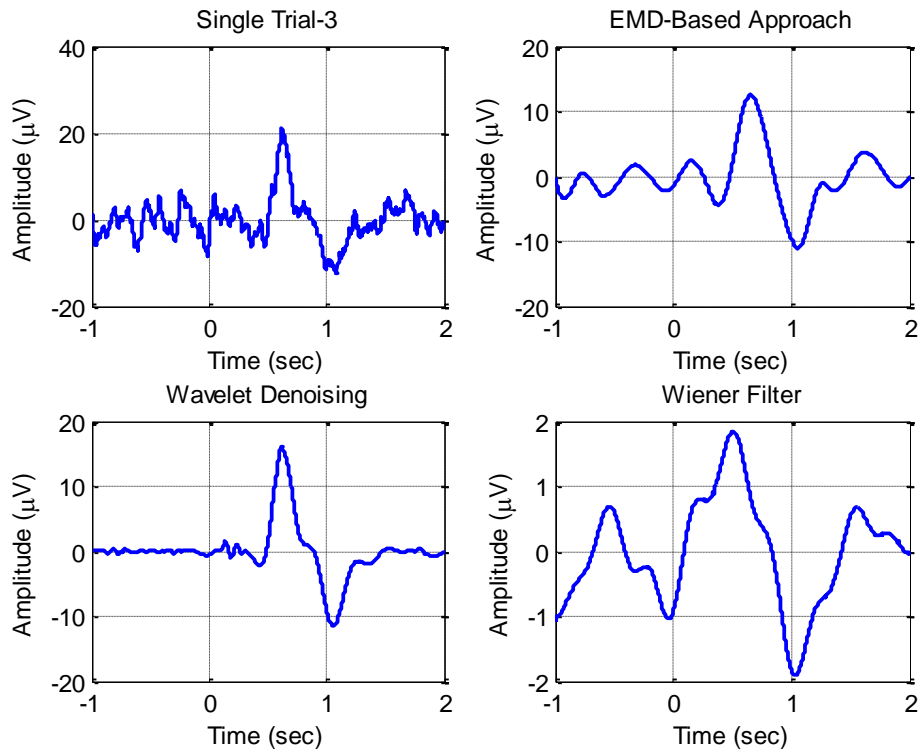
Figure 106. Original and all extracted single trial-3 for CO2 stimuli
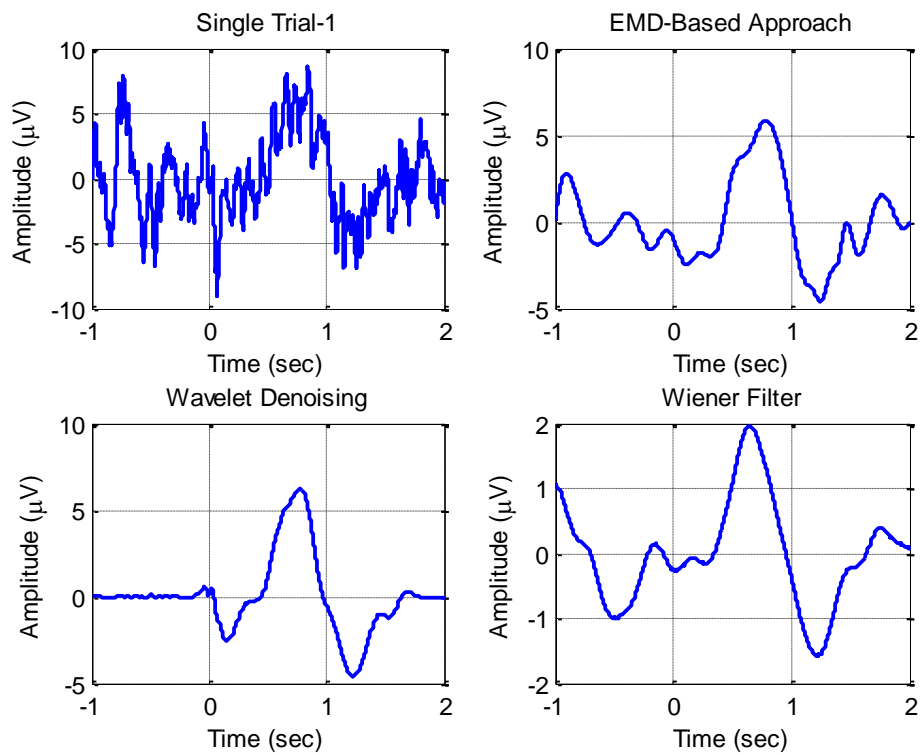
Figure 107.Original and all extracted single trial-1 for PEA stimuli

CHAPTER 6

ENHANCEMENT FACTOR APPROACH

In clinical conditions, recordings of CSEP and CSERP components (such as N1, P2) does not fully indicate the subject's olfactory performance accurately. They can be easily affected by subject's daily health state, vigilance, hormonal cycle, noise interference and etc. For this purpose, we have proposed a new approach called 'Enhancement Factor' for demonstration of the subject's olfactory performance independent from the basal activity of subject's, motor artifacts and noise interference from ambient.

In this approach, we intended to take into account the signal's root mean square (RMS) values of pre-stimulus and post-stimulus regions (see Figure 108).
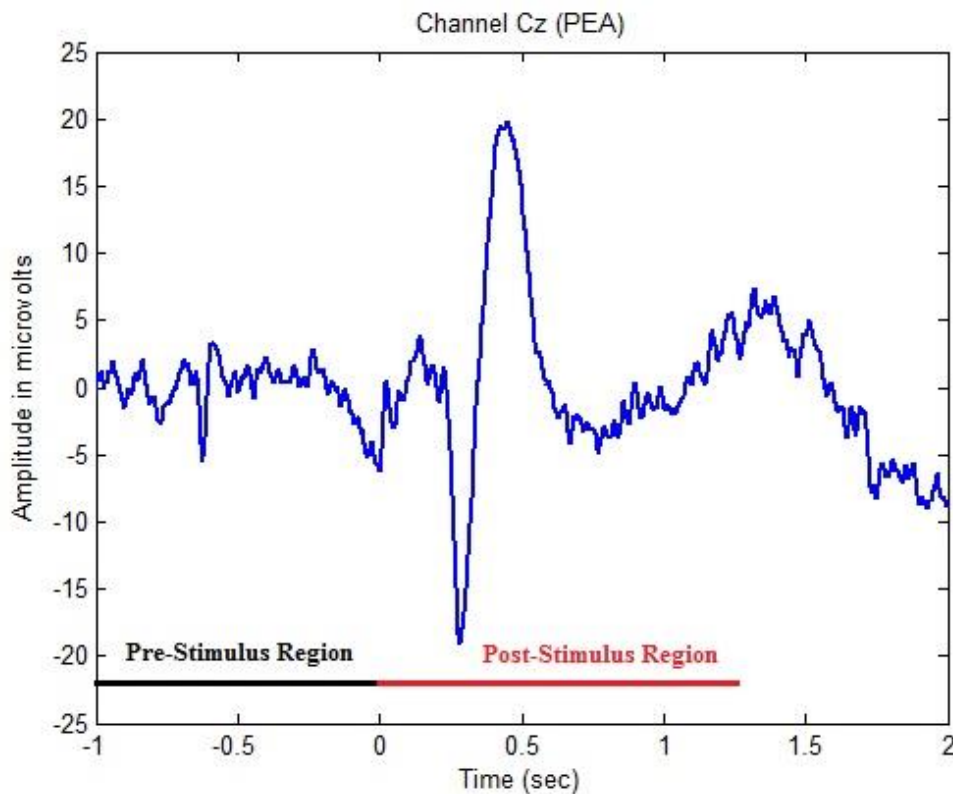
Figure 108. Subject's recorded EEG on CZ channel.

Then, Enhancement Factor (EF) can be calculated as,

$$EF = \frac{PostStimulus\ RMS - PreStimulus\ RMS}{PostStimulus\ RMS + PreStimulus\ RMS} \qquad (6.1)$$

Where RMS is defined as the root mean square root of the corresponding region of the signal f and is denoted as,

$$f_{RMS} = \sqrt{\frac{1}{T_2 - T_1} \int_{T_1}^{T_2} |f(t)|^2\ dt} \qquad (6.2)$$

In order to investigate the subject's objective smell performance, we have examined the correlations between TDI score of Sniffin' Stick test results and Enhancement Factor results. In this context, we have employed nineteen subjects to this process. In Table 20, totally 19 subjects' TDI scores and EF results are given.

Table 20. Subjects with EF and TDI scores

Subject no.	EF	TDI	Subject no	EF	TDI
1	0,0149	20,5	11	0,1496	0
2	0,3668	31,5	12	0,5898	25,5
3	0,093	20,75	13	0,492	36,5
4	0,0632	27,75	14	0,5168	34,5
5	0,0997	26,75	15	0,4613	31,5
6	0,1834	24.5	16	0,4138	26,5
7	0,2473	24.5	17	0,2643	26
8	0,2354	30.25	18	0,2641	35,25
9	0,1974	5	19	0,2189	24,5
10	0,0855	2			

All these calculated EF results and TDI scores have been conveyed to non-parametric Shapiro-Wilk normality test [127] by using SPSS predictive analytics software [128].

Shapiro-Wilk test is a way to see how data deviates from a comparable normal distribution. It compares the scores in the sample normally distributed with same mean and standard deviation. If the result is non-significant ($p>0.05$) it tells that data distribution is not far from normal distribution, however, if the test reaches significant

level (p<0.05) data's distribution is away from normal distribution. The test procedure is as follows;

- Obtain the values $x(i)$ for $i = 1, 2, ..., n$ that they came from normally distributed population.
- Calculate the a_i values for which is given as

$$(a_1, a_2, a_3, ..., a_n) = \frac{m^T V^{-1}}{(m^T V^{-1} V^{-1} m^T)^2} \tag{6.3}$$

Where $m = (m_1, m_2, ..., m_n)^T$ expected values for normally distributed samples and V denotes the covariance matrix.

- Finally the test statistics is calculated as

$$W = \frac{(\sum_{i=1}^{n} a_i x(i))^2}{\sum_{i=1}^{n} (x(i) - \bar{x})^2} \tag{6.4}$$

- If $W_{calculated} < W_{critical}$ distribution is away from normal distribution.

In Table 21, it is found that EF scores converged to normal distribution but TDI score didn't.

Table 21. Normality test results

Tests of Normality

	Kolmogorov-Smirnov[a]			Shapiro-Wilk		
	Statistic	df	Sig.	Statistic	df	Sig.
EF	,176	19	,125	,943	19	,299
TDI	,260	19	,001	,834	19	,004

a. Lilliefors Significance Correction

After these findings, EF values and TDI score were conveyed to Spearman Rank Order Correlation test. Spearman Rank Order Correlation is used to calculate the strength of the relationship between 2 variables. Spearman Rank Order Correlation Coefficient (rho) is calculated as,

$$\rho = \frac{\sum_i (x_i - \bar{x})(y_i - \bar{y})}{\sqrt{\sum_i (x_i - \bar{x})^2 \sum_i (y_i - \bar{y})^2}} \tag{6.5}$$

In Table 22, Spearman rank order correlation coefficient are given. The correlation coefficient between TDI scores and EF values is 0.617 *(r=.617, n=19, p<0.005)*.

According to these findings, these approach may be helpful for obtaining normative values and diagnosis of anosmia/hyposmia and normosmia symptoms for CSEP/CSERP. And also, with the help of the EF, it is possible to observe the status of subjects smell performance in different period of time.

Table 22. Spearman rank order correlation test results

Correlations

			EF	TDI
Spearman's rho	EF	Correlation Coefficient	1,000	,617[**]
		Sig. (1-tailed)	.	,002
		N	19	19
	TDI	Correlation Coefficient	,617[**]	1,000
		Sig. (1-tailed)	,002	.
		N	19	19

[**]. Correlation is significant at the 0.01 level (1-tailed).

CHAPTER 7

CONCLUSIONS

In this thesis, first of all, we reviewed the literature about insects and human olfactory system. How olfactory system interact with odorant molecules in periphery and how odorant information transferred to neural domain and also, how odorant information is processed in brain has been discussed in this thesis. After that, electronic nose, a device that imitates insects' olfactory system was reviewed briefly. In literature, there are many different approaches have been found. An interesting approach, CNN based e-nose structure has been investigated thoughtfully.

In the second part of this thesis, we have analyzed and reviewed the relationship between EEG and CSEP/CSERP which is denoted as responsiveness of the brain to chemosensory stimuli.

Wavelet entropy that is a measure that demonstrates complexity of signal, has been utilized to display the state transition in the neuronal structures in the brain to given chemosensory stimuli. We have found a significant entropy decrease occurs at nearly 0.5 seconds after the stimulus onset. It is thought that decrease in entropy concludes brain goes from disordered state to more ordered state upon information processing of chemosensory stimuli. After the obtaining the time dependent wavelet entropy, we have selected three distinct time windows from time evaluation of Shannon entropy. To demonstrate the meaningfulness of these entropy variations for all subjects, Friedman and Wilcoxon statistical test has been employed. Friedman test has found a meaningful increase and decrease of wavelet entropy within these chosen time windows for all subjects with an asymptotic significance 0.013 for PEA and 0.01 for CO_2. After those findings we have searched for the main source of these significance ratings. By utilizing the Wilcoxon test, we have observed that entropy decrease while transition from TW-1 to TW-2 and entropy increase while transition from TW-2 to TW-3 is of prime importance of these significance obtained from Friedman test. It can be stated that, through the instrument of chemosensory stimuli, complexity of brain decreases due to information processing of chemosensory stimuli within pyramidal cortical neurons in the brain.

After the wavelet entropy, we have used some signal processing techniques to obtain chemosensory related brain activity from ongoing EEG recordings. Wavelet denoising, Wiener Filter and EMD-Based techniques have been employed respectively for single trial and single subject responses. For single subject responses, we have employed Wavelet denoising and Wiener filtering techniques. By looking at the outcomes of Spearman rank order correlation tests, signal shapes and RMS values obtained from 0-1.2 seconds, Wavelet denoising can be thought as best choice for enhancing of SNR of the CSEP signals. And for single trial responses, we have evaluated all of these aforementioned techniques. Again, cross-correlation results, RMS values and signal shapes have been considered for performance analysis and the outcomes of these criteria displayed that EMD-Based techniques is most suitable techniques among them. But out main purpose was to relieve only chemosensory related activity from ongoing EEG activity. By considering the results in both single trial and single subject extracted CSEP, Wavelet denoising has become most successful technique among all others in the sense of SNR enhancement (i.e. extraction of CSEP).

In the final section of the thesis, our aim was to propose a metric for identification of smell performance that does not affected by daily basal activity of brain of subjects and away from subjective comments of expert. We have called this approach as "Enhancement Factor". According to the statistical test done with nineteen subjects, we have found a significant correlation between Sniffin' Stick Test scores and EF results. This might be indicate that EF approach could be used for diagnosis of some olfactory dysfunction and it can be a reliable tool for evaluation of the smell performance of subject's in different time courses.

Main aim of this thesis is to open a new perspective in the light of popular signal processing techniques to brain's responsiveness to chemosensory stimuli. In the literature there are many studies in which chemosensory responsiveness of brain has been investigated with electrophysiological techniques, however, there only very few studies utilized from time-frequency tools and filtering techniques and also, there are only one study that has employed EMD-Based technique for extraction of chemosensory related activity from EEG oscillations. In chapter 5, we have utilized the spectral criteria of this EMD-based technique to demonstrate the usefulness of this approach for chemosensory researches.

Briefly, this thesis contains some signal processing techniques which are new to chemosensory research, and some new approaches for development of a diagnostic approach for chemosensory studies.

For the future work, development of EF in the sense of correlation with TDI score can be vital for clinical and forensic case studies. And also, separation and estimation of the OEP/TEP in different types of odorant stimulus might be very helpful for clinical research area and it might be a key study for shortening the analysis time for a reliable results.

To best our knowledge, in the light of advanced signal processing studies especially in high frequency oscillatory activities might give very informative results. And also, with the help of improved denoising/filtering approaches, extraction of pure stimulus specific oscillatory activities without distorting the responsiveness, may be possible for future studies and it might help the exact evaluation of smell performance.

Besides them, instead of common CNN structure which is described in chapter 2, utilizing the memory property of memristor in CNN based e-nose system, which has been detailed in this thesis, might be a novel and interesting study for odor classification and odorant mixture separation.

REFERENCES

[1]   Auffarth, B., *Understanding smell—the olfactory stimulus problem.* Neuroscience & Biobehavioral Reviews, 2013. **37**(8): p. 1667-1679.

[2]   C.huart, T.H., Ph. Rombaux, A. Mouraux, *Clinical Usefulness and Feasibility of Time-Frequency Analysis of Chemosensory EventRelated Potentials.* Rhinology, 2013. **51**: p. 210-221.

[3]   Kaupp, U.B., *Olfactory signalling in vertebrates and insects: differences and commonalities.* Nature Reviews Neuroscience, 2010. **11**(3): p. 188-200.

[4]   Başar, E., et al., *Are cognitive processes manifested in event-related gamma, alpha, theta and delta oscillations in the EEG?* Neuroscience Letters, 1999. **259**(3): p. 165-168.

[5]   Berger, H., *Über das elektrenkephalogramm des menschen.* European Archives of Psychiatry and Clinical Neuroscience, 1929. **87**(1): p. 527-570.

[6]   Van Toller, S., et al., *An analysis of spontaneous human cortical EEG activity to odours.* Chemical senses, 1993. **18**(1): p. 1-16.

[7]   Finkenzeller, P., *Gemittelte EEG-potentiale bei olfactorischer reizung.* Pflüger's Archiv für die gesamte Physiologie des Menschen und der Tiere, 1966. **292**(1): p. 76-80.

[8]   Lorig, T.S., *The application of electroencephalographic techniques to the study of human olfaction: a review and tutorial.* International Journal of Psychophysiology, 2000. **36**(2): p. 91-104.

[9]   Kobal, G. and K. Plattig, *Objective olfactometry: methodological annotations for recording olfactory EEG-responses from the awake human.* EEG-EMG Zeitschrift für Elektroenzephalographie, Elektromyographie und verwandte Gebiete, 1978. **9**(3): p. 135.

[10]   Rombaux, P., C. Huart, and A. Mouraux, *Assessment of chemosensory function using electroencephalographic techniques.* Rhinology, 2012. **50**(1): p. 13-21.

[11]   Wetter, S. and C. Murphy, *A paradigm for measuring the olfactory event-related potential in the clinic.* International journal of psychophysiology, 2003. **49**(1): p. 57-65.

[12]   Kobal, G., et al., *" Sniffin'sticks": screening of olfactory performance.* Rhinology, 1996. **34**(4): p. 222-226.

[13]   Oniz, A., et al., *The Modified Sniffin'Sticks Test in Turkish Population Based on Odor Familiarity Survey.* Journal of Neurological Sciences, 2013. **30**(2).

[14] Doty, R.L., et al., *University of Pennsylvania Smell Identification Test: a rapid quantitative olfactory function test for the clinic.* The Laryngoscope, 1984. **94**(2): p. 176-178.

[15] Nordin, S., et al., *The Scandinavian Odor-Identification Test: development, reliability, validity and normative data.* Acta oto-laryngologica, 1998. **118**(2): p. 226-234.

[16] Lötsch, J. and T. Hummel, *The clinical significance of electrophysiological measures of olfactory function.* Behavioural brain research, 2006. **170**(1): p. 78-83.

[17] Cui, L. and W.J. Evans, *Olfactory event-related potentials to amyl acetate in congenital anosmia.* Electroencephalography and Clinical Neurophysiology, 1997. **102**(4): p. 303-306.

[18] Rombaux, P., et al., *Presence of olfactory event-related potentials predicts recovery in patients with olfactory loss following upper respiratory tract infection.* The Laryngoscope, 2010. **120**(10): p. 2115-2118.

[19] Frasnelli, J., B. Schuster, and T. Hummel, *Interactions between olfaction and the trigeminal system: what can be learned from olfactory loss.* Cerebral Cortex, 2007. **17**(10): p. 2268-2275.

[20] Barresi, M., et al., *Evaluation of olfactory dysfunction in neurodegenerative diseases.* Journal of the neurological sciences, 2012. **323**(1): p. 16-24.

[21] Morgan, C.D. and C. Murphy, *Olfactory event-related potentials in Alzheimer's disease.* Journal of the International Neuropsychological Society, 2002. **8**(06): p. 753-763.

[22] Mundiñano, I.-C., et al., *Increased dopaminergic cells and protein aggregates in the olfactory bulb of patients with neurodegenerative disorders.* Acta neuropathologica, 2011. **122**(1): p. 61-74.

[23] Haehner, A., T. Hummel, and H. Reichmann, *Olfactory loss in Parkinson's disease.* Parkinson's disease, 2011. **2011**.

[24] Meusel, T., et al., *The course of olfactory deficits in patients with Parkinson's disease—A study based on psychophysical and electrophysiological measures.* Neuroscience letters, 2010. **486**(3): p. 166-170.

[25] Mesholam, R.I., et al., *Olfaction in neurodegenerative disease: a meta-analysis of olfactory functioning in Alzheimer's and Parkinson's diseases.* Archives of neurology, 1998. **55**(1): p. 84-90.

[26] Welge-Lüssen, A., et al., *Olfactory-induced brain activity in Parkinson's disease relates to the expression of event-related potentials: a functional magnetic resonance imaging study.* Neuroscience, 2009. **162**(2): p. 537-543.

[27]   Murphy, C., *Age-related effects on the threshold, psychophysical function, and pleasantness of menthol.* Journal of Gerontology, 1983. **38**(2): p. 217-222.

[28]   Hummel, T., et al., *Chemosensory event-related potentials change with age.* Electroencephalography and Clinical Neurophysiology/Evoked Potentials Section, 1998. **108**(2): p. 208-217.

[29]   Morgan, C.D., et al., *Olfactory event-related potentials: older males demonstrate the greatest deficits.* Electroencephalogr Clin Neurophysiol, 1997. **104**(4): p. 351-8.

[30]   Toulouse, E. and N. Vaschide, *Mesure de l'odorat chez l'homme et chez la femme.* CR Soc Biol, 1899. **51**: p. 381-383.

[31]   Stuck, B., et al., *Chemosensory event-related potentials in relation to side of stimulation, age, sex, and stimulus concentration.* Clinical Neurophysiology, 2006. **117**(6): p. 1367-1375.

[32]   Olofsson, J.K. and S. Nordin, *Gender differences in chemosensory perception and event-related potentials.* Chemical senses, 2004. **29**(7): p. 629-637.

[33]   Lundström, J.N., et al., *Sex differentiated responses to intranasal trigeminal stimuli.* International journal of psychophysiology, 2005. **57**(3): p. 181-186.

[34]   Demiralp, T., et al., *Wavelet analysis of oddball P300.* International journal of psychophysiology, 2001. **39**(2): p. 221-227.

[35]   Morgan, C.D. and C. Murphy, *Differential effects of active attention and age on event-related potentials to visual and olfactory stimuli.* International Journal of Psychophysiology, 2010. **78**(2): p. 190-199.

[36]   Olofsson, J.K., et al., *Olfactory and chemosomatosensory function in pregnant women assessed with event-related potentials.* Physiology & behavior, 2005. **86**(1): p. 252-257.

[37]   Boesveldt, S., et al., *Signal-to-noise ratio of chemosensory event-related potentials.* Clinical neurophysiology, 2007. **118**(3): p. 690-695.

[38]   Covington, J.W., et al., *Normal aging and odor intensity effects on the olfactory event-related potential.* International Journal of Psychophysiology, 1999. **32**(3): p. 205-214.

[39]   Cain, W.S., *History of research on smell.* Handbook of perception, 1978. **6**: p. 197-229.

[40]   Wang, L., et al., *The correlation between physiological and psychological responses to odour stimulation in human subjects.* Clinical Neurophysiology, 2002. **113**(4): p. 542-551.

[41]   Lorig, T.S., D.H. Zald, and J.V. Pardo, *A computer-controlled olfactometer for fMRI and electrophysiological studies of olfaction.* Behavior Research Methods, Instruments, & Computers, 1999. **31**(2): p. 370-375.

[42]   Nordin, S., et al., *Olfactory event-related potentials in young and elderly adults: evaluation of tracking task versus eyes open/closed recording.* Chemical senses, 1999. **24**(4): p. 459-464.

[43]   Tonoike, M., et al. *Measurements Of Olfactory Evoked Potentials And Event Related Potentials Using Odorant Stimuli.* in *Engineering in Medicine and Biology Society, 1990., Proceedings of the Twelfth Annual International Conference of the IEEE.* 1990.

[44]   Rombaux, P., et al., *Assessment of olfactory and trigeminal function using chemosensory event-related potentials.* Neurophysiologie Clinique/Clinical Neurophysiology, 2006. **36**(2): p. 53-62.

[45]   Geisler, M.W. and C. Murphy, *Event-related brain potentials to attended and ignored olfactory and trigeminal stimuli.* International Journal of Psychophysiology, 2000. **37**(3): p. 309-315.

[46]   Stuck, B.A., et al., *Chemosensory event-related potentials during sleep—A pilot study.* Neuroscience letters, 2006. **406**(3): p. 222-226.

[47]   Ozkurt, N. and F.A. Savaci, *Determination of Wavelet Ridges of Nonstationary Signals by Singular Value Decomposition.* Circuits and Systems II: Express Briefs, IEEE Transactions on, 2005. **52**(8): p. 480-485.

[48]   Huart, C., et al., *Time-Frequency Analysis of Chemosensory Event-Related Potentials to Characterize the Cortical Representation of Odors in Humans.* PLoS ONE, 2012. **7**(3): p. e33221.

[49]   Quiroga, R.Q. and H. Garcia, *Single-trial event-related potentials with wavelet denoising.* Clinical Neurophysiology, 2003. **114**(2): p. 376-390.

[50]   Donoho, D.L., *De-noising by soft-thresholding.* Information Theory, IEEE Transactions on, 1995. **41**(3): p. 613-627.

[51]   Ahmadi, M. and R. Quian Quiroga, *Automatic denoising of single-trial evoked potentials.* NeuroImage, 2013. **66**(0): p. 672-680.

[52]   Effern, A., et al., *Time adaptive denoising of single trial event-related potentials in the wavelet domain.* Psychophysiology, 2000. **37**(6): p. 859-865.

[53]   Woody, C.D., *Characterization of an adaptive filter for the analysis of variable latency neuroelectric signals.* Medical and biological engineering, 1967. **5**(6): p. 539-554.

[54]   Iyer, D. and G. Zouridakis, *Single-trial evoked potential estimation: comparison between independent component analysis and wavelet denoising.* Clinical Neurophysiology, 2007. **118**(3): p. 495-504.

[55]   Huang, N.E., et al., *The empirical mode decomposition and the Hilbert spectrum for nonlinear and non-stationary time series analysis.* Proceedings of the Royal Society of London. Series A: Mathematical, Physical and Engineering Sciences, 1998. **454**(1971): p. 903-995.

[56]   Wu, C.-H., et al., *Empirical Mode Decomposition-Based Approach for Intertrial Analysis of Olfactory Event-Related Potential Features.* Chemosensory Perception, 2012. **5**(3-4): p. 280-291.

[57]   Daubechies, I., *Ten Lectures on Wavelets.* 1992: Society for Industrial and Applied Mathematics.

[58]   Rosso, O.A., *Entropy changes in brain function.* International Journal of Psychophysiology, 2007. **64**(1): p. 75-80.

[59]   Yordanova, J., et al., *Wavelet entropy analysis of event-related potentials indicates modality-independent theta dominance.* Journal of Neuroscience Methods, 2002. **117**(1): p. 99-109.

[60]   Rosso, O.A., S. Blanco, and A. Rabinowicz, *Wavelet analysis of generalized tonic-clonic epileptic seizures.* Signal Processing, 2003. **83**(6): p. 1275-1289.

[61]   Emre Cek, M., M. Ozgoren, and F. Acar Savaci, *Continuous time wavelet entropy of auditory evoked potentials.* Computers in Biology and Medicine, 2010. **40**(1): p. 90-96.

[62]   Shannon, C.E. and W. Weaver, *The Mathematical Theory of Communication.* 1949: University of Illinois Press.

[63]   Tsallis, C., *Possible generalization of Boltzmann-Gibbs statistics.* Journal of statistical physics, 1988. **52**(1-2): p. 479-487.

[64]   Quiroga, R.Q., et al., *Wavelet entropy in event-related potentials: a new method shows ordering of EEG oscillations.* Biological Cybernetics, 2001. **84**(4): p. 291-299.

[65]   Dumermuth, G., *EEG-brain dynamics: relation between EEG and brain evoked potentials.* Computer Programs in Biomedicine, 1982. **14**(2): p. 227-228.

[66]   Kermen, F., et al., *Molecular complexity determines the number of olfactory notes and the pleasantness of smells.* Scientific reports, 2011. **1**.

[67]   Ayhan, T., *Using Cnn Based Antennal Lobe Model To Increase Odor Classification*, in *Electronics and Communication Engineering.* 2010, Istanbul Technical University: Istanbul. p. 87.

[68]   Bhandawat, V., et al., *Sensory processing in the Drosophila antennal lobe increases reliability and separability of ensemble odor representations.* Nature neuroscience, 2007. **10**(11): p. 1474-1482.

[69]   Menini, A., *The neurobiology of olfaction.* 2010: CRC Press.

[70]   Deisig, N., M. Giurfa, and J.C. Sandoz, *Antennal lobe processing increases separability of odor mixture representations in the honeybee.* Journal of neurophysiology, 2010. **103**(4): p. 2185.

[71]   Muezzinoglu, M.K., et al. *Artificial olfactory brain for mixture identification.* in *Advances in Neural Information Processing Systems.* 2008.

[72]   Buck, L. and R. Axel, *A novel multigene family may encode odorant receptors: a molecular basis for odor recognition.* Cell, 1991. **65**(1): p. 175-187.

[73]   Brand, G., *Olfactory/trigeminal interactions in nasal chemoreception.* Neuroscience & Biobehavioral Reviews, 2006. **30**(7): p. 908-917.

[74]   Firestein, S., *How the olfactory system makes sense of scents.* Nature, 2001. **413**(6852): p. 211-218.

[75]   Huart, C., P. Rombaux, and T. Hummel, *Plasticity of the Human Olfactory System: The Olfactory Bulb.* Molecules, 2013. **18**(9): p. 11586-11600.

[76]   Leffingwell, J.C., *Olfaction–Update No. 5.* Leffingwell reports, 2002. **2**(1): p. 1-34.

[77]   Asena, E., *Anosmi ve Parosmi İle Seyreden Nörolojik Hastalıklarda Olfaktör Uyartılmış Potansiyeller*, in *Tıp Fakültesi.* 2007, Ege University: Izmir. p. 66.

[78]   Yazdani, A., et al. *Electroencephalogram alterations during perception of pleasant and unpleasant odors.* in *Quality of Multimedia Experience (QoMEX), 2012 Fourth International Workshop on.* 2012. IEEE.

[79]   Freeman, W.J., III, *The Physiology of Perception.* 1991.

[80]   Lazarini, F. and P.-M. Lledo, *Is adult neurogenesis essential for olfaction?* Trends in neurosciences, 2011. **34**(1): p. 20-30.

[81]   Bhatnagar, K.P., et al., *Number of mitral cells and the bulb volume in the aging human olfactory bulb: a quantitative morphological study.* The Anatomical record, 1987. **218**(1): p. 73-87.

[82]   Prescott, J., *The generalizability of capsaicin sensitization and desensitization.* Physiology & behavior, 1999. **66**(5): p. 741-749.

[83]   Sicuteri, F., et al., *Beneficial effect of capsaicin application to the nasal mucosa in cluster headache.* The Clinical journal of pain, 1989. **5**(1): p. 49-54.

[84]   Peris, M. and L. Escuder-Gilabert, *A 21st century technique for food control: Electronic noses.* Analytica Chimica Acta, 2009. **638**(1): p. 1-15.

[85]   Zhang, S., et al., *An entire feature extraction method of metal oxide gas sensors.* Sensors and Actuators B: Chemical, 2008. **132**(1): p. 81-89.

[86]   Gardner, J. and P.N. Bartlett, *Sensors and Sensory Systems for an Electronic Nose.* 1992: Springer.

[87]   Ying, Z., et al., *A study on QCM sensor for identification of acetone vapor.* COMPEL: The International Journal for Computation and Mathematics in Electrical and Electronic Engineering, 2010. **29**(2): p. 477-483.

[88]   Bicego, M., *Odor classification using similarity-based representation.* Sensors and Actuators B: Chemical, 2005. **110**(2): p. 225-230.

[89]   Nimsuk, N. and T. Nakamoto. *Study of Odor Classification in Dynamically Changing Concentration using QCM Sensor Array and Short-Time Fourier Transform.* in *Solid-State Sensors, Actuators and Microsystems Conference, 2007. TRANSDUCERS 2007. International*. 2007.

[90]   Vergara, A., et al., *On the performance of gas sensor arrays in open sampling systems using Inhibitory Support Vector Machines.* Sensors and Actuators B: Chemical, 2013. **185**(0): p. 462-477.

[91]   Mumyakmaz, B., et al., *A study on the development of a compensation method for humidity effect in QCM sensor responses.* Sensors and Actuators B: Chemical, 2010. **147**(1): p. 277-282.

[92]   Dutta, R., et al., *Stochastic resonance-based electronic nose: A novel way to classify bacteria.* Sensors and Actuators B: Chemical, 2006. **115**(1): p. 17-27.

[93]   Phaisangittisagul, E. and H.T. Nagle, *Predicting odor mixture's responses on machine olfaction sensors.* Sensors and Actuators B: Chemical, 2011. **155**(2): p. 473-482.

[94]   Phaisangittisagul, E. *Outlier detection for machine olfaction based on odor-type signatures.* in *Electrical Engineering/Electronics, Computer, Telecommunications and Information Technology, 2009. ECTI-CON 2009. 6th International Conference on*. 2009. IEEE.

[95]   Acevedo, F.J., et al., *Probabilistic support vector machines for multi-class alcohol identification.* Sensors and Actuators B: Chemical, 2007. **122**(1): p. 227-235.

[96]   Muezzinoglu, M.K., et al., *Acceleration of chemo-sensory information processing using transient features.* Sensors and Actuators B: Chemical, 2009. **137**(2): p. 507-512.

[97]   Trincavelli, M., S. Coradeschi, and A. Loutfi, *Odour classification system for continuous monitoring applications.* Sensors and Actuators B: Chemical, 2009. **139**(2): p. 265-273.

[98]   Phaisangittisagul, E. *Transient feature extraction for machine olfaction based on Wavelet decomposition.* in *Electrical Engineering/Electronics, Computer, Telecommunications and Information Technology, 2008. ECTI-CON 2008. 5th International Conference on.* 2008.

[99]   Ehret, B., et al., *A new feature extraction method for odour classification.* Sensors and Actuators B: Chemical, 2011. **158**(1): p. 75-88.

[100]   Chua, L.O. and L. Yang, *Cellular neural networks: theory.* Circuits and Systems, IEEE Transactions on, 1988. **35**(10): p. 1257-1272.

[101]   Yalçin, M.E., J.A.K. Suykens, and J. Vandewalle, *Cellular Neural Networks, Multi-scroll Chaos and Synchronization.* 2005: World Scientific.

[102]   Ayhan, T. and M.E. YALÇIN, *An application of small-world cellular neural networks on odor classification.* International Journal of Bifurcation and Chaos, 2012. **22**(01).

[103]   Pearson, K., *LIII. On lines and planes of closest fit to systems of points in space.* The London, Edinburgh, and Dublin Philosophical Magazine and Journal of Science, 1901. **2**(11): p. 559-572.

[104]   Vapnik, V., *The nature of statistical learning theory.* 2000: springer.

[105]   Worrell, G., *High-frequency oscillations recorded on scalp EEG.* Epilepsy Currents, 2012. **12**(2): p. 57-58.

[106]   Jurcak, V., D. Tsuzuki, and I. Dan, *10/20, 10/10, and 10/5 systems revisited: their validity as relative head-surface-based positioning systems.* Neuroimage, 2007. **34**(4): p. 1600-1611.

[107]   Kropotov, J., *Quantitative EEG, event-related potentials and neurotherapy.* 2010: Academic Press.

[108]   Sanei, S. and J.A. Chambers, *EEG signal processing.* 2008: Wiley. com.

[109]   Başar, E., et al., *Gamma, alpha, delta, and theta oscillations govern cognitive processes.* International Journal of Psychophysiology, 2001. **39**(2): p. 241-248.

[110]   Doty, R.L. and C. Press, *Handbook of olfaction and gustation.* 2003: Marcel Dekker New York.

[111]   Mouraux, A. and G.D. Iannetti, *Across-trial averaging of event-related EEG responses and beyond.* Magnetic Resonance Imaging, 2008. **26**(7): p. 1041-1054.

[112] Simon, S.A. and M.A. Nicolelis, *Methods in chemosensory research*. 2010: CRC Press.

[113] Tateyama, T., et al., *Relation of olfactory event-related potentials to changes in stimulus concentration.* Electroencephalography and Clinical Neurophysiology/Evoked Potentials Section, 1998. **108**(5): p. 449-455.

[114] Emre Cek, M., *Analysis of Observed Chaotic Data*, in *Electrical and Electronics Engineering*. 2004, Izmir Institute of Technology: Izmir. p. 101.

[115] Mallat, S., *A Wavelet Tour of Signal Processing: The Sparse Way*. 2008: Elsevier Science.

[116] Quiroga, R.Q., *Quantitative Analysis of EEG signals: Time-Frequency Methods and Chaos Theory* in *Institute of Physiology and Institute of Signal Processing*. 1998, Medical University Lübeck: Germany. p. 146.

[117] Addison, P.S., *The Illustrated Wavelet Transform Handbook: Introductory Theory and Applications in Science, Engineering, Medicine and Finance*. 2010: Taylor & Francis.

[118] Delprat, N., et al., *Asymptotic wavelet and Gabor analysis: Extraction of instantaneous frequencies.* IEEE transactions on Information Theory, 1992. **38**(2): p. 644-664.

[119] Cai, T.T. and B.W. Silverman, *Incorporating information on neighbouring coefficients into wavelet estimation.* Sankhyā: The Indian Journal of Statistics, Series B, 2001: p. 127-148.

[120] Rosso, O.A., et al., *Wavelet entropy: a new tool for analysis of short duration brain electrical signals.* Journal of neuroscience methods, 2001. **105**(1): p. 65-75.

[121] Bradley, A.P. and W. Wilson, *On wavelet analysis of auditory evoked potentials.* Clinical Neurophysiology, 2004. **115**(5): p. 1114-1128.

[122] Wiener, N., *Extrapolation, interpolation and smoothing of stationary time series, 1949.* New York.

[123] Vaseghi, S.V., *Wiener Filters*, in *Advanced Digital Signal Processing and Noise Reduction*. 2001, John Wiley & Sons, Ltd. p. 178-204.

[124] Haykin, S., *Adaptive filter theory, 1996*. 2000, Prentice-Hall, Upper Saddle River, New Jersey.

[125] Flandrin, P., G. Rilling, and P. Goncalves, *Empirical mode decomposition as a filter bank.* Signal Processing Letters, IEEE, 2004. **11**(2): p. 112-114.

[126] Xuan, Z., S. Xie, and Q. Sun. *The Empirical Mode Decomposition Process of Non-stationary Signals*. in *Measuring Technology and Mechatronics Automation (ICMTMA), 2010 International Conference on*. 2010.

[127] Shapiro, S.S. and M.B. Wilk, *An analysis of variance test for normality(complete samples)*. 1964, JSTOR.

[128] Pallant, J., *SPSS survival manual: A step by step guide to data analysis using SPSS*. 2010: McGraw-Hill International.